STUDY OF FAST TIME SCALE PHENOMENA IN PLASMAS

By

Sita Sundar

INSTITUTE FOR PLASMA RESEARCH, GANDHINAGAR.

A thesis submitted to the
Board of Studies in Physical Sciences

In partial fulfillment of the requirements

For the Degree of

DOCTOR OF PHILOSOPHY

of

HOMI BHABHA NATIONAL INSTITUTE

August 2012

Homi Bhabha National Institute

Programme: Ph.D.

Board of Studies in PHYSICAL **Sciences**

1. Name of the Constituent Institution: Instite for Plasma Research

2. Name of the Student: Sita Sundar

3. Enrolment Number: PHYS 06 200704010

4. Date of Enrolment in HBNI: September 3, 2007

5. Date of Submission of Thesis: August 31, 2012

6. Title of the Thesis: Study of Fast Electron Time Scale Phenomena in Plasmas

7. Composition of the Doctoral Committee:

Sr No	Composition	Designation in HBNI	Name
a.	**Chairman**	Senior Professor	Prof. Abhijit Sen
b.	**Convener** (Guide)	Associate Professor	Prof. Amita Das
c.	**Co-Guide**, if any		
d.	**Member**		Prof. Y. C. Saxena
e.	**Member**	Assistant Professor	Dr. Sudip Sengupta
f.	**The Technology Adviser**, if any	**Invitee**	

8. Number of Doctoral Committee Meetings held with respective dates: 5

(1) 06/10/2008 (2) 25/11/2009 (3) 30/08/2010 (4) 26/07/2011

(5) 25/05/2012

9. Name and Organization of the Examiner 1: G. Ravindra Kumar, TIFR Mumbai

Recommendations of the Examiner 1 (Thesis Evaluation) (i) accepted, (ii) accepted after revisions, or (iii) rejected:

10. Name and Organization of the Examiner 2: F. Pegoraro, Universita' di Pisa, Pisa

Recommendations of the Examiner 2 (Thesis Evaluation) (i) accepted, (ii) accepted after revisions, or (iii) rejected:

Name & Signature of Dean-Academic, CI: Dr. S. Mukherjee

S Mukherjee
06/11/2012

Recommendations of the Viva Voce Board

1. **Date of Viva Voce Examination:** 06/11/2012

2. **Recommendations for the award of the Ph.D. degree: Recommended / ~~Not Recommended~~**
   (If Recommended, give summary of main findings and overall quality of thesis)
   (If Not Recommended, give reasons for not recommending and guidelines to be communicated by Convener of the Doctoral committee to the student for further work)

This is a thesis of a very high quality, reporting substantial advances in a topical research area. The role of the Kelvin-Helmholtz instability in the fast ignition of laser fusion is a very important insight. So are the soliton instability questions addressed in the second part.

The candidate made a sound and coherent presentation in the Viva-Voce and answered questions satisfactorily.

Overall, this has been a very good all round effort, which should provoke more research and advances.

G. Ravindra Kumar
06/11/12

Abhijit
6/11/2012

In case Not Recommended, another date will be fixed by the Dean-Academic, CI, which shall not be earlier than a month after and not later than six months from the date of first viva.

Date: 06/11/2012

Name and Signature of the Viva Voce Board (Doctoral Committee and External Examiner):

1. G. Ravindra Kumar — G. Ravindra Kumar
2. Prof. Abhijit Sen — Abhijit
3. Prof. Amita Das — Amita Das
4. Prof. Y. C. Saxena — YCSaxena
5. Dr. Sudip Sengupta. — SSengupta

CERTIFICATION FROM GUIDE

This is to certify that viva voce of **Ms. Sita Sundar** took place on 6th November 2012 in the Institute for Plasma Research, Bhat, Gandhinagar, in the presence of all the following Doctoral Committee members and the external referee **Dr. G. Ravindra Kumar.**

Prof. Abhijit Sen (Chairman) Abhijit

Prof. Amita Das (Guide) Amita Das.

Prof. Y. C. Saxena (Member) YCSaxena

Dr. Sudip Sengupta (Member) Sengupta

The corrections as indicated in the thesis evaluation report of both the referees, have been incorporated in this copy of the thesis.

Amita Das.

Date: 06.11.2012

(Prof. Amita Das)

Guide

DECLARATION

I, Sita Sundar, hereby declare that the investigation presented in the thesis has been carried out by me. The work is original and the work has not been submitted earlier as a whole or in part for a degree/diploma at this or any other Institution or University.

Sita Sundar

Sita Sundar

I hereby certify that I have read this dissertation prepared under my direction and recommend that it may be accepted as fulfilling the dissertation requirement.

Amitā Das.

Guide: Prof. Amita Das

STATEMENT BY THE AUTHOR

This dissertation has been submitted in partial fulfillment of requirements for an advanced degree at Homi Bhabha National Institute (HBNI) and is deposited in the Library to be made available to borrowers under rules of the HBNI.

Brief quotations from this dissertation are allowable without special permission, provided that accurate acknowledgement of source is made. Requests for permission for extended quotation from or reproduction of this manuscript in whole or in part may be granted by the Competent Authority of HBNI when in his or her judgment the proposed use of the material is in the interests of scholarship. In all other instances, however, permission must be obtained from the author.

Sita Sundar

Sita Sundar

ACKNOWLEDGEMENTS

This thesis would not have been completed without the support and guidance from many people, whom I would like to thank heart and soul. First and foremost, I wish to express my utmost gratitude to my supervisor Prof Amita Das for her excellent guidance and support. She always encouraged me to learn new techniques and understand the Physics. Despite her other obligations, she has always shared her invaluable time with me for the scientific discussions. I owe a lot to you for the valuable advice and constructive criticism. Thank you Ma'am!

She and the other Doctoral Committee members, Prof. Abhijit Sen(Chairman), Prof. Y.C. Saxena(Member), Dr. Sudip Sengupta(Member), guided me throughout the Research Program, never accepting less than my best efforts. I thank them all.

I would also like to acknowledge and extend my heartfelt gratitude to Prof. Kaw for all those precious moments he shared with me from his busy schedule for scientific discussions.

I am also extremely indebted to Dr. R. Ganesh, Dr. Prabal Chattopadhyaya, Dr. Joydeep Ghosh, Dr. Srinivasan, Dr. Manoj Warrier, Raj Singh, Ritesh Sugandhi, Prof. R. Jha, Dr. S. Deshpande, Dr. Indranil Bandyopadhyaya, Dr. S. Mukherjee, Dr. Sudip Sengupta for providing very good training during the course work. I express my sincere thanks to Academic Dean, Dr. Mukherjee for his timely help. I would like to extend my sincere gratitude to Shravan, Smita, Pragnya Pathak, Arundhati Das, Sambhawi, Hemant Joshi, Shailendra Trivedi, Sutapa Ranjan and all Library and Computer Centre Staff members for the use of their resources, such as online databases and library, without which the compilation of this thesis would have been extremely complicated. I expand my thanks to Sourbhan, Khanduri, Dinesh Nair, Vartak, Savai, Sirin, Silel for their help they rendered.

I am delighted that here I have an opportunity to acknowledge the cooperation of my batchmates Kshitish, Prabal, Sanjib, Ashwin, Ujjwal, Vikram, Tayyab, Linthish, Deepak, Arvind. I further extend my thanks to Jyotirmoy, Neeraj, Pintu, Ritu, Rajneesh, Maya, Kishor, Vikrant, Sunita, Shekhar, Jugal, Satya, Sharad, Sushil, Rameswar, Manjeet, Pravesh, Sayak, Soumen, Aditya, Shailaja, Sushmita, Shefali, Swati Baruah, Sarveshwar, Sapna, Vidhi, Deepa, Akanksha, Mangi, Neeraj, Chandrasekhar, Meghraj, Vara, Harish, Rupendra, Bibhu, Samir and Saleem.

A special thanks to Sanat, Gurudatt and Avadhesh for going the extra mile with the kind of feedback that put flesh on the bones. Thanks are due to Pratibha for sharing her thoughts and time with me and feeding me on Special Saturdays. At this juncture, it is a pleasant task to express my thanks to Sanat and Dharodi for the proofreading. I am thankful to my friends Madhumita, Garima, Pratima, Ravi Shankar, Farzad, Ashish, Moumita, Sangeeta Singh, Anjali Gautam, Archana Tiwari and Chaitali.

I would like to acknowledge my University Reader, Dr. Bhabani Prasad Mandal, for the constant support and encouragement he provided throughout my Ph.D. tenure.

Most especially to my family, words alone cannot express what I owe them for their encouragement and whose patient love enabled me to complete this thesis. I dedicate this thesis to my family members for their unconditional love and support in every way possible throughout the process of this Research period, this thesis and beyond. And especially to God, who made all things possible.

List of Publications

Publications in Peer Reviewed Journals:

1. **Detailed Characterization of Relativistic Electromagnetic Solitons in Cold Plasma** ,
   Sita Sundar and Amita Das
   Physics of Plasmas (*to be submitted*).

2. **Perturbative analysis of sheared flow Kelvin-Helmholtz instability in a weakly relativistic magnetized electron fluid**,
   Sita Sundar, Amita Das, and Predhiman Kaw
   Physics of Plasmas 19, 052105 (2012).

3. **Relativistic electromagnetic flat top solitons and their stability**,
   Sita Sundar, Amita Das, Vikrant Saxena, Predhiman Kaw, and Abhijit Sen
   Physics of Plasmas 18, 112112 (2011).

4. **Free energy source for flow shear driven instabilities in electron-magnetohydrodynamics**,
   Sita Sundar and Amita Das
   Physics of Plasmas 17, 042106 (2010).

5. **Electron velocity shear driven instability in relativistic regime**,
   Sita Sundar and Amita Das
   Physics of Plasmas 17, 022101 (2010).

6. **Role of natural length and time scales on shear driven two-dimensional electron magnetohydrodynamic instability**,
   Gurudatt Gaur, Sita Sundar, Sharad K. Yadav, Amita Das, Predhiman Kaw, Sharveshwar Sharma
   Physics of Plasmas 16, 072310 (2009).

Abstract

Plasma is a very complex medium. A typical plasma medium is a charged many body system which generates and responds to electromagnetic fields and behaves in a collective fashion. Often, simplifications in such a complex plasma system are desirable. A gross simplification is possible by adopting a macroscopic fluid picture wherein properties averaged over a large number of particles constitute a small fluid element whose propagation can be followed up in space and time. Furthermore, due to the huge difference in the masses of the constituent species of the plasma (ions are typically 1840 times heavier than electrons), their response times are very different. Hence, a further simplification is possible if the phenomena under consideration falls under the time scale regime where only one of the constituent regime can have a dominant response. The exploitation of such time scale separation has led to various simplified models for plasma depiction. Based on the idea of the exploitation of time scale separation, plasma phenomena can be broadly categorized into two groups: (a) Slow ion time scale phenomena, where one can assume instantaneous response of electrons and (b) fast electron time scale phenomena, for which ions are assumed to provide merely a stationary neutralizing background. In both the regimes of (a) and (b) further simplifications are possible and have been adopted in literature, based on more definite information about the phenomena under consideration. While the regime of ion response has been studied extensively since almost a century and interesting studies are still being pursued in this area, the phenomena associated with fast electron time scale response has been relatively less explored. It is only recently (with the advent of fast high power lasers) that the laboratory plasma can be triggered to respond and diagnosed at these time scales, and studies in this regime have gained prominence.

We have chosen to investigate some fundamental issues which also have practical relevance in the regime of fast electron time scale response in plasmas. In particular, the thesis explores the electron shear flow driven instabilities and coherent nonlinear solutions that may form in this domain of plasma response. The magnetized and relativistic nature of the electron fluid produces interesting features in the electron shear flow driven Kelvin - Helmholtz (KH) like mode of the plasma. The study concerning this instability has been presented in the part - I of the thesis. In part - II, the study of the existence of nonlinear coherent structure

in the coupled laser plasma system has been presented. The dynamical evolution of some of the solutions and questions pertaining to the stability of some of these structures have also been looked at.

The sheared electron flow in the non-relativistic regime has often been described by a reduced fluid Electron Magnetohydrodynamic (EMHD) model. EMHD model describes the dynamics of magnetized electron fluid in the presence of self-consistent and external electric and magnetic field on time scales in between electron and ion gyrofrequencies. Here, ion dynamics is completely ignored and role of ions is simply to provide neutralizing background. The electron fluid is assumed to be incompressible in this limit, the density perturbations as well as the displacement current are assumed to be negligible in this case.

The EMHD model resembles closely the neutral hydrodynamic fluid system and hence the characteristic neutral fluid instabilities are also present here as well, albeit with appropriate modifications due to magnetized character of the electron fluid. The distinction and similarities of the KH mode in neutral fluid and the EMHD has been outlined in the past by several authors. The sheared flow of electrons also constitutes a sheared current in the plasma. It has so far not been clear, which between the two, the current shear or the velocity shear, was responsible for the instability of sheared electron flow configuration. It is for this reason that this mode has often been also referred to as the sausage and/or kink mode [1, 2], the nomenclature used when the current shear produces instability in a plasma. We have employed a generalised Electron Magnetohdrodynamic description to distinguish a sheared current flow configuration from the case with velocity shear, by choosing an appropriately tailored inhomogeneous electron density profile. The instability studies carried out for the two configuration then clearly shows that in 2-D the instability is driven by the shear in electron flow velocity, and hence it is a KH like mode. The interpretations for certain characteristic features, such as existence of a threshold wavenumber along the flow direction and the excitation of sharper scales in the direction normal to both shear and flow directions, the order of magnitude estimation of the growth rate etc., from physical considerations of the release in the free energy source has also been provided by us.

An important practical implication of the KH instability driven by a sheared electron current flow can be in the context of fast ignition (FI) mechanism of laser fusion [1–6]. The FI is a variant of the inertial confinement fusion scheme in which the task of material compression is separated from that of ignition by employing two separate laser pulses. While the compression is done by a slow nanosecond laser pulse, for ignition one employs a fast sub-picosecond laser. The ignitor pulse is unable to penetrate the overdense compressed target core and instead produces hot energetic electrons which propagate towards the compressed target core. It is desirable that these energetic electrons dump their energy in the compressed core of the target to produce the hot spot for ignition. The transport of energetic electrons in the plasma, is therefore an important issue. The flow of energetic electrons is typically countered by reverse shielding current provided by the background plasma immediately. The forward and background currents, upon suffering Weibel, tearing and coalescence instability produce cylindrical current channels. The central portion of which carries the forward current and the external cylindrical shell carries the reverse shielding current. The flow of electrons in the cylinder along its axis, therefore, has sufficient shear in the radial direction. This sheared flow configuration would in general be susceptible to the KH instability. However, since the energetic electron flow can be relativistic, it is important that the relativistic effects on the EMHD KH mode be understood. For this purpose, we have carried out a detailed investigation of the KH mode in the relativistic regime.

Our studies on the KH mode for the sheared electron flow which is relativistic reveals that there are characteristic differences with the nonrelativistic case. We have shown that the incorporation of displacement current (as the flows are now relativistic) has little influence on the mode. However, as the relativistic mass factor can also be sheared, we observe that the possibility of exciting modes sharper than the velocity shear scale in the flow direction exists. We also show that the unstable domain of the wave-number space is considerably wider in this case and the mode does not remain purely growing but acquires a real frequency even for a purely antisymmetric velocity profile. We have provided an understanding of these features observed in the strongly relativistic regime as resulting from the shear in the relativistic mass factor γ_0.

The results of the weakly relativistic case observed from numerical analysis has also been reproduced by a perturbative analytic treatment. A good matching between the numerical exact results for the maximum growth rate and the threshold wave vector has been demonstrated by us.

In the second part of the thesis, we have looked at the problem of the coupling of the laser and the plasma medium. We have, in this context, sought exact propagating nonlinear coherent solutions for the coupled set [7–14]. Existence of several distinct varieties of solutions have been demonstrated. The different structures occur in a different parametric domain of the frequency λ vs the propagation speed β. Some solutions occur in a continuum band of the λ vs β plane while others are only permitted in discrete regime and satisfy certain eigen value condition. We have carried out a detailed characterization of these solutions and have also provided a physical interpretation of their existence in the particular regime of the λ vs β parametric space.

We notice that for solutions moving with the group velocity of $\beta = 0$ and/or very small, the assumption of static ions should not be made. We, therefore incorporated the effect of ion dynamics and investigated the eigen spectra afresh. We notice several additional new varieties of solitonic structures in this case. We also observe that the bright soliton solutions (with light pulse trapped within the central region) are not permitted at low group velocities in this case. Instead dark solitonic structures can form. At the edge, a particular variety of flat top solutions are shown to exist.

A detailed dynamical evolution of the flat top solutions have also been carried out. The studies show that the flat top solutions propagate stably for several plasma periods. However, they are observed to be susceptible to an instability, which has been identified as the backward Brillouin instability process. In the cold plasma, it is a quasi-mode where the role of temperature is played by the electron quiver velocity.

Further extension of our work in both the problems can be carried out. The linear analysis of the relativistic flow shear driven instability in EMHD is useful in understanding the basic physics of the excitation of the unstable mode but nonlinear studies are very important. With the nonlinear studies we will be able to have deeper insights regarding the evolution properties, saturation etc. The nonlinear studies of the relativistic EMHD mode would be crucial for the estimation of the effective transport properties of the electron flow. This is specially pertinent, as pointed out by us, in the context of FI concept of laser fusion.

The dynamical evolution of flat-top solitons has shown that they develop a backward Brillouin scattering instability. It would be interesting to see how some of the stable structures behave when the two-dimensional perturbations allow for a side scattering process. The three-dimensional generalization, the effect of relativistic temperature on the stability properties and dynamics of electromagnetic solitons are other issues of interest for future investigation.

Contents

List of Figures

List of Tables

Chapter 1

Introduction

The thesis is devoted to the study of certain fundamental aspects of the plasma behaviour pertaining to those time scales at which the lighter electron species have a dominant dynamical role. Simplified fluid models (existing as well as extended) based on the idea of time scale separation have been adopted to study certain frontier issues of fundamental as well as applied interest in this regime. These issues illustrate both cases e.g. wherein only electron dynamical response is important and when the retention of the coupling of the electron dynamical response with the slow response of heavier ion species is crucial.

One of the ways in which a plasma can be triggered to respond at the fast electron response scales is through ultra fast short intensity lasers. In this thesis, we have explored both situations, namely the evolution of a disturbed plasma once the laser pulse has left and the other case when the laser light is present and plasma continues to interact with it.

1.1 Motivation

The understanding of evolution of any system of interest is an issue of prime importance. The laws of physics attempt at providing such an understanding. The difficulty, however, often lies with the huge number of degrees of freedom associated with any given system which needs to be evolved by appropriate equations of motion for its proper and complete understanding. Such a difficulty is often overcome by invoking suitable set of approximations. For instance, in the particular case of plasma medium an illustration of such approximations can be gleaned by looking at its properties and the descriptions that are normally adopted to understand its evolution under various circumstances. A typical plasma medium consists of a collection of positively and negatively charged ions and electron species respectively. The particle number density and the temperature range wherein the plasma state of matter is observed in the universe, covers a very wide range. This has been depicted in the plot of Fig. 1.1. Clearly, any of these plasma systems constitutes a very large number of particles, the evolution of each of the particles ultimately determines the overall evolution of the system.

1.2 Adoption of fluid model

To understand the overall evolution of any large system with large number of particles, one is not interested in observing developments at individual particle level. A gross simplification is possible by adopting a macroscopic picture instead, wherein properties averaged over a large number of particles constitute a small fluid element whose propagation can be followed up in space and time. This is the basis of

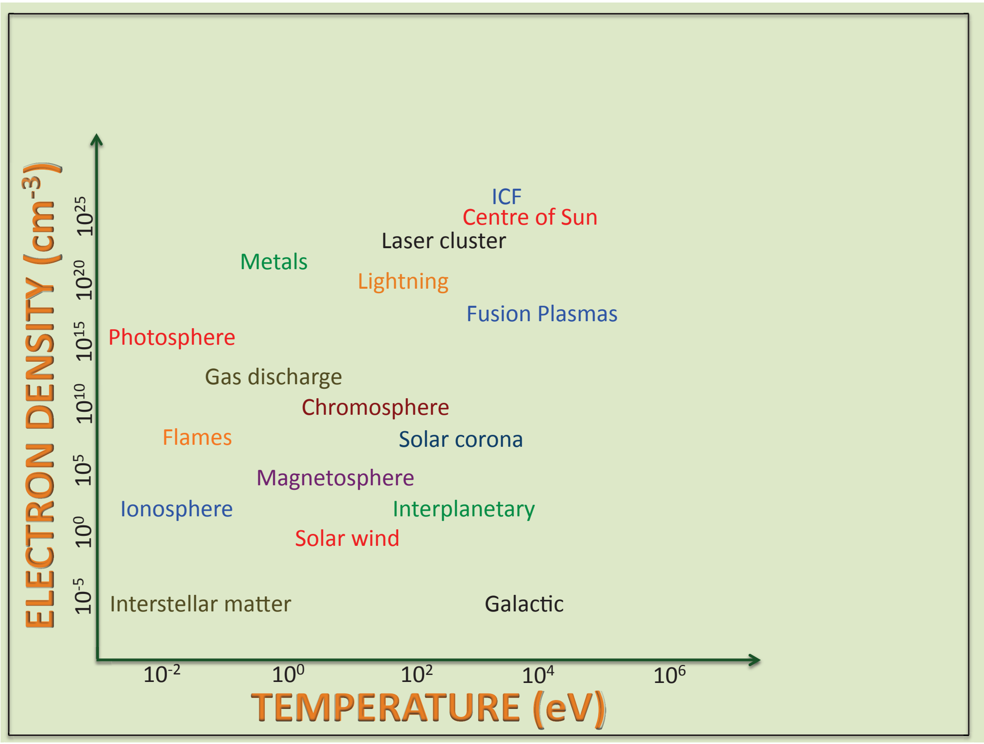

Figure 1.1: Overview of plasmas in the density-temperature plane.

the development of fluid models. In the context of plasmas a two fluid depiction corresponding to the evolution of ion and electron species has been adopted. Furthermore, since the charge species of plasma responds to the electromagnetic fields and is also responsible for the generation of electric and magnetic fields, the two fluid depiction for ion and electron species has to be coupled with the Maxwell's equation which describe the evolution of electric and magnetic fields. Even though such a fluid based description provides for a huge simplification, it may still contain a lot of unnecessary and complicated details for the depiction of certain phenomena, thereby shrouding the physics germane to that. A further simplification is possible by defining the time scale regime of the phenomena of interest and concentrating on possible simplified description which would be adequate for it. We discuss this procedure in the next section.

1.3 Exploitation of time scale separation

As mentioned earlier the plasma medium consists of two kind of species, namely the ions and the electrons. There is a huge difference in the masses of these two species. The ions are typically 1836 times (or more) massive compared to electrons which constitute the lighter species of the medium. The two species have very different response times due to the disparity of their masses. It is, thus, possible to exploit the time scale separation to simplify the two fluid model, coupled to the Maxwell's set of equations, further. The exploitation of scale separation has led to various reduced models for plasma depiction. For instance, the Magnetohydrodynamic (MHD) fluid model represents a model of magnetized ion fluid pertaining to the slow response of the heavier ion species. For the lighter electron species, one assumes an instantaneous response by ignoring the electron inertial effects. At the other limit are phenomena associated with fast electron time scales. In this case, the heavier ion species, which are considerably slower than electrons, are assumed to provide only for a neutralizing static background. This is a regime where we concentrate upon in this thesis. Certain specific issues in the frontier areas of research pertaining to this time scale regime have been conceptualized by us. There are, however, also cases where even though the dominant dynamical response is that of electron species, the ion dynamics in some reduced approximate sense does have interesting role to play. We illustrate this regime in the case of slowly moving coherent soliton solutions for the coupled laser plasma system.

1.4 Fast electron time scale phenomena

Our interest in the study of fast electron time scale phenomena in plasmas is motivated by the recent technological advancements. The development of ultra intense short pulse lasers have now made it possible to conduct various laboratory experiments in this domain. By using these laser pulses a laboratory plasma can be triggered to respond at the fast time scales associated with electron dynamics. In addition, novel diagnostic techniques have also been developed which are now capable of capturing the response at such time scales. Thus, plasma response associated with faster electron species is an area of growing current research interest.

Furthermore, phenomena at these time scales have relevance in various applications. Some frontier research applications are that of the Fast Ignition (FI) concept of Inertial Confinement Fusion (ICF), laser and beam based particle acceleration schemes and so on. The questions pertaining to certain astrophysical puzzles associated with the rapid reconnection of magnetic field resulting in rapid release of energy bursts in solar flares etc., are also believed to be governed by phenomena occurring at these time scales.

The model description in this regime is provided by the electron fluid continuity and momentum equations. While any electrostatic phenomena with a static distribution of ion charges would involve an additional Poisson's equation alone, for the electromagnetic case one needs to couple these equations with Ampere's and Faraday's law as well. There is a further possibility of simplification in the electromagnetic case when the phase and group speeds associated with the phenomena is much slower than the speed of light and/or the typical time scales are slower than the electron plasma period. For these cases, it is possible to ignore the electron continuity equation by invoking the assumption of negligible electron density fluctuation. The displacement current can also be ignored in this limit. The model then reduces to an extremely interesting form and is known as the Electron Magnetohydrodynamic (EMHD) model. The EMHD model has a very simplified form wherein the governing equations can be cast entirely in terms of the evolution equation of the magnetic field alone. We have chosen to investigate the understanding of certain phenomena associated with the EMHD domain of plasma response in this thesis.

1.5 Review of Earlier Works

While the plasma behaviour at slow ion time scales has been contemplated extensively, studies related to fast electron response time scales have been rare. The reason is also apparent from the fact that most laboratory experiments could explore till recent times only slow ion time scale phenomena. With the advent of high power fast femtosecond lasers, a relatively unexplored regime of fast electron dynamical response came within the realm of observation in the laboratory.

The new regime offers several interesting fundamental aspects of exploration in which there has been a considerable increase in recent activity. The new regime has its own set of linear response, instabilities, coherent solutions and turbulent features. The possibility of performing controlled experiments in this area has helped in gaining insights of the topic and motivated theoretical and numerical work in the area.

Several applications which existed as mere theoretical ideas now have become an experimental reality. For example the entire area of laser and plasma based particle acceleration schemes has produced significant results in recent times. The particle energy doubling of 42GeV electrons in a metre-scale plasma wakefield accelerator has been achieved [18]. New ideas to improve upon the qualities of the accelerated particles are being proposed and pursued. The table top nature of the experiments have led to a variety of medical applications. Newer schemes of fusion e.g. FI, which relies on the transport of energetic electrons through plasma have been proposed.

We have touched upon two specific areas pertaining to this regime of plasma response. These two have been presented in Part - I and part - II of the thesis. The part - I of the thesis deals with the Kelvin - Helmholtz like instability (driven by a sheared fluid flow configuration) for the electron flow. In the second part, the possible existence and stability of the nonlinear coherent solutions of the coupled laser plasma system has been explored.

1.6 Content and organization of the thesis

As mentioned in the introduction we have chosen to investigate some fundamental issues which also have practical relevance in the regime of fast electron time scale response in plasmas. For this purpose, we have chosen to divide the thesis in two parts. The first part deals with instabilities in this regime. In particular, we have chosen to study some salient features of the electron shear flow driven Kelvin - Helmholtz instability that can get excited in a variety of circumstances. In part - II, the study of the existence of nonlinear coherent structure in the coupled laser plasma system has been investigated. The dynamical evolution of some of the solutions and questions pertaining to their stability have also been looked at.

In Chapter 2, we describe the governing equations that are employed for the exploration of the phenomena in the regime of the fast electron time scale dynamics. The complete set corresponds to the electron fluid (momentum and the continuity equations) coupled with the Maxwell set of equations. The reduction of the equations under various approximations to simpler forms have also been described in detail in the chapter. The relativistic generalization of the equations have also been shown. These equations have been utilized to address issues pertaining to the topic of shear flow driven instability in Part - I and the possible coherent solutions for the coupled laser plasma system in Part - II of the thesis.

The first part of the thesis (Chapters 3, 4 and 5) deals with the evolution of sheared electron flow configuration against a stationary neutralizing background of ions. The possibility of the occurrence of such a sheared electron flow configuration has been envisaged in a variety of astrophysical as well as laboratory plasma experiments. For instance, in the context of fast ignition (a frontier concept in the inertial confinement fusion in which the task of compression and heating are carried out by separate laser pulses), such a configuration arises during the ignition phase. The ignitor pulse, which is supposed to carry and deposit energy at an appropriate spot for ignition, cannot penetrate the overdense region of the target. It generates energetic electrons at the critical density surface. One hopes that these energetic electrons would deposit energy at the appropriate location for the creation of hot spot for ignition. However, as these energetic electrons move towards the compressed core of the target, its current is shielded by a reverse cold electron current from the background plasma. The forward and reverse currents get spatially separated by the Weibel instability. The subsequent tearing and Coalescence modes lead to the formation of cylindrical current channels. These cylindrical channels carry the forward current due to energetic electrons in their central region and in the outer annular region, the background shielding current flows. Thus, radially the electron flow has a sheared flow configuration. The entire process leading to the formation of sheared electron configuration has been shown in the schematic of Fig. 1.2.

Any fluid with a sheared flow configuration is susceptible to the Kelvin - Helmholtz mode. The subsequent nonlinear phase of the instability determines the transport of the fluid. If the flow remains laminar, the friction and viscous drag would be small and remain classical. On the other hand if the flow is turbulent, the drag can be very high. One, therefore, expects the same to happen in the context of sheared flow of electrons through a plasma. However, electrons being a charged magnetized fluid, it has subtle differences with a normal hydrodynamic fluid. Some of these differences have been highlighted in recent studies. We have

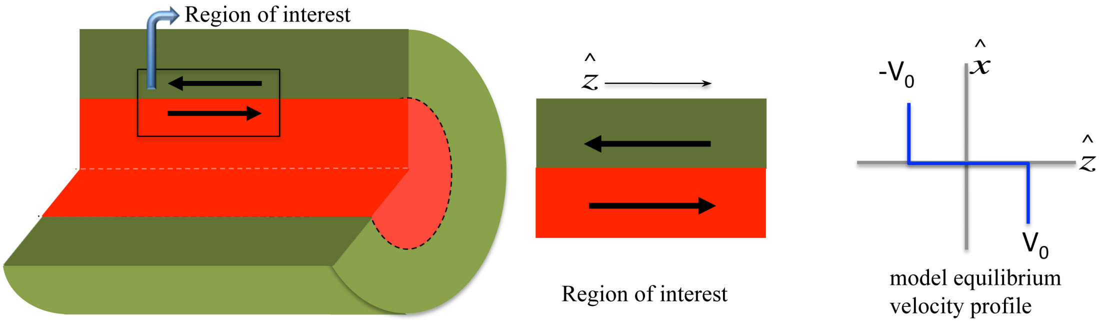

Figure 1.2: The schematic of a filament consisting of forward and reverse shielding current. This particular shear profile is modelled by a step velocity profile. For the transition layer having finite shear width, it can be modelled by tangent hyperbolic shear flow.

provided a detailed physical description and understanding of the instability in Chapter 3.

In the case of FI as well as in most circumstances of laboratory as well as astrophysical situations, the electron flow can be relativistic. The dependence of mass on velocity in the case of relativistic flow introduces a new effect in the sheared flow case. The relativistic mass now has a sheared profile in space. The growth rate and the mode structure in this case has been obtained numerically and studied extensively by us. It is observed that there are certain interesting new additional features associated with the relativistic effect on the unstable KH mode arising through the shear in the profile of the mass. These details have been presented and discussed in detail in Chapter 4 of the thesis. We have also carried out a perturbative analytical calculation for the weakly relativistic case. A comparison with the exact numerical eigen evaluation shows good agreement for the growth rate of the maximally growing mode and the threshold wavenumber in the weakly relativistic case. The details of the perturbative analytic calculation and its comparison with the exact numerical results have been provided in Chapter 5.

In the Part - II of the thesis, we investigate the possible coherent nonlinear solutions of the coupled laser plasma system. We also explore the dynamical evolution of some of these solutions. The coupled laser plasma system constitutes a strongly nonlinear system. The coherent solutions in such a system can play promising role in terms of carriers of information and energy from one point to another. It is, therefore, important to seek the parametric domain of their possible existence and also to have an idea of the time scale of their stable existence.

The coupled laser plasma system is a strongly nonlinear medium. A low intensity laser cannot penetrate an overdense region of plasma. However, at higher intensities the laser can evacuate the electrons by its ponderomotive pressure. Furthermore, at higher intensities the electrons can be driven to relativistic speeds, thereby reducing the plasma frequency and enabling the possibility of laser penetration. Thus, a pulse of high intensity laser light can get trapped in a plasma medium by creating a cavity for itself. The high intensity central region alters the property of the plasma medium, for it to survive as a propagating wave, whilst at the edges where its intensity is usually low it is unable to creep out. Usually this forms the basis of the exact coherent nonlinear solutions of the laser plasma system. A detail description of this has been carried out. Possible coherent structures in the laser frequency vs. the group velocity of the pulse structure have been identified. Chapter 6 contains the detailed description about these solutions. It is also noticed that when the ion dynamical response is altogether ignored, stable solutions with zero group velocity can be found. However, in such a scenario when the pulse is at rest, it would not be correct to ignore the ion dynamics. This is an example where the coupling to ion motion becomes important, even though the laser frequency can be pretty high to influence ion motion in any fashion. These details have been described in Chapter 6. It is observed that several new variety of solutions can be found when the ion response is incorporated. The spectrum also exhibits new features.

The dynamical evolution of a particular flat-top variety of solutions formed in the presence of ion response has also been studied numerically. It is observed that as these solutions propagate, they show initial stable propagation for several plasma periods, but ultimately disintegrate as a result of a backward Brillouin instability. Chapter 7 contains the description of the flat top solution, its dynamical evolution and the identification of the instability process.

Finally, in chapter 8 we summarize our studies and point out at the possible issues for future exploration of the work presented in the thesis.

Part I

Problem one

Chapter 2

Governing Models to describe plasma dynamics at fast electron time scales

We have adopted fluid model for our studies, which provides a simplified description of plasma evolution. In general, a two fluid description for the ion and electron species coupled with the Maxwell's set of equations govern the properties of plasma evolution. However, due to huge difference in the mass of the constituent species, electrons and ions (at least a factor of 1840) in a plasma their response time differ considerably and further simplifications are possible. In this chapter we concentrate on the simplifications that can be made when the concerning phenomena occur at a time scale at which the lighter electron species has a dominant dynamical role to play. We also illustrate the simplifications due to reduced dimensionality, non - relativistic nature and incompressible situation that may arise in different contexts.

2.1 Governing Equations for fast time scale phenomena: The most general case

At fast electron time scales, the ions are assumed to play a subsidiary role of providing a static neutralizing background. The governing equations for a relativistic electron fluid in three dimensions is then provided by the electron momentum equation

$$\frac{\partial\left(\gamma_e\vec{v}_e\right)}{\partial t}+\vec{v}_e\cdot\nabla\left(\gamma_e\vec{v}_e\right)=-\frac{e}{m_e}\left\{\vec{E}+\frac{\vec{v}_e\times\vec{B}}{c}\right\}-\frac{\nabla p_e}{m_e n_e} \tag{2.1}$$

and the electron continuity equation

$$\frac{\partial n_e}{\partial t}+\nabla\cdot\left(n_e\vec{v}_e\right)=0 \tag{2.2}$$

where e and m_e denote the charge and rest mass of electron. The number density, fluid velocity and the pressure of the electron species is denoted by n_e, $\vec{v_e}$ and p_e respectively. The evolution of electron fluid is governed by the Lorentz force which depends on the externally applied as well as the self consistent electric and magnetic field, denoted here by conventional symbols of $\vec{E}$ and $\vec{B}$ respectively. Here, $\gamma_e=1/\sqrt{1-v_e^2/c^2}$ is the relativistic factor of the electron fluid. The electron momentum equation can also be expressed alternatively in terms of the scalar potential φ and the magnetic vector potential $\vec{A}$ as

$$\frac{\partial}{\partial t}\left(m_e\gamma_e\vec{v_e}-\frac{e\vec{A}}{c}\right)=\vec{v}_e\times\nabla\times\left(m_e\gamma_e\vec{v_e}-\frac{e\vec{A}}{c}\right)+\nabla\left(e\varphi-\frac{m_e}{2}\gamma_e v_e^2\right)-\frac{\nabla p_e}{n_e} \tag{2.3}$$

The electron fluid being charged, its flow produces a current and often a charge separation, and is thus responsible for the generation of self consistent electric and magnetic field. These fields can be evaluated with the help of the Maxwell's equations. Thus the coupled set of Eqs. (2.1)-(2.2) along with the Maxwell's equations provided below describe the complete evolution of the system in this case. The Ampere's law from the Maxwell's set of equation

$$\begin{aligned} \nabla \times \vec{B} &= \frac{4\pi}{c}\vec{J} + \frac{1}{c}\frac{\partial \vec{E}}{\partial t} \\ \nabla \times \nabla \times \vec{A} &= -\frac{4\pi}{c} e n_e \vec{v}_e - \frac{1}{c}\frac{\partial}{\partial t}\left(\nabla\varphi + \frac{1}{c}\frac{\partial \vec{A}}{\partial t}\right) \end{aligned} \tag{2.4}$$

along with the Poisson's equation

$$\nabla^2 \varphi = -4\pi e(n_0 - n_e) \tag{2.5}$$

defines the model. Where n_0 and $\vec{J}$ are the background plasma density and electron current density respectively.

An important issue in all physics problems is the choice of normalizations. It is convenient and advisable to use the typical time scales pertaining to the problem under consideration for normalization purposes.

2.2 Approximations and reduced models

In section - I, we presented the most general set of evolution equations. It is still quite complicated. Depending on the specific nature of the problem several simplifications are possible. Apart from the simplifications arising due to reduced dimensionality and/or due to the non relativistic nature, there are some interesting approximations in which the above set of equations take very simplified forms. We discuss those cases, here, one by one. These equations have been adopted in the subsequent chapters of the thesis to explore a specific question.

2.2.1 EMHD

When the electron fluid flow can be considered incompressible, the evolution equations take a very simplified form as we show below. The flow can be treated as incompressible when the density perturbations of the fluid can be ignored. Thus, the electron continuity equation becomes irrelevant. This is the case, when not only the equilibrium state but also the time evolution preserves quasi - neutrality. Thus, the Poisson's equation reduces to $\nabla^2\varphi \approx 0$ and the displacement current in the Maxwell's equations can also be treated as negligible. One should in principle retain the displacement current for relativistic studies. However, under the approximation of the typical time scale concerning the system to be much slower than those of the electron plasma period, ignoring displacement current and treating the electron fluid as incompressible are reasonable. For a cold unmagnetized electron fluid, this can happen when the time scales are slower than the electron plasma period, i.e. $\omega << \omega_{pe}$. In the magnetized case, the condition is $\omega << \omega_{pe}^2/\omega_{ce}$ [19]. For a warm electron plasma this would require the electron flow to be subsonic.

Under these conditions the set of Eqs. (2.1)-(2.5) can be simplified and take the following form

$$\frac{\partial}{\partial t}(\nabla \times \vec{P}) = \nabla \times [\vec{v_e} \times (\nabla \times \vec{P})] \tag{2.6}$$

Here, $\vec{P} = \gamma_e \vec{v_e} - (e/m_e c)\vec{A}$. It should be noted that the evolution in this case can be described entirely in terms of the evolution of the magnetic field. The instantaneous magnetic field is related to the electron flow by the relationship

$$\vec{v_e} = -\frac{c}{4\pi n_e}\nabla \times \vec{B} \tag{2.7}$$

The magnetic field evolution thus provides the complete description of the system. In the reduced 2-D case, the above equations take a further simplified form. In the 2-D $x - z$ plane the EMHD equations can be expressed in terms of evolution of two scalar fields, which define the total magnetic field as $\vec{B} = b\hat{y} + \hat{y} \times \nabla\psi$. Consequently, the electron velocity can be expressed in terms of these two scalar fields as $\vec{v_e} = -\nabla \times \vec{B} = \hat{y} \times \nabla b - \hat{y}\nabla^2\psi$ [20].

$$\begin{aligned} \frac{\partial}{\partial t}(\nabla^2 b - b) + \hat{y} \times \nabla b \cdot \nabla\nabla^2 b - \hat{y} \times \nabla\psi \cdot \nabla\nabla^2\psi &= 0 \\ \frac{\partial}{\partial t}(\nabla^2\psi - \psi) + \hat{y} \times \nabla b \cdot \nabla(\nabla^2\psi - \psi) &= 0 \end{aligned} \tag{2.8}$$

Here, $\hat{y}$ denotes the symmetry direction. Eq. (2.8) has been expressed in normalized variables. Magnetic field has been normalized by a typical amplitude of B_{00}, the time by the corresponding electron gyro-period $\omega_{ce}^{-1} = (eB_{00}/m_e c)^{-1}$ and length by the electron skin depth $d_e = c/\omega_{pe}$. The Eqs. (2.13) can be further simplified when the electron flow is also confined in the 2-D plane. It is interesting to note that in the limit of $k^2 d_e^2 >> 1$, where k is the wavevector along with $\psi = 0$, reduces the coupled set of Eq. (2.8) to the Navier Stokes equations in 2-D for an incompressible neutral fluid hydrodynamics,

$$\frac{\partial}{\partial t}\nabla^2 b + \hat{y} \times \nabla b \cdot \nabla\nabla^2 b = 0 \tag{2.9}$$

here b can be identified with the velocity potential. Thus, when the scales of the phenomena under consideration become smaller and/or comparable to the electron skin depth the electron fluid behaves like a neutral hydrodynamic fluid.

This model has been extensively employed by us in Part - I of the thesis (Chapters 3-5) where we have explored various aspects of the flow shear driven Kelvin -

Helmholtz (KH) like instability in the context when the electron flow is sheared.

2.2.2 GEMHD

The EMHD model has been generalized recently to consider cases where the background plasma is inhomogeneous. In these cases if one still assumes the response to remain quasineutral (if the two conditions $\omega << \omega_{pe}$ and $\omega << \omega_{pe}^2/\omega_{ce}$ continue to be satisfied at all locations), the electron density though a function of space, can remain independent of time. The effect of inhomogeneous plasma density introduces an additional term in the governing equations, Eqs. (2.6) as now the electron velocity and the current in the medium are not related only by a constant scalar multiplier. The curl of the momentum equations for the GEMHD model in the normalized form are as follows [21]

$$\frac{\partial \vec{g}}{\partial t} = \nabla \times [\vec{v_e} \times \vec{g}] \tag{2.10}$$

where

$$\vec{v_e} = -\frac{1}{n_e}\nabla \times \vec{B}; \quad \vec{g} = \frac{\nabla^2 \vec{B}}{n_e} - \nabla\left(\frac{1}{n_e}\right) \times \left(\nabla \times \vec{B}\right) - \vec{B} \tag{2.11}$$

Normalizations introduced are same as in the previous section. The density is normalized by a typical value n_{00}. In the 2-D case, magnetic field being divergence-less, can now be expressed in terms of two scalar fields as $\vec{B} = b\hat{y} + \hat{y} \times \nabla\psi$, which in turn simplifies the Eqs. (2.10-2.11) to

$$\frac{\partial}{\partial t}\left\{b - \nabla \cdot \left(\frac{\nabla b}{n_e}\right)\right\} + \hat{y} \times \nabla b \cdot \nabla \left[\frac{1}{n_e}\left\{b - \nabla \cdot \left(\frac{\nabla b}{n_e}\right)\right\}\right] + \hat{y} \times \nabla\psi \cdot \nabla\left(\frac{\nabla^2\psi}{n_e}\right) = 0 \tag{2.12}$$

and

$$\frac{\partial}{\partial t}\left\{\psi - \frac{\nabla^2\psi}{n_e}\right\} + \frac{\hat{y}\times\nabla b}{n_e}\cdot\nabla\left\{\psi - \frac{\nabla^2\psi}{n_e}\right\} = 0 \qquad (2.13)$$

where $\hat{y}$ is the symmetry axis. Thus, b represents the magnetic field component along the symmetry direction and the magnetic field along x and z directions are $\partial\psi/\partial z$, and $-\partial\psi/\partial x$, respectively. When the flow of electron fluid is confined in the 2-D plane it takes the following form :

$$\frac{\partial}{\partial t}\left\{b - \nabla\cdot\left(\frac{\nabla b}{n_e}\right)\right\} + \hat{y}\times\nabla b\cdot\nabla\left[\frac{1}{n_e}\left\{b - \nabla\cdot\left(\frac{\nabla b}{n_e}\right)\right\}\right] \qquad (2.14)$$

When the electron plasma density n_e is constant, the above coupled set of Eqs. (2.13-2.13) reduce to the EMHD Eqs. (2.8) in 2-D.

2.2.3 Weakly relativistic case

In general, incompressibility cannot be a good approximation when the electron flow is relativistic. The flow speed being comparable to speed of light, the displacement current has to be retained. Furthermore, if the temperature is finite, the flow will always be supersonic and hence density fluctuation would be present and continuity equation would need to be retained.

Some simplification is, however, possible in the weakly relativistic case of cold electron fluid. Here, $v_e/c < 1$ and can be treated as a small parameter for expansion. In this case assuming if condition $\omega << \omega_{pe}$ holds, we can still ignore the continuity equation. We, however, retain the displacement current contribution as v_e/c is small but not negligible. In this limit, the governing equations are

$$\nabla^2 b - \mathcal{A}\sigma^2\frac{\partial^2 b}{\partial t^2} = \left(\frac{\partial v_{ex}}{\partial z} - \frac{\partial v_{ez}}{\partial x}\right) \qquad (2.15)$$

$$\frac{\partial(\xi - b)}{\partial t} + \vec{v_e} \cdot \nabla(\xi - b) = 0 \quad (2.16)$$

where v_{ex} and v_{ez} are the x and z component of the electron fluid velocity v_e. Here, $\sigma = \omega_{ce0}/\omega_{pe}$ where ω_{ce0} is the electron gyroperiod. An extra coefficient $\mathcal{A}$ is introduced to signify the contribution of displacement current. The coupled set of Eqs. (4.8-4.9) along with

$$\nabla^2 \gamma_e v_{ex} = \frac{\partial \xi}{\partial z}; \quad \nabla^2 \gamma_e v_{ez} = -\frac{\partial \xi}{\partial x} \quad (2.17)$$

can now be employed to study the electron velocity shear driven instability in the relativistic regime. Here $\xi = \nabla \times \gamma_e \vec{v}_e$. If one ignores the displacement current also, one obtains a simplified generalization of the EMHD equation for the weakly relativistic case.

$$\frac{d^2 v_{x1}}{dx^2} + 3\frac{d\left(\log \gamma_0\right)}{dx}\frac{dv_{x1}}{dx} - \left(\frac{k_z^2}{{\gamma_0}^2} + \frac{1}{{\gamma_0}^3} - \frac{k_z\left((\gamma_0 v_{z0})'' - v_{z0}\right)}{\bar{\omega}{\gamma_0}^3}\right) v_{x1} = 0 \quad (2.18)$$

This equation has been used earlier [22] to evaluate the relativistic correction of the KH growth rate for the specific case of step velocity profile.

We have considered the Eqs. (4.8)-(4.10) and Eq. (2.18) to show that a profile with finite shear width exhibits new features in the KH instability which primarily arise as the relativistic mass now has a sheared profile.

2.3 Other effects

For the study of phenomena at fast electron time scales, we wish to point out here that the ion response can be altogether ignored. However, it is not possible to do so in all cases. We cite here an example where the retention of ion response would become necessary.

In the context of light wave propagation through the plasma medium, the electron species typically has the maximal role to play. The electrons acquire a quiver velocity due to the transverse oscillating electric field associated with the light wave. Thus, the propagation of electromagnetic waves with frequencies lower than the electron plasma period completely get screened and are unable to propagate inside the plasma. The waves with higher frequency do propagate inside the plasma but with reduced group velocity. In the context of high intensity light waves, various nonlinear effects come into play and it is possible to have exact pulse like localized structures which can propagate with slow group velocity [23]. Theoretical analysis based on ignoring the ion response completely, have predicted existence of even static structures. Even though the light trapped inside such structures oscillate rapidly and would not be able to influence ion response, the ponderomotive force associated with the static structure would ultimately trigger the evolution of ions. In such cases, therefore, a coupling between ion and electron response time scales would occur and the ion response should be retained. The coupled set of fluid Maxwell's equations in such cases will have additional equations for the momentum and continuity equations of ions as follows.

$$\begin{aligned} \frac{\partial n_e}{\partial t} + \nabla \cdot (n_e \vec{v_e}) = 0 \\ \frac{\partial n_i}{\partial t} + \nabla \cdot (n_i \vec{v_i}) = 0 \end{aligned} \tag{2.19}$$

$$\begin{aligned}
\left[\frac{\partial}{\partial t} + \vec{v_e} \cdot \nabla\right] \vec{p_e} &= -e\left(\vec{E} + \frac{\vec{v_e} \times \vec{B}}{c}\right) \\
\left[\frac{\partial}{\partial t} + \vec{v_i} \cdot \nabla\right] \vec{p_i} &= e\left(\vec{E} + \frac{\vec{v_i} \times \vec{B}}{c}\right) \qquad (2.20)
\end{aligned}$$

$$\begin{aligned}
\nabla \times \vec{B} &= \frac{4\pi}{c}\vec{J} + \frac{1}{c}\frac{\partial \vec{E}}{\partial t} \\
\nabla \times \vec{E} &= -\frac{1}{c}\frac{\partial \vec{B}}{\partial t} \\
\nabla \cdot \vec{E} &= -4\pi e(n_e - n_i) \\
\nabla \cdot \vec{B} &= 0 \qquad (2.21)
\end{aligned}$$

The 1-D version of these equations have been utilized by us to seek specific coherent solutions pertaining to the coupled laser plasma system in Part - II of the thesis.

2.4 Summary

We have provided a brief description of the set of governing equations that have been employed in the thesis for studying various phenomena associated with the fast electron dynamics in plasmas.

Chapter 3

Physics of flow shear driven instabilities in EMHD

In Chapter 2 we have shown that the incompressible electron flows can be depicted by Electron - Magnetohydrodynamic (EMHD) model. This model resembles the neutral hydrodynamic fluid model in the limit when the scale lengths are comparable to or smaller than the electron skin depth. It is, therefore, suggestive that the electron flow in the limit of EMHD description will be plagued by similar instabilities that plague any hydrodynamic fluid system. One of the prominent fluid instabilities is the shear flow driven Kelvin - Helmholtz (KH) mode. The interest in the study of this particular mode has been motivated both by fundamental considerations as well as due to the relevance of this mode in the frontier Fast Ignition (FI) concept of Inertial confinement Fusion (ICF) scheme [24]. This mode has also been extensively explored [25] in the context of a sheared electron flow configuration within the framework of EMHD depiction. It has been observed that the magnetized character of the electron flow introduces certain differences. These differences along with similarities with the fluid KH mode have been pointed out in earlier studies [25].

In this chapter, we have provided a detailed physical description of the shear flow driven Kelvin - Helmholtz (KH) mode in the context of electron fluid. In particular, we have shown that the free energy source of the mode is the shear in the flow velocity and not the sheared current configuration. We have also provided an order of magnitude estimate of the growth rate purely from physical considerations associated with the release of free energy in exciting the mode. In 3-D systems, the behaviour of the mode has also been physically interpreted.

3.1 Introduction

The fast time scale phenomena occurring at electron time scales are often depicted by a simplified single electron fluid treatment of the Electron Magnetohydrodynamics (EMHD) model [19, 20, 26]. The model has been investigated for the study of electron time scale phenomena by several authors [27–32]. The model ignores the dynamical response of the heavier ion species. Ions are assumed to provide merely a neutralizing stationary background. In addition, the model does not incorporate effects related to the electron density perturbations and the displacement current contribution in the Ampere's law is also not retained. Under such simplifications, the model can be completely represented in terms of a nonlinear evolution equation for the magnetic field. The model has also been generalized to incorporate effects due to the background plasma density inhomogeneity (G-EMHD) recently [5, 21].

The EMHD model which represents the magnetized electron fluid description reduces to the neutral hydrodynamic fluid dynamics at scales shorter than the electron skin depth. Thus, the characteristic neutral fluid instabilities are present here as well, albeit with appropriate modifications due to the magnetized character of the electron fluid. In some recent works [1, 2, 21, 22, 25, 33–35], the velocity shear driven instabilities have been studied extensively in the context of the EMHD model. The mode compares closely with the Kelvin - Helmholtz mode of the neutral hydrodynamic fluid [24]. Since the shear in velocity is also associated with the current gradients in a typical scenario of EMHD phenomena, the mode has often also been identified as current gradient driven sausage and kink-like mode. In this chapter, we distinguish the two cases of current and velocity shear by choosing an inhomogeneous density plasma. Since the current is the product of velocity and density, the inclusion of density gradient can distinguish between current and velocity shear configurations. It should be noted that the equilibrium density inhomogeneity cannot relax in a cold collisionless plasma. Thus, there is no free energy available for excitation of any instability with the density inhomogeneity. The distinct cases of velocity and current shear are then analyzed with the help of G-EMHD equations Eq. (2.12)-(2.13) to show that the free energy associated with a sheared velocity configuration is necessary for the instability. The presence of current gradient without a sheared velocity configuration is unable to excite any instability. Another possible way to distinguish between the velocity and current shear driven cases is by considering an electron-positron (or a two electron fluid) system. The importance of velocity shear for instability has also been demonstrated by studying a combined electron - positron two fluid system within the EMHD formalism. On the basis of these analyses we conclude that the flow shear driven instabilities in the context of EMHD are, in fact, a modified fluid Kelvin - Helmholtz mode.

3.1.1 Flow with current shear only

We consider a neutral, cold inhomogeneous plasma with density variation along x. For the analysis pertaining to this section, we consider the electron species to be having a constant $\hat{z}$ directed flow. The electron flow along $\hat{z}$ produces a current along $\hat{z}$ and an associated magnetic field along $\hat{y}$ direction Fig. 3.1. Since

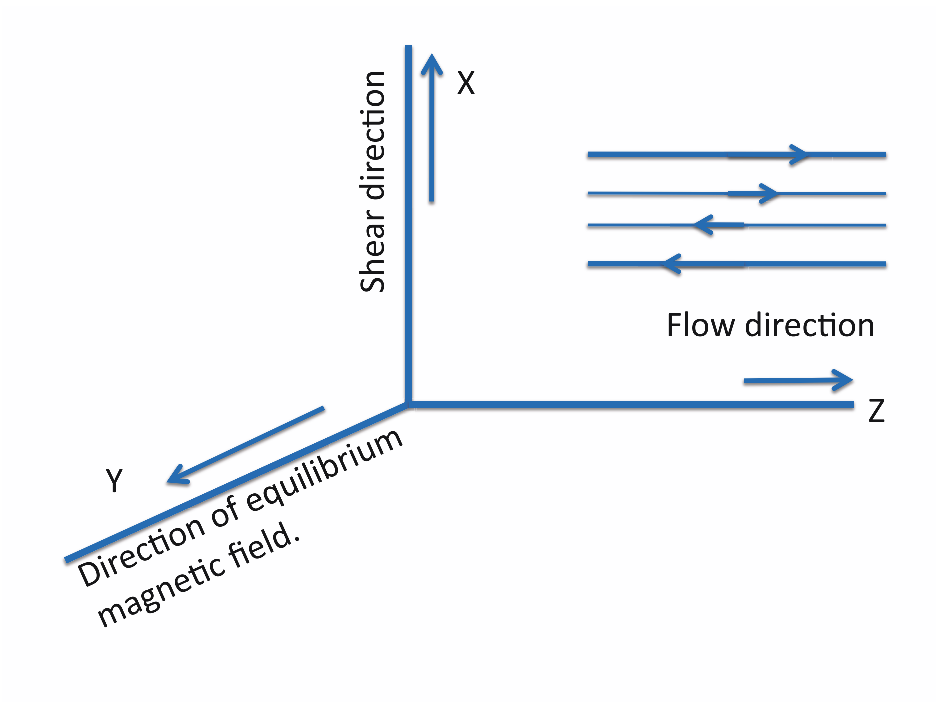

Figure 3.1: The equilibrium electron flow configuration

the plasma/electron density profile varies along x, a constant shearless $\hat{z}$ directed velocity flow produces a sheared electron current flow. We emphasize here that incorporating a density inhomogeneity in a cold collisionless plasma does not contribute towards an additional free energy source for instability to the system.

We now investigate with the aforementioned configuration, a possible excitation of the pure current shear driven instability within the EMHD formalism. We first consider a simplified case when the perturbations are confined in the 2-D $x-z$ plane of Fig. 3.1. For this particular configuration, even the perturbed magnetic field would also be directed along $\hat{y}$. Earlier studies [25] have already shown that for a homogeneous plasma, a sheared velocity (producing a sheared current configuration as well) excites unstable modes in the 2-D $x-z$ plane. Here, as stated earlier we have an inhomogeneous plasma density with variations along x, enabling shearless electron flow velocity along $\hat{z}$ producing a sheared current configuration. This system is then depicted by the 2-D G-EMHD evolution equation, Eq. (2.14) for the magnetic field component b along $\hat{y}$.

$$\frac{\partial}{\partial t}\left[b-\nabla\cdot\left(\frac{\nabla b}{n}\right)\right]+\hat{y}\times\nabla b\cdot\nabla\left[\frac{1}{n}\left\{b-\nabla\cdot\left(\frac{\nabla b}{n}\right)\right\}\right]=0 \tag{3.1}$$

The current shear along x produces an equilibrium magnetic field b_0. The equilibrium velocity along $\hat{z}$, though finite, however, has been chosen to have no dependence on x. Thus,

$$\hat{z}v_0=\frac{\hat{y}\times\nabla b_0}{n_0}=-\frac{1}{n_0}\frac{db_0}{dx}\hat{z}=const \tag{3.2}$$

Linearizing the G-EMHD equations around this equilibrium and Fourier analyzing in z and t, ($exp(ik_z z-i\omega t)$) we obtain the following differential equation with ω as the eigen value.

$$\frac{1}{n_0}\frac{d^2b_1}{dx^2}+\frac{d}{dx}\left(\frac{1}{n_0}\right)\left(\frac{db_1}{dx}\right)-\left(1+\frac{k_z^2}{n_0}\right)b_1+\frac{1}{\bar{\omega}}\frac{d}{dx}\left(\frac{b_0}{n_0}\right)k_zb_1=0 \tag{3.3}$$

Here $\bar{\omega}=\omega-k_zv_0$ and we have used the condition of the constancy of $(1/n_0)(db_0/dx)$ in our derivation. The eigen value ω decides whether or not the system is unstable for any given choice of the equilibrium profiles of b_0 and n_0. Here, for the specific choice of a shearless electron flow, the profiles of b_0 and n_0 are constrained to obey the relationship of Eq. (3.2). Multiplying Eq. (3.3) by b_1^* and integrating over x gives

$$\int \left[\frac{1}{n_0} \left| \frac{db_1}{dx} \right|^2 + \left(1 + \frac{k_z^2}{n_0}\right) | b_1 |^2 \right] dx - \frac{1}{\bar{\omega}} \int \frac{d}{dx}\left(\frac{b_0}{n_0}\right) k_z | b_1 |^2 dx = 0 \quad (3.4)$$

Here, the perturbations have been assumed to vanish at the boundaries. It should be noted that v_0 being independent of x, we could take $\bar{\omega}$ outside the integrand. Clearly, from Eq. (3.4) we have

$$\omega = k_z v_0 + \frac{\displaystyle\int_{-\infty}^{\infty} \frac{d}{dx}\left(\frac{b_0}{n_0}\right) k_z | b_1 |^2 dx}{\displaystyle\int_{-\infty}^{\infty} \left[\frac{1}{n_0} \left| \frac{db_1}{dx} \right|^2 + \left(1 + \frac{k_z^2}{n_0}\right) | b_1 |^2 \right] dx} \quad (3.5)$$

showing that ω is real. Thus, the current shear configuration in the absence of velocity shear can not be unstable to the excitation of 2-D modes in the $x - z$ plane.

We now consider perturbations in the $x - y$ plane, referred as kink geometry in earlier publications [2, 33], for the possible excitation of instability in the absence of velocity shear. In this case too, as the perturbations are confined in a 2-D plane, the EMHD evolution equations, Eq. (2.8) can be cast in terms of two scalar fields. However, in this case the equilibrium magnetic field along $\hat{y}$ lies in $x - y$ plane, which couples the two scalar fields unlike the previous case. The total magnetic field in terms of the two scalar fields can be written as $\vec{B} = \hat{z}\phi + \hat{z} \times \nabla\psi$ and the evolution equations are

$$\frac{\partial}{\partial t}\left\{\phi - \nabla \cdot \left(\frac{\nabla\phi}{n}\right)\right\} + \hat{z} \times \nabla\phi \cdot \nabla \left[\frac{1}{n}\left\{\phi - \nabla \cdot \left(\frac{\nabla\phi}{n}\right)\right\}\right]$$
$$+ \hat{z} \times \nabla\psi \cdot \nabla \left(\frac{\nabla^2\psi}{n}\right) = 0 \quad (3.6)$$

$$\frac{\partial}{\partial t}\left\{\psi - \frac{\nabla^2\psi}{n}\right\} + \frac{\hat{z}\times\nabla\phi}{n}\cdot\nabla\left\{\psi - \frac{\nabla^2\psi}{n}\right\} = 0 \tag{3.7}$$

We now linearize these equations in the presence of an equilibrium magnetic field $\hat{y}b_0 = \hat{y}d\psi_0/dx$ arising from the electron flow along $\hat{z}$. The electron flow velocity is related to the magnetic field and plasma density in the G-EMHD formalism through $\vec{v} = -\nabla\times\vec{B}/n_0$ and the current as $\vec{J} = \nabla\times\vec{B}$. As before, we choose a sheared equilibrium current flow along $\hat{z}$ but the x dependence of plasma density is chosen so as to have no shear in the flow velocity. Thus,

$$v_0 = -\frac{1}{n_0}\frac{db_0}{dx} = -\frac{1}{n_0}\frac{d^2\psi_0}{dx^2} = constant$$

Linearizing Eqs. (3.6) and (3.7) we obtain

$$\frac{\partial}{\partial t}\left\{\phi_1 - \nabla\cdot\left(\frac{\nabla\phi_1}{n_0}\right)\right\} + \hat{z}\times\nabla\psi_0\cdot\nabla\left(\frac{\nabla^2\psi_1}{n_0}\right) = 0 \tag{3.8}$$

$$\frac{\partial}{\partial t}\left\{\psi_1 - \nabla\cdot\left(\frac{\nabla\psi_1}{n_0}\right)\right\} + \frac{\hat{z}\times\nabla\phi_1}{n_0}\cdot\nabla\psi_0 = 0 \tag{3.9}$$

Fourier analyzing in y and t we obtain

$$\left(1+\frac{k_y^2}{n_0}\right)\phi_1 - \frac{d}{dx}\left(\frac{1}{n_0}\frac{d\phi_1}{dx}\right) - \frac{k_y b_0}{\omega n_0}\left(\frac{d^2\psi_1}{dx^2} - k_y^2\psi_1\right) = 0 \tag{3.10}$$

$$\left(1+\frac{k_y^2}{n_0}\right)\psi_1 - \frac{1}{n_0}\frac{d^2\psi_1}{dx^2} + \frac{k_y b_0}{\omega n_0}\phi_1 = 0 \tag{3.11}$$

Multiplying Eq. (3.10) by ϕ_1^* and Eq. (3.11) by $(k_y^2 - d^2/dx^2)\psi_1^*$ and integrating over x yields

$$\int \left\{ \left(1+\frac{k_y^2}{n_0}\right) \mid \phi_1 \mid^2 + \frac{1}{n_0} \left| \frac{d\phi_1}{dx} \right|^2 + k_y^2 \left(1+\frac{k_y^2}{n_0}\right) \mid \psi_1 \mid^2 \right.$$
$$\left. + \left| \frac{d\psi_1}{dx} \right|^2 + \frac{1}{n_0} \left| \frac{d^2\psi_1}{dx^2} \right|^2 \right\} dx$$
$$+ \frac{k_y}{\omega} \int \frac{b_0}{n_0} \left\{ k_y^2(\phi_1^*\psi_1 + \phi_1\psi_1^*) - \left(\phi_1^* \frac{d^2\psi_1}{dx^2} + \phi_1 \frac{d^2\psi_1^*}{dx^2} \right) \right\} dx = 0$$

upon summing the two equations.

In this case too, ω is real as it can be expressed as a ratio of two real integrals. Thus, there are no unstable eigen modes when the variations are confined to the $x - y$ plane. For the general 3-D perturbation, a similar energy integral equation with two terms can be constructed. In the absence of velocity shear $1/\bar{\omega} = 1/(\omega - k_z v_0)$ can be taken outside the integral. Similar arguments follow which lead to the conclusion that no unstable eigen mode exist in the absence of velocity shear.

3.1.2 Flow with velocity shear only

We now consider another example to show the relevance of free energy associated with the velocity shear to be behind the excitation of flow shear driven modes in the context of EMHD formalism. We consider an electron - positron plasma. Ions may or may not be present in this case. A sheared equilibrium flow velocity in both of these species is chosen so as to have no currents. We show that in this case, there indeed exist unstable modes.

For this system of electron positron plasma, we now obtain the governing set of equations. The curl of the momentum equation for both electron as well as positron can be expresses using Eq. (2.6) where, $\vec{P} = \vec{v} + (q/m_e c)\vec{A}$ and $q = \pm e$ for electron and positron respectively. For variations confined in the 2-D x-z plane, $\nabla \times \vec{P}$ has only $\hat{y}$ component and the equation can be written as

$$\frac{\partial}{\partial t}(\nabla \times \vec{P})_y + \vec{v} \cdot \nabla(\nabla \times \vec{P})_y = 0 \tag{3.12}$$

An equilibrium fluid flow of the form $v_0(x)\hat{z}$ is assumed (i.e. directed along $\hat{z}$ with x dependent sheared profile). We linearize the Eq. (3.12) and Fourier analyze the linear perturbations in z and t to obtain

$$\frac{d^2 v_{x1}}{dx^2} - k_z^2 v_{x1} + \frac{q}{e} i k_z b_1 - \frac{k_z}{(\omega - k_z v_0)}(\frac{q}{e} B_0' - v_0'')v_{x1} = 0 \tag{3.13}$$

We have used the same normalizations as in the previous section for Eq. (3.13). The equations for the electron and positron fluid with density n_{0e} and n_{0p} respectively and flowing with an equilibrium velocity of $v_{0e}(x)\hat{z}$ and $v_{0p}(x)\hat{z}$ can be written as

$$\frac{d^2 v_{xe}}{dx^2} - k_z^2 v_{xe} - i k_z b_1 - \frac{k_z}{(\omega - k_z v_0)}(B_0' + v_{0e}'')v_{xe} = 0 \tag{3.14}$$

$$\frac{d^2 v_{xp}}{dx^2} - k_z^2 v_{xp} + i k_z b_1 + \frac{k_z}{(\omega - k_z v_0)}(B_0' - v_{0p}'')v_{xp} = 0 \tag{3.15}$$

The current in the system is the sum of electron and positron currents, which produces a total magnetic field $B\hat{y} = (B_0 + b_1)\hat{y}$. Here, B_0 is the magnetic field due to the equilibrium current and b_1 arises from the perturbed current. From Ampere's law we have

$$dB_0/dx = B_0' = J_0 = n_{0p}v_{0p} - n_{0e}v_{0e}.$$

The perturbed flow of the two fluids is assumed to be incompressible under the approximation that time scales considered are much slower than the effective plasma frequency. The perturbed flow being in the 2-D $x - z$ plane, we have $-ik_z b_1 = n_{0p}v_{xp} - n_{0e}v_{xe}$.

The instability due to shear flow for single electron fluid cases studied earlier, had contributions from both the terms B_0' and v_0''. Also, for this case, since the current was also carried by the electron fluid, we had $v_0 = -B_0'$, the distinction between velocity and current shear could not be made. For the two fluid electron - positron system, we make a distinction between the two by choosing the total equilibrium current to be zero, i.e. $B_0' = n_{0p}v_{0p} - n_{0e}v_{0e} = 0$. The shear in velocity flow of the two fluids continues to be finite, whereas since the current is zero everywhere, the current shear is also zero for this case.

For this simplified case, we multiply Eq. (3.14) with $n_{0e}v_{xe}^*$ and Eq. (3.15) with $n_{0p}v_{xp}^*$ and integrate with respect to x to obtain

$$\begin{aligned}
&n_{0e}\int\left\{k_z^2\mid v_{xe}\mid^2+\left|\frac{dv_{xe}}{dx}\right|^2\right\}dx+n_{0p}\int\left\{k_z^2\mid v_{xp}\mid^2+\left|\frac{dv_{xp}}{dx}\right|^2\right\}dx\\
&+n_{0e}^2\int\mid v_{xe}\mid^2 dx+n_{0p}^2\int\mid v_{xp}\mid^2 dx-n_{0p}n_{0e}\int\{v_{xe}^*v_{xp}+v_{xp}^*v_{xe}\}dx\\
&+n_{0e}k_z\int\left\{\frac{v_{0e}''}{\omega_e-k_zv_0}\mid v_{xe}\mid^2\right\}dx\\
&+n_{0p}k_z\int\left\{\frac{v_{0p}''}{\omega_p-k_zv_0}\mid v_{xp}\mid^2\right\}dx=0
\end{aligned}\qquad(3.16)$$

We have eliminated b_1 in terms of v_{xp} and v_{xe} in the above derivation. The first five terms in Eq. (3.16) are real. Thus, the equation can be satisfied for an imaginary value of ω if and only if the coefficient of ω_i vanishes (where ω_i represents the imaginary part of ω). This implies

$$n_{0e}\int\frac{\mid v_{xe}\mid^2}{\mid\omega_e-k_zv_0\mid^2}v_{0e}''dx+n_{0p}\int\frac{\mid v_{xp}\mid^2}{\mid\omega_p-k_zv_0\mid^2}v_{0p}''dx=0\qquad(3.17)$$

Since, the total equilibrium current has been chosen to be zero, we have $v_{0p} = (n_{0e}/n_{0p})v_{0e}$. For the analysis, in this section, we have chosen the electron and positron densities to be homogeneous, thus $v''_{0p} = (n_{0e}/n_{0p})v''_{0e}$. Thus, the equilibrium velocity v_{0p} and its derivatives can be expressed in terms of v_{0e} and its derivatives. The condition for imaginary values of ω provided by Eq. (3.17) can then be satisfied only for those equilibrium flows which have an inflection point. It should be noted that unlike the case considered in the previous section, here $\bar{\omega}_e = \omega - k_z v_{0e}$ and $\bar{\omega}_p = \omega - k_z v_{0p}$, both are functions of x and hence cannot be taken outside the integral. This has led to a possibility that ω can have a imaginary part. This analysis, however, only provides a necessary condition for instability.

We would now show explicitly that the instability exists by evaluating the growth rate. We choose for the purpose of illustration, a simple case for which the equilibrium velocity of both electron and positron flows have a simple form of a step profile, viz. $v_{0e} = -V_0 + 2V_0\Theta(x)$, and $v_{0p} = (-V_0 + 2V_0\Theta(x))(n_{0e}/n_{0p})$. It should be noted that this choice ensures that the total equilibrium current in the system is zero. In region I $(-\infty < x \leq 0)$ and II $(0 \leq x < \infty)$ the Eqs. (3.14)-(3.15) can be separately written as :

$$\begin{aligned} &\frac{d^2 v_{eI,II}}{dx^2} - k_z^2 v_{eI,II} + n_{0p} v_{pI,II} - n_{0e} v_{eI,II} = 0 \\ &\frac{d^2 v_{pI,II}}{dx^2} - k_z^2 v_{pI,II} - n_{0p} v_{pI,II} + n_{0e} v_{eI,II} = 0 \end{aligned} \tag{3.18}$$

Eq. (3.18) is solved in the two regions separately. The growth rate is then determined by ensuring the continuity of the following functions at $x = 0$

$$f_{1e} = \bar{\omega}_e \frac{dv_{xe}}{dx} + k_z v'_{oe} v_{xe}; \qquad f_{2e} = \frac{v_{xe}}{\bar{\omega}_e}$$
$$f_{1p} = \bar{\omega}_p \frac{dv_{xp}}{dx} + k_z v'_{op} v_{xp}; \qquad f_{2p} = \frac{v_{xp}}{\bar{\omega}_p} \tag{3.19}$$

We choose $v_{e,p}$ as $\sim exp(px)$ to solve the homogeneous coupled set given by Eq. (3.18). This yields the following equation for p

$$p^4 - (2k_z^2 + n_{0e} + n_{0p})p^2 + (k_z^2 + n_{0e})(k_z^2 + n_{0p}) - n_{0p}n_{0e} = 0$$

The double quadratic equation for p is solved leading to ${p_+}^2 = k_z^2 + n_{0e} + n_{0p}$ and ${p_-}^2 = k_z^2$, corresponding to the $\pm$ sign of the two solutions of p^2. Defining ${q_\pm}^2 = (k_z^2 + n_{0e} - p_\pm)/n_{0p}$ we obtain ${q_+}^2 = -1$, and ${q_-}^2 = n_{0e}/n_{0p}$. Since the solution should vanish at $\pm\infty$, we make the following choices for the solutions in the two regions:

$$v_{eI} = Aexp(p_+x) + Bexp(p_-x),$$

$$v_{pI} = {q_+}^2 Aexp(p_+x) + {q_-}^2 Bexp(p_-x),$$

$$v_{eII} = Cexp(-p_+x) + Dexp(-p_-x),$$

$$v_{pII} = {q_+}^2 Cexp(-p_+x) + {q_-}^2 Dexp(-p_-x).$$

Now, utilizing the matching conditions of Eq. (3.19) and eliminating the coefficients, we obtain the dispersion relation as $det||M|| = 0$, where the matrix M is defined as follows

$$\begin{vmatrix} 1/\Omega_+ & 1/\Omega_+ & -1/\Omega_- & -1/\Omega_- \\ -1/\Omega_{s+} & \sigma/\Omega_{s-} & 1/\Omega_{s-} & -\sigma/\Omega_{s-} \\ \Omega_+ p_+ & \Omega_+ p_- & p_+\Omega_- & \Omega_- p_- \\ -p_+\Omega_{s+} & \sigma p_-\Omega_{s+} & -\Omega_{s-}p_+ & \sigma p_-\Omega_{s-} \end{vmatrix}$$

Here, $\Omega_{s\pm} = \omega \pm \sigma k_z v_{0e}$, $\quad \Omega_\pm = \omega \pm k_z V_0$ and $\sigma = n_{0e}/n_{0p}$.

Now, $det||M|| = 0$ gives

$$\omega^2 = [k_z^2 v_{0e}^2/(2(1+\sigma)^2 p_- p_+)][-(\sigma(\sigma-1)^2(p_+^2+p_-^2)+(\sigma^4+6\sigma^2+1)p_+p_-) \\ \pm\{(\sigma(\sigma-1)^2(p_+^2+p_-^2)+(\sigma^4+6\sigma^2+1)p_+p_-)^2-(2\sigma(1+\sigma)p_+p_-)^2\}^{1/2}]. \tag{3.20}$$

For the particular case of $n_{0e} = n_{0p} = 1$, we have $v_{0e} = v_{0p}$ and $\omega^2 = -k_z^2 v_{0e}^2$. This exhibits that the mode is purely growing despite the fact that the plasma is currentless. It clearly shows that the mode is driven by the velocity shear. Furthermore, it needs to be emphasized here that the growth rate in this particular currentless case is identical to that of the velocity shear driven Kelvin - Helmholtz instability, for a step velocity shear profile of a neutral hydrodynamic fluid. Thus, in the absence of current, the mode is the pure Kelvin-Helmholtz mode. It should be noted that for the EMHD case with current, the growth rate $\gamma = k_z V_0\sqrt{(1+4k_z^2)/(3+4k_z^2)}$. The factor inside the square root appearing for this case arises due to the fact that the electron current influences the instability but is not responsible for it.

3.2 Free energy for flow shear driven instability in EMHD

We have shown that the flow shear driven modes can be excited within the EMHD formalism only if the free energy source is available in velocity shear. The presence of current shear alone is not sufficient to excite the instability. This can be understood from the physical grounds also. An electron fluid moving with a constant velocity (contributing to the current) can always be transformed to a frame in which it is at rest. In this frame, there is no free energy source available with the electron fluid. Such a frame transformation leads to the motion of background ions in the opposite direction, which is now responsible for current flow in this frame. However, since the ions do not have any dynamical role within the EMHD formalism, there is no mechanism by which any energy can be tapped from the ion fluid. This clearly shows that there can be no instability in the absence of velocity shear.

We now look at some other interesting aspects of this instability using physical arguments based on the availability of free energy from velocity shear. In Fig. 3.2, we show a surface plot of the growth rate for the typical case of a single electron fluid with tangent hyperbolic velocity profile (considered in a number of previous studies) as a function of k_z and k_y.

As specified earlier, the equilibrium flow is along $\hat{z}$ and is sheared along the $\hat{x}$ direction. Some characteristic features of the instability are that the unstable wavenumber along the flow direction $\hat{z}$ has a threshold $k_{zth} \leq 1/\epsilon$ (where ϵ is the width of the velocity shear layer). Thus, the unstable perturbations with

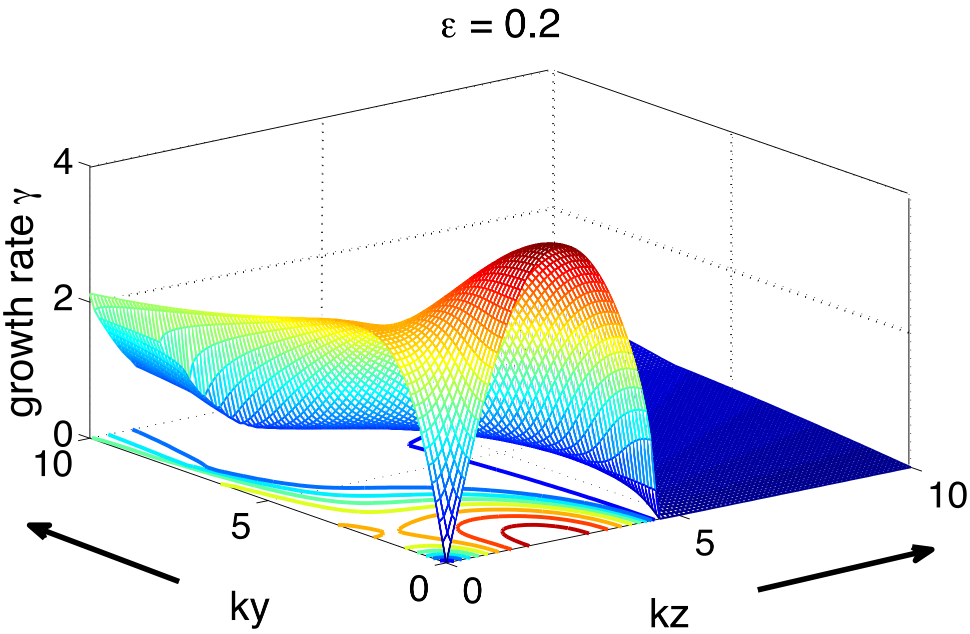

Figure 3.2: A surface and contour plot of the growth rate for the velocity shear driven mode in the $k_y - k_z$ plane. The equilibrium velocity profile chosen as $v_0 = V_0 tanh(x/\epsilon)$. Here, $\epsilon = 0.2$ is the shear width in units of electron skin depth.

variations confined in the flow - shear plane ($x - z$ plane), have a non - local character. However, this is not so for those perturbations which have variations in the $x-y$ plane. The growth rate here too shows a maxima at some k_y but extends far beyond $1/\epsilon$. These observations have been noted in earlier studies [2]. Here, we try to provide a physical understanding of these features.

When the variations of the perturbations are confined to the $x - z$ plane the equilibrium flow lines along $\hat{z}$ have to bend along $\hat{x}$ as shown in Fig. 3.3. The unstable eigen mode structure resembles a sheared flow, orthogonal to the original flow direction as illustrated in Fig. 3.3. The shear scale length of the eigen mode structure is of the order of k_z^{-1}. Since the free energy for the instability is provided by the sheared flow configuration, the unstable eigen functions themselves cannot have scales sharper than shear scale, ϵ. This is responsible for the threshold on the wavenumber k_z. On the other hand, when the variations of the perturbations are confined in the $x-y$ plane, the flow lines do not have to bend, but they merely get shuffled around as shown in Fig. 3.3. It can be seen that in this case much sharper scales along $\hat{y}$ can be generated which hardly cost any kinetic energy. In EMHD, however, the equilibrium magnetic field lines are along $\hat{y}$. Thus, for this particular case of finite k_y the magnetic field lines have to bend. The predominant energy expenditure in this case is thus for the creation of magnetic energy associated with field line bending. As it is well known in EMHD, the magnetic energy associated with any mode is down by a factor of k^2 as compared to the kinetic energy. The energy requirement for unstable modes with $x-y$ variation being predominantly magnetic is much less at higher k_y than at a corresponding high value of k_z. This explains the extended range of k_y in comparison to k_z for instability.

The typical value of the growth rate being of the $\mathcal{O}(k_z V_0)$ can also be understood from energetics of the unstable mode. It has been observed in simulations that the original equilibrium shear width of ϵ as a result of the instability, typically gets broadened and saturates at an effective value of the shear width $\epsilon_{eff} = 1/k_z$. For simplicity, we represent the original equilibrium velocity flow profile within the shear layer as $v_i(x) = V_0 x/\epsilon$ and the final relaxed profile as $v_f(x) = V_0 x/\epsilon_{eff}$. The longitudinal kinetic energy that gets released due to this change is

$$\begin{aligned} \Delta K.E. &= \frac{V_0^2}{\epsilon_{eff}} \int_0^{\epsilon_{eff}} \left\{ \frac{x^2}{\epsilon^2} - \frac{x^2}{\epsilon_{eff}^2} \right\} dx \\ &= V_0^2 \left\{ \frac{1}{\epsilon^2} - \frac{1}{\epsilon_{eff}^2} \right\} \frac{\epsilon_{eff}^2}{3} \approx \frac{V_0^2}{k_z^2 \epsilon^2} \end{aligned} \tag{3.21}$$

We have replaced ϵ_{eff} by $1/k_z$ and approximated $\epsilon_{eff} >> \epsilon$ for writing the last expression in the Eq. (3.21). This kinetic energy would be released due to the re-

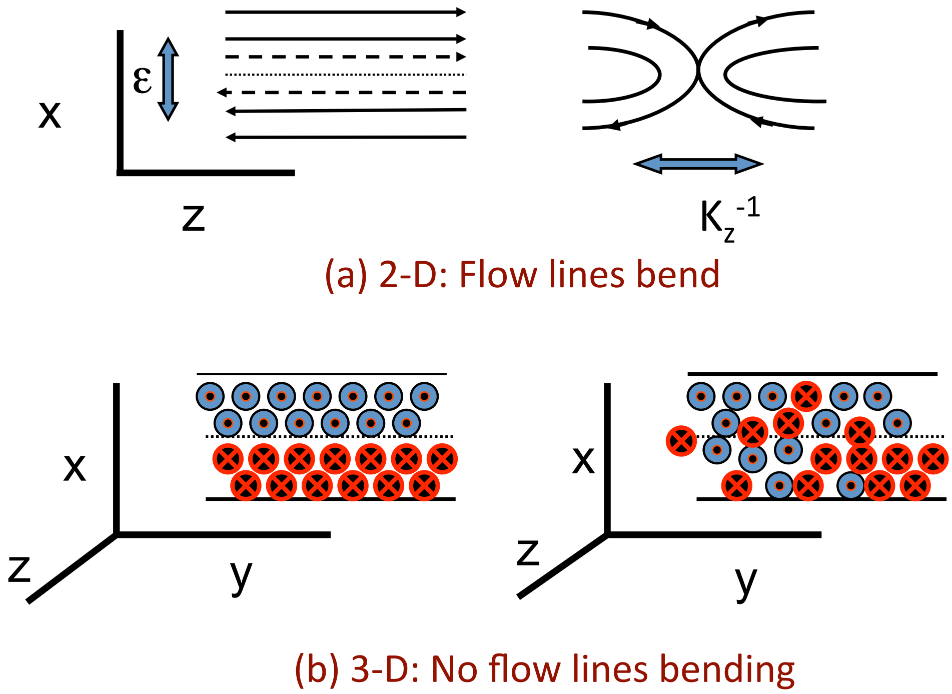

Figure 3.3: (a) A schematic showing the flow configuration after KH destabilization in 2-D. It can be seen that the destabilized flow configuration results in a sheared flow orthogonal to the original shear flow, with a shear width given by k_z^{-1}. (b) For perturbation scales along the third $\hat{y}$ direction, the flow lines do not have to bend. They merely get shuffled around to generate short scales along $\hat{y}$.

arrangement in the velocity configuration resulting from the instability. The fluid due to the KH mode attains a transverse velocity in the $\hat{x}$ direction. This velocity would be of the order of $\sim \omega\epsilon_{eff}$ (as ϵ_{eff} is distance covered in a typical time scale of the mode). Here, ω is the typical time scale associated with the growing mode. A symmetric profile for which we have estimated ΔKE, the mode is purely growing and hence $\omega \sim \gamma$ represents the growth rate. The kinetic energy required for this transverse motion ought to be less than the kinetic energy released from the original flow along $\hat{z}$ estimated in Eq. (3.21). Thus, we have

$$\omega^2 \epsilon_{eff}^2 = \frac{\omega^2}{k_z^2} \leq \frac{V_0^2}{k_z^2 \epsilon^2}$$

Since $k_z \epsilon \leq 1$, for instability we obtain $\omega \leq k_z V_0$. In fact, the growth rate for a step profile is $k_z V_0$ and for a finite shear width (e.g. piecewise linear and/or tangent hyperbolic), the maximum growth rate is always less than this value. The typical estimate for growth rate is thus $\mathcal{O}(k_z V_0)$.

3.3 Summary

We have discussed various aspects of the free energy source for the flow shear driven instability in the context of Electron - Magnetohydrodynamic (EMHD) system, which is a fluid depiction of fast electron time scale phenomena in plasma. The EMHD model resembles closely the neutral hydrodynamic fluid system and hence the characteristic neutral fluid instabilities are present here as well, albeit with appropriate modifications due to the magnetized character of the electron fluid.

One of the prominent fluid instability namely the Kelvin - Helmholtz mode driven by the velocity shear has been studied in great detail recently. In the context of EMHD, however, the flow of electrons is solely responsible for the current in the medium (the heavier ion species merely provides a neutralizing stationary background at fast time scales). Since, the shear in electron flow also corresponds to a sheared current configuration, the electron flow shear instability has often been characterized as both the velocity shear driven KH like mode as well as the current gradient driven sausage and/or kink like modes [1, 2, 22, 25, 33]. We studied two cases to distinguish between the current and velocity shear equilibrium configurations to show that the free energy source for the flow shear driven instability is essentially the kinetic energy of the electron flow.

The G-EMHD model equations [5, 21] are used for the evolution of an inhomogeneous density plasma. The density inhomogeneity distinguishes between the current and velocity shear configurations. It should be noted that under the cold plasma approximation, the presence of density inhomogeneity does not add any new free energy source. The analysis then clearly shows that there is no instability in the absence of velocity shear. We also use a sheared two fluid uni-directional electron - positron (or oppositely directed two electron fluids) to illustrate that even in the absence of any current (and consequently any current shear) the sheared velocity flow excites a KH-like mode. The instability is thus a fluid KH mode and not a sausage or kink like mode. Furthermore, in recent publications [1, 2, 22, 35] it has been shown that as shear width of the flow is made broader in comparison to electron skin depth, thereby reducing the role of electron inertia related terms, the growth rate of the instability diminishes. This also demonstrates that the electron inertia plays a crucial role for the instability. The free energy for the instability is essentially the kinetic energy of the electron sheared flow. The role of the kinetic energy as the free energy source for the instability has been explicitly demonstrated by us in previous section where the typical estimate of the growth rate of the mode is evaluated from kinetic energy released during the course of the instability. A couple of other characteristic features (e.g. existence of a threshold wavenumber along the flow direction but excitation of sharper scales in the direction normal to both shear and flow directions) associated with the instability have also been interpreted using physical considerations.

In this chapter, we have discussed the various aspects of flow shear driven KH-like instability using EMHD model for non-relativistic flows. But in many physical experiments like Fast-Ignition(FI) concept of inertial fusion, the flow velocity is often relativistic. It would be pertinent to study the KH-like flow shear driven instability for relativistic flows. So, to supplement this study, in the next chapter, we have incorporated relativistic effects. There, we will see the role of relativity on the flow shear driven instability within the purview of EMHD model.

Chapter 4

Electron Velocity Shear Driven Instability in Relativistic Regime

The electron flow in laboratory as well as astrophysical situations can often be relativistic. The present chapter discusses the role of relativity on the shear flow driven instability associated with the electron fluids. Both cases of weak and strong relativistic regime have been explored. It is observed that when the flow is weakly relativistic the growth rate diminishes and the domain of the unstable wave number also shrinks. However, when the flow is strongly relativistic additional features emerge. The growth rate as a function of wave number is no longer a single humped curve but additional peaks emerge. The unstable domain of wave numbers gets broader and can even exceed the threshold wave vector domain of the non-relativistic case. The difference between the weak and strong relativistic behaviour has been interpreted as an effect due to shear flow influencing the relativistic mass factor of the fluid.

4.1 Introduction

The sheared electron flow configuration occurs in a variety of contexts such as astrophysical jets, laser plasma interaction experiments, fast ignition studies, etc. The electron velocity in these situations is often in the Relativistic regime. It is, therefore, important to understand the role of relativistic effects on the electron velocity shear driven instability. The flow of lighter electron species being of main concern in these cases, the dynamical response of heavier ion species is negligible and can be ignored. The ions are, therefore, treated as merely a stationary neutralizing background. The fluid Electron Magnetohydrodynamics (EMHD) model [19–21, 26, 29–32, 34, 35], therefore, seems an appropriate framework for the study of these phenomena. As we have already discussed in Chapter 2 and Chapter 3, the EMHD model ignores the displacement current contribution in the Ampere's law and provides description for non-relativistic incompressible electron flows [19–21, 26, 29–32, 34, 35]. The generalization of the model for weakly relativistic flows (where ignoring displacement current continues to be a good approximation) has been made earlier [22]. However, with the advent of high power femtosecond lasers, plasma can be triggered to respond at very fast time scales with its electron component in *strongly* relativistic regime. In this strongly relativistic regime, ignoring displacement current can no longer be considered a good approximation. This chapter discusses the extension of the EMHD model to a strongly relativistic regime. In the limiting case when the phenomenon under consideration is slower than the electron plasma period (e.g. very dense plasmas), the electron density perturbations can be ignored and the relativistic electron fluid can still be considered as an incompressible fluid. The response of the electron fluid in this limit is purely electromagnetic. We concentrate in this particular regime to analyze the behaviour of the electron velocity shear driven modes.

The influence of relativistic effects on the flow shear driven Kelvin - Helmholtz (KH) instability [24] has been studied by Bodo *et al.* [36] in the context of compressible neutral hydrodynamic fluid. The characteristic features of the linear instability for an abrupt step function velocity profile were delineated for various Mach numbers and the inclination of the wave number with respect to the flow direction, in the study by Bodo *et al.* [36]. The KH like instability for the magnetized electron fluid has been investigated in the non-relativistic limit in considerable detail in some recent studies [25, 33, 35]. It was observed that the magnetized character of the electron fluid makes it somewhat distinct from the hydrodynamic KH mode. There have been suggestions lately [5, 33, 37] that this instability might have an important role in the context of the propagation of energetic electrons in the ignition phase of Fast Ignition (FI) experiments [3, 6, 38]. The electron in such experiments being strongly relativistic, it is necessary to study the role of relativity on the growth of the mode. Such a study would also have relevance in some astrophysical contexts, where one often encounters a strongly relativistic sheared electron flow (e.g. astrophysical electron jets, etc.). It is, therefore, of importance to study the influence of relativistic motion on the shear driven mode for electron fluids. Present chapter aims at this objective.

An important observation gleaned from these studies is that the role of displacement current is negligible in the present incompressible limit. Our studies also show that the growth rate for the relativistic case for an abrupt step function velocity differs only slightly from the non - relativistic expression. Thus, the typical estimates of growth rate in a relativistic situation, when evaluated from a simplified non relativistic expression, produce only a small deviation. The relativistic effect, however, manifests as extended unstable wave number domain, for gradually varying realistic velocity profiles in the strongly relativistic regime. In this case (unlike the conventional KH instability), the threshold wave number along the flow direction, is no longer constrained by the inverse of the shear width of the velocity profile [1, 2, 35]. Also, the mode no longer remains a purely growing mode, instead it acquires a real frequency even for an antisymmetric (e.g. tangent hyperbolic) shear velocity profile. The appearance of these new features have been understood by realizing that the presence of shear in the velocity, also produces a shear in the relativistic mass factor, γ_0. The shear in the relativistic mass factor is sharper (due to its nonlinear dependence on velocity) in the strongly relativistic regime and is responsible for the expanded domain of the unstable wave numbers. Furthermore, it has been shown that for this case, the Rayleigh criteria of instability can be satisfied even when the wave function is not localized symmetrically about the velocity null point. This produces a Doppler shifted real frequency.

4.2 Governing Equations

The electron time scale phenomena in relativistic regime can be described by the coupled set of Maxwell's and the relativistic electron fluid equations. We restrict to the case where the electron fluid is either cold or it has a non - relativistic temperature. The set of Eqs. (2.1)-(2.5) discussed in Chapter 2, describe the most general set of governing equations. We now seek simplified limits of this set. We consider the variations to be confined in the 2-D $x - z$ plane. The $\hat{y}$

axis represents the symmetry direction. The ion species of the plasma forms a stationary neutralizing background of homogeneous density at the time scales of interest. The electron flow velocity (both equilibrium and the perturbed) and consequently the associated current is assumed to lie in the 2-D, $x-z$ plane. For this simplified case, the magnetic field component along the symmetry axis $\hat{y}$ is the only relevant component. Thus, we choose to represent the magnetic field in terms of a single scalar field $\vec{B}=b\hat{y}$. Similarly, the relativistic fluid vorticity $\nabla\times\gamma_e\vec{v}_e$ in this case has only one scalar component directed along the symmetry axis $\xi\hat{y}$. In the Ampere's law, due to the existence of displacement current, one is not able to express the electron velocity directly in terms of magnetic field here, as is done in the context of conventional non-relativistic EMHD model. Taking the $\hat{y}$ component of the curl of Eqs. (2.3)-(2.4) yield the following equations for the fields ξ and b respectively:

$$\begin{aligned}\left\{\frac{\partial}{\partial t}+\vec{v}_e\cdot\nabla\right\}\left(m\xi-\frac{e}{c}b\right) &= -\left(m\xi-\frac{e}{c}b\right)\nabla\cdot\vec{v}_e \\ &- \left\{\frac{\partial}{\partial z}\left(\frac{1}{n_e}\frac{\partial p_e}{\partial x}\right)-\frac{\partial}{\partial x}\left(\frac{1}{n_e}\frac{\partial p_e}{\partial z}\right)\right\}\end{aligned}\tag{4.1}$$

$$\frac{1}{c^2}\frac{\partial^2 b}{\partial t^2}-\nabla^2 b=-\frac{4\pi e}{c}\left\{n_e\left(\frac{\partial v_{xe}}{\partial z}-\frac{\partial v_{ze}}{\partial x}\right)+v_{xe}\frac{\partial n_e}{\partial z}-v_{ze}\frac{\partial n_e}{\partial x}\right\}\tag{4.2}$$

The divergence of the electron momentum equation yields the following equation for $\chi=\nabla\cdot\gamma_e\vec{v}_e$

$$\begin{aligned}m\left\{\frac{\partial\chi}{\partial t}+\vec{v}_e\cdot\nabla\chi\right\} &= \frac{e}{c}\left\{\frac{\partial}{\partial x}(v_{ze}b)-\frac{\partial}{\partial z}(v_{xe}b)\right\}+e\nabla^2\varphi-\nabla\cdot\left(\frac{\nabla p_e}{n_e}\right) \\ -m&\left\{\frac{\partial v_{xe}}{\partial x}\frac{\partial\gamma_e v_{xe}}{\partial x}+\frac{\partial v_{ze}}{\partial x}\frac{\partial\gamma_e v_{xe}}{\partial z}+\frac{\partial v_{xe}}{\partial z}\frac{\partial\gamma_e v_{ze}}{\partial x}+\frac{\partial v_{ze}}{\partial z}\frac{\partial\gamma_e v_{ze}}{\partial z}\right\}\end{aligned}\tag{4.3}$$

The evolution of fields n_e, ξ, b and χ through Eqs. (2.5),(4.1)-(4.3) represent a complete and a consistent set of coupled equations for analysis under the condition of (i) stationary neutralizing ions (ii) two dimensionality, and (iii) absence of in-plane magnetic field component. The other fields φ, v_{xe} and v_{ze} can be determined from Poisson's equation along with

$$\nabla^2 \gamma_e v_{xe} = \partial\chi/\partial x + \partial\xi/\partial z$$
$$\nabla^2 \gamma_e v_{ze} = \partial\chi/\partial z - \partial\xi/\partial x. \tag{4.4}$$

The various constants π, e, c etc., from Eqs. (4.1)-(4.3) can be absorbed by appropriate normalization. We choose to normalize the magnetic field by a typical amplitude B_{00}, time by the gyroperiod $\omega_{ce0}{}^{-1}$ corresponding to B_{00} and length by the electron skin depth $d_e = c/\omega_{pe}$ (where $\omega_{pe}^2 = 4\pi n_{0e} e^2/m$). The normalized equations can then be written as

$$\nabla^2 b - \sigma^2 \frac{\partial^2 b}{\partial t^2} = \left\{ n_e \left(\frac{\partial v_{xe}}{\partial z} - \frac{\partial v_{ze}}{\partial x} \right) + v_{xe} \frac{\partial n_e}{\partial z} - v_{ze} \frac{\partial n_e}{\partial x} \right\} \tag{4.5}$$

$$\frac{\partial(\xi - b)}{\partial t} + \vec{v_e} \cdot \nabla(\xi - b) = -(\xi - b)(\nabla \cdot \vec{v}_e) \tag{4.6}$$

$$\begin{aligned} &\frac{\partial\chi}{\partial t} + \vec{v}_e \cdot \nabla\chi = \sigma^2(n_e - 1) + \frac{\partial(b v_{ze})}{\partial x} - \frac{\partial(b v_{xe})}{\partial z} - \nabla^2 p_e \\ &- \left[\frac{\partial v_{xe}}{\partial x}\frac{\partial \gamma_e v_{xe}}{\partial x} + \frac{\partial v_{ze}}{\partial z}\frac{\partial \gamma_e v_{ze}}{\partial z} + \frac{\partial v_{xe}}{\partial z}\frac{\partial \gamma_e v_{ze}}{\partial x} + \frac{\partial v_{ze}}{\partial x}\frac{\partial \gamma_e v_{xe}}{\partial z} \right]. \end{aligned} \tag{4.7}$$

We have eliminated φ from Eq. (4.7) by using Poisson's equation, Eq. (2.5). The continuity equation for density remains unaltered. The symbol $\sigma = \omega_{ce0}/\omega_{pe}$ and $\gamma_e = 1/\sqrt{1 - \sigma^2 v_e^2}$. It is clear that the inclusion of effects related to the displacement current has complicated the governing equations considerably in comparison to the conventional EMHD model. While the EMHD equations under identical conditions of 2-D variation and the absence of electron flow along symmetry direction can be expressed solely in terms of one field (namely the magnetic field component along the symmetry direction b), here, on the other hand one has to consider the evolution of four fields (b, n_e, ξ and χ). Moreover, Eq. (4.5) contains second derivative with respect to time.

We now seek possible limits in which further simplifications are possible. Considering a pure electromagnetic mode in a homogeneous plasma, one can ignore electron density perturbations under the approximation of $\omega < \omega_{pe}$. This corresponds to incompressible flows for which $\nabla \cdot \vec{v}_e$ should also be zero. The displacement current contribution continues to be present through the $\partial^2 b/\partial t^2$ term in Eq. (4.5). This is, thus, a case when $\nabla \times \vec{v}_e$ is more prominent than the $\nabla \cdot \vec{v}_e$. The simplified equations in this limit can thus be written as

$$\nabla^2 b - \mathcal{A}\sigma^2 \frac{\partial^2 b}{\partial t^2} = \left(\frac{\partial v_{xe}}{\partial z} - \frac{\partial v_{ze}}{\partial x} \right) \tag{4.8}$$

$$\frac{\partial(\xi - b)}{\partial t} + \vec{v} \cdot \nabla(\xi - b) = 0 \tag{4.9}$$

The coupled set of Eqs. (4.8)-(4.9) along with

$$\nabla^2 \gamma_e v_{xe} = \frac{\partial \xi}{\partial z}; \quad \nabla^2 \gamma_e v_{ze} = -\frac{\partial \xi}{\partial x} \tag{4.10}$$

to determine the velocity, would be employed to study the electron velocity shear driven instability in the relativistic regime. It should be noted that we have added an extra coefficient $\mathcal{A}$ in the L.H.S. of the second term of Eq. (4.8). Two cases $\mathcal{A} = 0$ and $\mathcal{A} = 1$ would be considered to identify the role of displacement current term. Choosing $\mathcal{A} = 0$, the contribution of the displacement current gets ignored. In the next section, we obtain the linearized equations for a sheared relativistic electron velocity flow equilibrium.

4.3 Linearized Equations

We consider an electron flow $v_{0z}(x)\hat{z}$, which is directed along the $\hat{z}$ axis and has a sheared profile along x as the equilibrium. This equilibrium flow produces an equilibrium vorticity $\xi_0\hat{y} = -(\partial(\gamma_0 v_{z0})/\partial x)\hat{y}$. The linearized equations around this equilibrium can then be written as

$$\mathcal{A}\sigma^2\frac{\partial^2 b_1}{\partial t^2} - \frac{\partial^2 b_1}{\partial x^2} - \frac{\partial^2 b_1}{\partial z^2} = \left(\frac{\partial v_{z1}}{\partial x} - \frac{\partial v_{x1}}{\partial z}\right) \tag{4.11}$$

$$\frac{\partial(\xi_1 - b_1)}{\partial t} + v_{z0}\frac{\partial(\xi_1 - b_1)}{\partial z} + v_{x1}\frac{\partial(\xi_0 - b_0)}{\partial x} = 0 \tag{4.12}$$

Expressing ξ_1 in terms of v_{x1} and taking Fourier Transform of Eqs. (4.11)-(4.12) along $\hat{z}$ and time we obtain

$$\begin{aligned} -\mathcal{A}\omega^2\sigma^2 b_1 - \frac{d^2 b_1}{dx^2} &= -k_z^2 b_1 + \frac{i}{k_z}\left[\frac{d^2 v_{x1}}{dx^2} - k_z^2 v_{x1}\right] \\ (\bar{\omega})\left[{\gamma_0}^3\frac{d^2 v_{x1}}{dx^2} - k_z^2\gamma_0 v_{x1} - ik_z b_1 + 3{\gamma_0}^5\sigma^2 v_{z0}v_{z0}^{'}\frac{dv_{x1}}{dx}\right] & \\ +k_z\left[(\gamma_0 v_{z0})^{''} - v_{z0}\right] v_{x1} &= 0 \end{aligned} \tag{4.13}$$

where $\bar{\omega} = \omega - k_z v_{z0}$. For $\mathcal{A} = 0$, the equations reduce to the previous case of pure EMHD studies for linear shear flow instability in 2-D. It can be shown from Eq. (4.13) that for a step velocity profile, following four functions f_1,f_2,f_3, and f_4

should be continuous at the boundary separating different regions of flow velocity:

$$\begin{aligned}
f_1 &= b_1' + \frac{iv_{x1}'}{k_z} \\
f_2 &= b_1 + i\frac{v_{x1}}{k_z} \\
f_3 &= {\gamma_0}^3(\bar{\omega}v_{x1}' + k_z v_{z0}' v_{x1}) \\
f_4 &= \frac{v_{x1}}{\bar{\omega}}
\end{aligned} \tag{4.14}$$

Thus, while obtaining the eigen functions, one must ensure the continuity of these functions.

4.4 Step profile

We consider, in this section, the simplest step velocity profile to study the role of relativistic effects on the growth rate of shear driven modes. The step velocity profile corresponds to two adjoining regions of oppositely streaming electrons. In Region I ($-\infty < x < 0$), the electron flow velocity $v_{z0}(x)\hat{z} = -V_0$ and in Region II ($0 < x < \infty$), the flow velocity is chosen as $v_{z0}(x)\hat{z} = V_0$. In the two regions, the equations can then be written separately as

$$\begin{aligned}
\frac{d^2 b_{I,II}}{dx^2} + \alpha_{I,II} b_{I,II} + \beta_{I,II} v_{xI,II} &= 0 \\
\frac{d^2 v_{xI,II}}{dx^2} + \mu_{I,II} b_{I,II} + \delta_{I,II} v_{xI,II} &= 0
\end{aligned} \tag{4.15}$$

with the coefficients α_r, β_r, γ_r, and δ_r (the suffix r stands for the two regions) as constants (independent of x) defined as follows

$$\alpha_{I,II} = \left(\mathcal{A}\omega^2\sigma^2 - k_z^2 - 1/{\gamma_0}^3\right), \qquad \beta_{I,II} = \mp(iV_0)/{\gamma_0}^3\Omega_{\pm} + ik_z/{\gamma_0}^2 - ik_z$$

$$\delta_{I,II} = \left(-k_z^2/{\gamma_0}^2 \pm k_z V_0/{\gamma_0}^3\Omega_\pm\right), \qquad \mu_{I,II} = -ik_z/{\gamma_0}^3$$

Here, $\Omega_\pm = \omega \pm k_z V_0$. The coupled set defined by Eq. (4.15) can be solved assuming the form $\sim exp(p_r x)$ for the solution.

$$\begin{aligned}\left(p_r^2 + \alpha_r\right) b_r + \beta_r v_{xr} &= 0 \\ \left(p_r^2 + \delta_r\right) v_{xr} + \mu_r b_r &= 0\end{aligned} \tag{4.16}$$

which gives, $p_r^2 = (1/2)\left[-\left(\alpha_r + \delta_r\right) \pm \sqrt{\left(\alpha_r - \delta_r\right)^2 + 4\beta_r\mu_r}\right]$. Thus, there are two roots each for p_I^2 and p_{II}^2 corresponding to the $\pm$ sign before the square root. Upon substituting for $\alpha_{I,II}$, $\beta_{I,II}$, $\mu_{I,II}$, and $\delta_{I,II}$ we obtain the expression for the roots as

$$p_{I\pm}^2 = \pm\frac{1}{2}\left\{\left(\mathcal{A}\omega^2\sigma^2 - \left(\frac{\omega + 2k_zV_0}{\Omega_+{\gamma_0}^3}\right) - {k_z}^2{v_{z0}}^2\right)^2 + \frac{4{k_z}^2}{{\gamma_0}^6}\left(\gamma_0 - {\gamma_0}^3 - \frac{v_{z0}}{k_z\Omega_+}\right)\right\}^{1/2}$$
$$+\left\{k_z^2\left(1 - \frac{{v_{z0}}^2}{2}\right) + \frac{\omega}{2{\gamma_0}^3\Omega_+} - \frac{\mathcal{A}\omega^2\sigma^2}{2}\right\}$$

$$p_{II\pm}^2 = \pm\frac{1}{2}\left\{\left(\mathcal{A}\omega^2\sigma^2 - \left(\frac{\omega - 2k_zV_0}{\Omega_-{\gamma_0}^3}\right) - {k_z}^2{v_{z0}}^2\right)^2 + \frac{4{k_z}^2}{{\gamma_0}^6}\left(\gamma_0 - {\gamma_0}^3 + \frac{v_{z0}}{k_z\Omega_-}\right)\right\}^{1/2}$$
$$+\left\{k_z^2\left(1 - \frac{{v_{z0}}^2}{2}\right) + \frac{\omega}{2{\gamma_0}^3\Omega_-} - \frac{\mathcal{A}\omega^2\sigma^2}{2}\right\}$$

Using the condition that the solutions of Eq. (4.15) should vanish at $\pm\infty$, we have the following expression for them

$$b_I = b_{I+}exp(p_{I+}x) + b_{I-}exp(p_{I-}x); \qquad b_{II} = b_{II+}exp(-p_{II+}x) + b_{II-}exp(-p_{II-}x)$$

$$v_{xI} = v_{xI+}exp(p_{I+}x) + v_{xI-}exp(p_{I-}x); \; v_{xII} = v_{xII+}exp(-p_{II+}x) + v_{xII-}exp(-p_{II-}x)$$

Here, $p_{r\pm}$ are chosen as the positive square root of $p_{r\pm}^2$. The solutions contain eight unknown coefficients which have to be determined. There are only four matching conditions to be satisfied in terms of the continuity of the four functions in the two regions, as already discussed in the previous section. It should be noted that the coefficients of one of the fields, viz., v_x can be expressed in terms of b by using Eq. (4.16). This gives

$$v_{xI,II\pm} = \left(\frac{ik_z}{\delta_{I,II} + p_{I,II\pm}^2} \right) b_{I,II\pm}$$

This leaves us with four unknown coefficients $v_{xI,II\pm}$ which have to satisfy the four matching conditions. In order to obtain a non trivial solution, the determinant of the coefficient matrix $\bar{M}$ should be zero. The condition $det||M|| = 0$ then determines the eigen value ω. Upon applying the matching conditions, the coefficient matrix M can be expressed as follows

$$\begin{vmatrix} p_{I+}\left(1-\frac{1}{q_{I+}^2}\right) & p_{I-}\left(1-\frac{1}{q_{I-}^2}\right) & p_{II+}\left(1-\frac{1}{q_{II+}^2}\right) & p_{II-}\left(1-\frac{1}{q_{II-}^2}\right) \\ \left(1-\frac{1}{q_{I+}^2}\right) & \left(1-\frac{1}{q_{I-}^2}\right) & \left(-1+\frac{1}{q_{II+}^2}\right) & \left(-1+\frac{1}{q_{II-}^2}\right) \\ p_{I+}\left(\frac{\Omega_+}{q_{I+}^2}\right) & p_{I-}\left(\frac{\Omega_+}{q_{I-}^2}\right) & p_{II+}\left(\frac{\Omega_-}{q_{II+}^2}\right) & p_{II-}\left(\frac{\Omega_-}{q_{II-}^2}\right) \\ \left(\frac{1}{\Omega_+ q_{I+}^2}\right) & \left(\frac{1}{\Omega_+ q_{I-}^2}\right) & -\left(\frac{1}{\Omega_- q_{II+}^2}\right) & -\left(\frac{1}{\Omega_- q_{II-}^2}\right) \end{vmatrix}$$

where $\delta_r + p_{r\pm}^2 = q_{r\pm}^2$. In the Fig. 4.1, we have shown the surface and contour plot of one of the roots of this determinant. For subsequent analysis, we choose the normalizing magnetic field B_{00} (for any given density n_{0e}) so as to have $\sigma = 1$. The eigen value ω as a function of k_z and V_0 can be obtained from the roots of the equation $det \mid\mid M \mid\mid= 0$. The root with maximum value of $Im(\omega)$ provides for the maximum growth rate of the instability. The corresponding eigen vector is the maximally growing mode of the system. The growth rate in the absence of displacement current contribution Γ_{WR} can be obtained analytically (by substituting $\mathcal{A} = 0$ in the equation $det \mid\mid M \mid\mid= 0$) as

$$\Gamma_{WR} = k_z V_0 \sqrt{(1 + 4k_z^2\gamma_0)/(3 + 4k_z^2\gamma_0)}. \tag{4.17}$$

This expression for Γ_{WR} has also been obtained in an earlier publication by Das *et al.* [22]. The non-relativistic expression Γ_{NR} results simply by substituting $\gamma_0 = 1$ in Eq. (4.17). The difference between the expressions of Γ_{WR} and the Γ_{NR} (for same V_0) is very small. Hence the curves corresponding to these growth rates as a function of k_z overlap in the subplots (a) and (b) of Fig. 4.2. The small difference

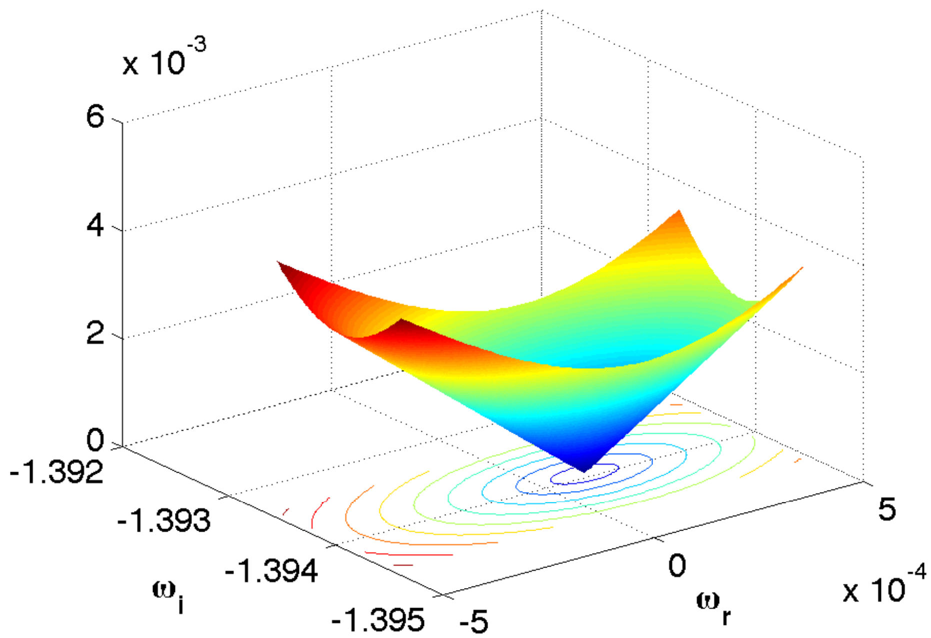

Figure 4.1: The contour as well surface plot of one of the roots obtained after solving the determinant $det||M|| = 0$. Here, $k_z = 2$.

between Γ_{WR} and Γ_{NR} has been shown in subplot (c) of Fig. 4.2. The plot clearly shows that the difference maximizes at an intermediate k_z. This difference at

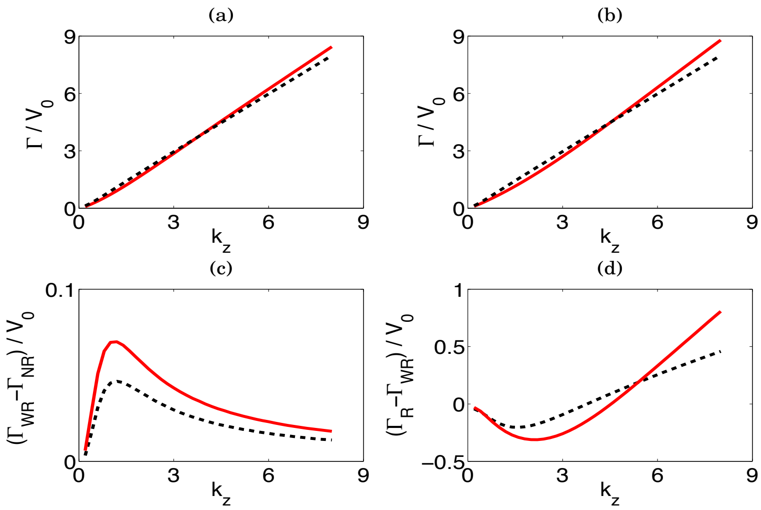

Figure 4.2: The plot of various limiting forms of the growth rates for a step velocity shear profile. Subplot (a) show for $V_0 = 0.8$ the relativistic growth rate Γ_R/V_0 for $\mathcal{A} = 1$ (solid line) as a function of k_z. The dashed line represents the non relativistic Γ_{NR}/V_0 and also the relativistic growth rate Γ_{WR}/V_0 evaluated for $\mathcal{A} = 0$. The difference between Γ_{WR}/V_0 and Γ_{NR}/V_0 is very small to be seen in the plot. Subplot (b) is similar to (a) but here $V_0 = 0.9$. Subplot (c) shows the plot of $(\Gamma_{WR} - \Gamma_{NR})/V_0$ as a function of k_z for $V_0 = 0.8$ (dashed line) and $V_0 = 0.9$ (solid line). Subplot (d) is for $(\Gamma_R - \Gamma_{WR})/V_0$ as a function of k_z for $V_0 = 0.8$ (dashed line) and $V_0 = 0.9$ (solid line).

intermediate range of k_z increases with V_0. From the expression, Eq. (4.17) also, it is clear that both, at very small and very large values of k_z, the two expressions asymptote towards $k_z V_0$ and $k_z V_0/\sqrt{3}$ respectively. We would also like to emphasize here that small difference simply means that the expressions for the growth rates in relativistic and non-relativistic cases for the step profile are typically very similar. Since V_0 is comparable to the speed of light (unity in the present normalizations) for the relativistic case and is much smaller in the non-relativistic situations, the value of the growth rate for relativistic flows would indeed be much higher than that for non-relativistic cases. The small difference in Fig. 4.2 merely suggests that the use of non-relativistic expression for evaluating the growth rate in relativistic cases would not cause any significant error. We now study the role of displacement current on the mode by choosing $\mathcal{A} = 1$. The thick solid line of subplots (a) and (b) of Fig. 4.2 show the the growth rate Γ_R as a function of k_z for $V_0 = 0.8$ and 0.9 respectively. The value of Γ_R is smaller than Γ_{WR} for lower k_z values, however at higher k_z, $\Gamma_R > \Gamma_{WR}$. The difference between the two increases monotonically with k_z and V_0 as illustrated in the subplot (d) of Fig. 4.2 . It basically means that the displacement current plays negligible role at small and intermediate wave numbers. The figure, however, suggests that at higher wave numbers the differences could be significant. However, only for the unrealistic step function velocity profile, there exist all higher values of the wave number k_z which can be destabilized. When a realistic profile of the velocity shear is chosen such as the tangent hyperbolic function, there exists a threshold on the wave number k_{zth} (inversely proportional to shear width) [1, 2] beyond which the growth rate vanishes. It will be shown in the next section that for the entire range of wave numbers for which the mode can be excited the contribution of displacement current is insignificant.

4.5 Tangent hyperbolic velocity profile

In this section, we consider a shear flow profile which has a finite width ϵ and has a tangent hyperbolic form $v_{z0}(x) = V_0 \tanh(x/\epsilon)$. The growth rate in this case is obtained numerically by solving for the eigen value ω from Eqs. (4.11)-(4.12). In Fig. 4.3 and 4.4, we show the plot of the growth rate and the real frequency

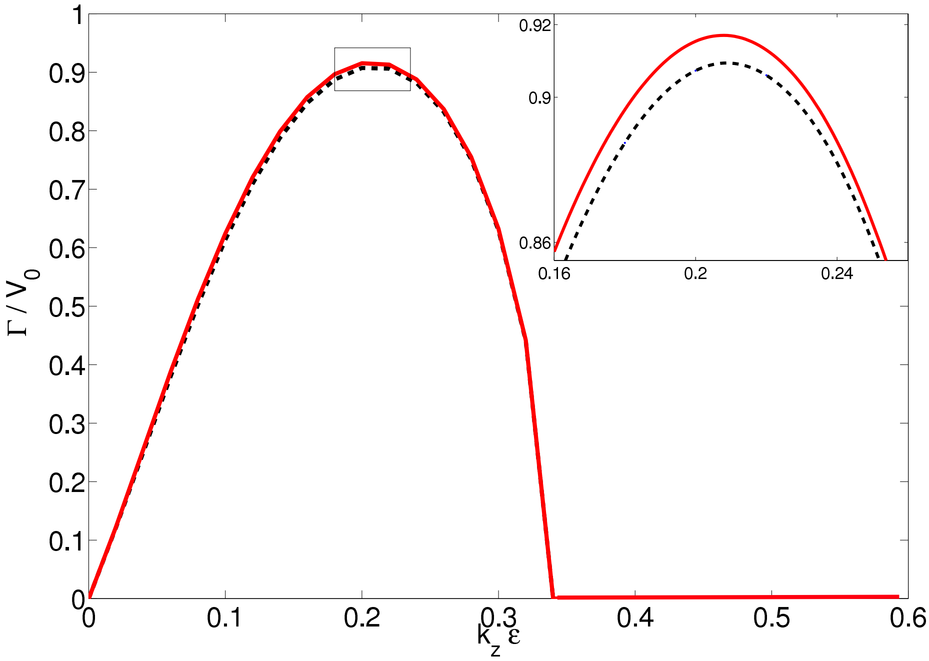

Figure 4.3: The growth rate for a tangent hyperbolic sheared velocity profile of the form $v_{z0} = V_0 \tanh(x/\epsilon)$. Here, $V_0 = 0.8$ and $\epsilon = 0.1$ has been chosen. The solid and dashed lines show the plot of Γ_R/V_0 and Γ_{WR}/V_0 respectively, as a function of $k_z\epsilon$. The inset shows the plot over an extended scale. The eigen value is purely growing for this case.

as a function of $k_z\epsilon$ for $V_0 = 0.8$ and $V_0 = 0.9$ respectively. The two figures provide comparison between Γ_{WR} (growth rate in the absence of the contribution from displacement current, i.e. for $\mathcal{A} = 0$) and Γ_R (when $\mathcal{A} = 1$). The inset in Fig. 4.3 shows this difference in an expanded scale. The figures, thus, suggest that the difference between Γ_R and Γ_{WR} is quite small over the entire regime of k_z. Thus, the role of the displacement current, in the incompressible limit that we are considering here, appears negligible.

The figures show that in the relativistic case too there exists a threshold value of k_z beyond which the growth rate vanishes. An interesting observation is that while

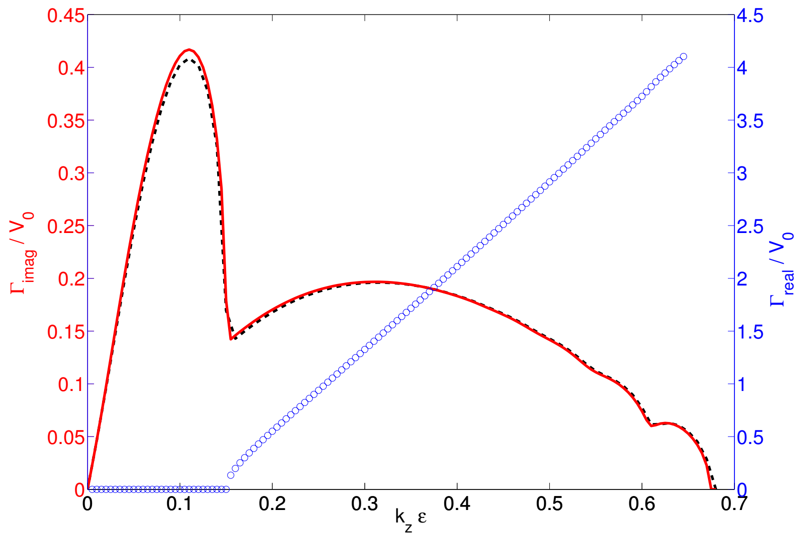

Figure 4.4: The growth rate for a tangent hyperbolic sheared velocity profile of the form $v_{z0} = V_0 \tanh(x/\epsilon)$. Here, $V_0 = 0.9$ and $\epsilon = 0.1$ has been chosen. The solid and dashed lines show the plot of Γ_R/V_0 and Γ_{WR}/V_0 respectively, as a function of $k_z\epsilon$. The eigen value acquires a real frequency indicated by a line with open circles beyond $k_z\epsilon \approx 0.15$ for this case.

the form of the growth rate curve in Fig. 4.3 is very similar to the non-relativistic growth rates obtained in the earlier publications [1, 2], the plot of Fig. 4.4 for $V_0 = 0.9$ has certain distinctions. The contribution due to displacement current continues to be small even when $V_0 = 0.9$. The mode, however, shows certain distinct features in this case, where relativistic effects are expected to be comparatively stronger. The typical KH mode in EMHD in the non-relativistic formulation is a purely growing mode (no real frequency associated with the growing mode). Also, the growth rate curve exhibits only a single maxima as a function of k_z in the non-relativistic limit. We observe that while the plot of Fig. 4.3 for $V_0 = 0.8$ exhibits these features, this is not so for $V_0 = 0.9$. There appear multiple peaks in the growth rate plot (see Fig. 4.4) and the mode also acquires a real frequency after the first peak. We have also repeated our investigation for other values of V_0. We conclude from these studies that smaller values of V_0 exhibit the typical trait of KH mode (single maxima of the growth rate curve and the purely growing character). However, at higher values of V_0, multiple peaks appear in the growth rate curve and the mode does not remain purely growing beyond the first peak. A real frequency also gets associated with the subsequent peaks of the curve. We, therefore, feel that the mode corresponding to subsequent peaks is somewhat distinct from the pure velocity shear mode that we have been acquainted with. In the later part of this section we will trace the origin of this distinction in detail.

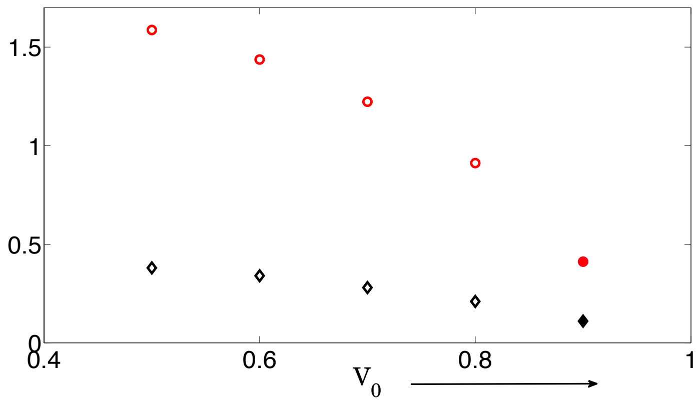

Figure 4.5: The maximum growth rate Γ_{Rmax}/V_0 (maximized over k_z) (hollow circles) and the threshold value of the wave vector k_{zth} (hollow diamond) as a function of V_0 . These points represent only those values of V_0 which are comparatively lower and produce a single peak in the plot of the growth rate vs. the wave number. The points, indicated by the dark filled circle and diamond in the figure correspond to the maximum growth rate divided by V_0 and the threshold wave number for the first peak of the purely growing mode of Fig. 4.4 respectively.

The other observations in the relativistic regime for smaller values of V_0 (e.g. purely growing modes with only *single peak* in the growth rate curve) show a monotonic decrease of Γ_{max}/V_0 with V_0. The points denoted by hollow circles in Fig. 4.5 illustrate this. One also observes that the threshold of the wave number, viz. k_{zth} (indicated by hollow diamonds in Fig. 4.5) also reduces with increasing V_0. Thus, the domain of unstable wave number seems to diminish with increasing speed. The last two points in the figure shown by dark filled circle and also a dark filled diamond has been put only for the purpose of illustration. These points are for $V_0 = 0.9$ and correspond to the Γ_{max}/V_0 (filled circle) maxima of the first peak, and that value of k_z (filled diamond) beyond which the growth rate acquires a real frequency. Note that this can be looked upon as the expected value of the threshold wave number, had only the first peak corresponding to purely growing mode been present in the growth rate plot. These points also seem to follow the consistent trend. The real k_{zth} for $V_0 = 0.9$, however, is much higher than that for $V_0 = 0.8$ as can be seen from the comparison of Fig. 4.3 and Fig. 4.4. This again suggests that the data corresponding to the first peak for $V_0 = 0.9$ is perhaps consistent with the overall trend with respect to V_0. However, the subsequent peaks of the growth rate of Fig. 4.4 appearing at higher values of V_0 have distinctly different characteristics. As we increase the value of V_0 further to 0.95, the growth rate curve in Fig. 4.6 shows that the domain of unstable wave numbers corresponding to the purely growing mode, shrinks to zero.

However, the subsequent peak with real frequency broadens up and the threshold of the wave number for the instability can be seen to exceed even the inverse shear width of the velocity profile, viz., $1/\epsilon$. This is a very interesting result as it shows that the unstable wave number domain increases in the strongly relativistic regime and scales even shorter than the shear width of the velocity profile are unstable.

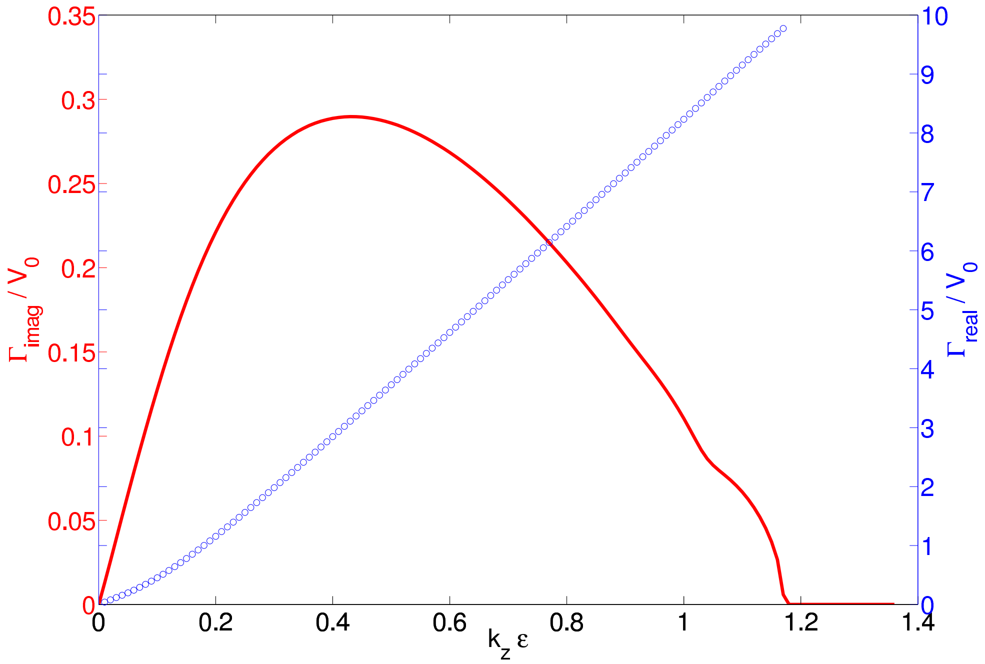

Figure 4.6: The growth rate for a tangent hyperbolic sheared velocity profile of the form $v_{z0} = V_0 \tanh(x/\epsilon)$. Here, $V_0 = 0.95$ and $\epsilon = 0.1$ has been chosen. The eigen value has real frequency over the entire domain of unstable wave numbers as shown by the curve with open circles.

Let us now try to understand the novel characteristic features of the growth rate curve as a function of $k_z\epsilon$ observed in the plots of Fig. 4.4 and Fig. 4.6. The contribution of displacement current has been found to be negligible in all studies, hence we consider the approximation of $\mathcal{A} = 0$ in Eqs. (4.11)-(4.12) and try to obtain a necessary condition for instability. For $\mathcal{A} = 0$, Eqs. (4.11)-(4.12) can be combined and written as

$$\frac{d^2 v_{x1}}{dx^2} + 3\frac{d\left(\log \gamma_0\right)}{dx}\frac{dv_{x1}}{dx} - \left(\frac{k_z^2}{{\gamma_0}^2} + \frac{1}{{\gamma_0}^3} - \frac{k_z\left((\gamma_0 v_{z0})'' - v_{z0}\right)}{\bar{\omega}{\gamma_0}^3}\right) v_{x1} = 0 \tag{4.18}$$

Using the transformation $v_{x1} = U/{\gamma_0}^{3/2}$, Eq. (4.18) the equation reduces to a simpler form

$$\frac{d^2U}{dx^2} + \mathcal{Q}U = 0 \tag{4.19}$$

where

$\mathcal{Q} = -\left(1/{\gamma_0}^3\bar{\omega}\right)\left(\bar{\omega}\left(k_z^2\gamma_0 + 1\right) - k_z\left((\gamma_0 v_{z0})'' - v_{z0}\right)\right) - \frac{3}{2}\left(\log\gamma_0\right)'' - \frac{9}{4}\left((\log\gamma_0)'\right)^2.$

Multiplying (4.19) by U^* and integrating by parts with respect to x leads to

$$\int\left[\mid \frac{dU}{dx}\mid^2 + \left(1 + \frac{k_z^2}{{\gamma_0}^2} + \frac{3}{2}(\log\gamma_0)'' + \frac{9}{4}\left((\log\gamma_0)'\right)^2\right)\mid U\mid^2\right]dx$$
$$- \int \frac{\left((\gamma_0 v_{z0})'' - v_{z0}\right)}{\bar{\omega}{\gamma_0}^3}k_z \mid U\mid^2 dx = 0 \tag{4.20}$$

where perturbations are assumed to vanish at the boundaries (i.e. at $x = \pm\infty$). The first term in the above integral equation is real and positive. The second term can also be written as

$$k_z\int \bar{\omega}\frac{\left((\gamma_0 v_{z0})'' - v_{z0}\right)}{\mid\bar{\omega}\mid^2 {\gamma_0}^3}\mid U\mid^2 dx \tag{4.21}$$

Eq. (4.20) can then be satisfied for an imaginary value of ω only if the coefficient of imaginary part of ω vanishes, all other terms being real in the equation. This implies

$$\int \frac{\left((\gamma_0 v_{z0})'' - v_{z0}\right)}{\mid\bar{\omega}\mid^2 {\gamma_0}^3}\mid U\mid^2 dx = 0 \tag{4.22}$$

Hence, it is clear that the necessary condition for instability implies [24] that $v_{z0} - (\gamma_0 v_{z0})''$ should change sign, all other factors being positive in the integrand. For the non-relativistic case, as well as the case when V_0 has a low value (e.g. 0.8 chosen in our plots), the sign $v_{z0} - (\gamma_0 v_{z0})''$ changes only once over a width of ϵ as shown in Fig. 4.7. However, when the value of V_0 is chosen to be high (e.g. 0.9

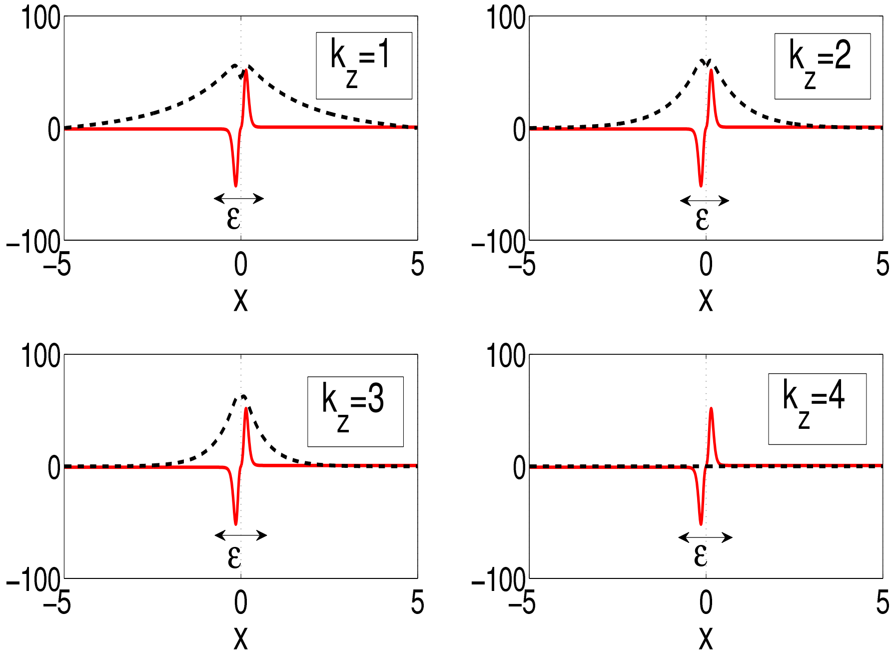

Figure 4.7: The four subplots show $v_0 - (\gamma_0 v_0)''$ (solid line) and the eigen function $| v_{x1} |^2$ (dashed line) as a function of x for the tangent hyperbolic equilibrium shear profile flow for different values of k_z. Here, $V_0 = 0.8$ and $\epsilon = 0.1$.

and above) the tangent hyperbolic profile of v_{z0} also produces a strong shear in the relativistic mass factor γ_0. This, then changes the sign of $v_{z0} - (\gamma_0 v_{z0})''$ more than once, and over much shorter width than ϵ as can be seen from Fig. 4.8 and Fig. 4.9 for $V_0 = 0.9$ and $V_0 = 0.95$ respectively. We feel that for the additional peaks in the growth rate plot of Fig. 4.4 and for the entire region of unstable wave number domain shown in Fig. 4.6, the shear in the relativistic mass factor γ_0 is responsible.

This has been made more evident by plotting the corresponding eigen functions

$\mid v_{x1} \mid^2$ also as dotted lines in Fig. 4.7, Fig. 4.8 and Fig. 4.9. For $V_0 = 0.8$ in Fig. 4.7 the eigen function can be seen to be symmetric and localized around $x = 0$ (the point where v_{z0} is zero) for $k_z = 1, 2, 3$. Since $k_z = 4$ is higher than k_{zth} the eigen function is zero everywhere in the fourth subplot of this figure.

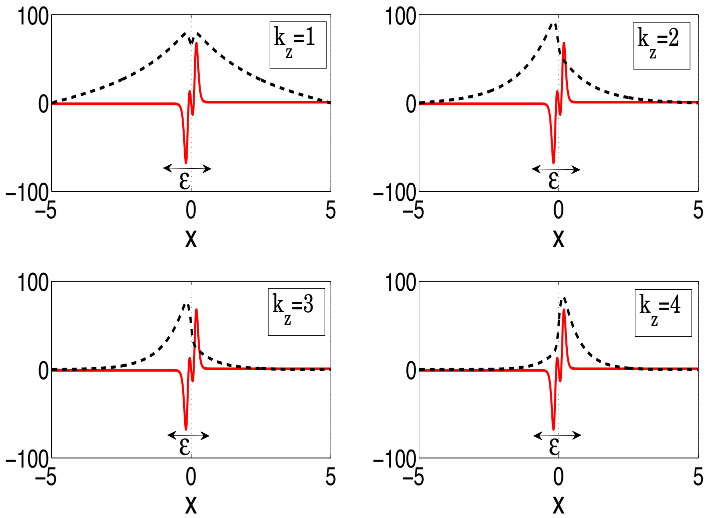

Figure 4.8: The four subplots show $v_0 - (\gamma_0 v_0)''$ (solid line) and the eigen function $\mid v_{x1} \mid^2$ (dashed line) as a function of x for the tangent hyperbolic equilibrium shear profile flow for different values of k_z. Here, $V_0 = 0.9$ and $\epsilon = 0.1$.

For the plots of Fig. 4.8, only $k_z = 1$ lies in the region of the first peak of Fig. 4.8. All other values of k_z chosen for the various subplots of Fig. 4.8 (e.g. $2, 3, 4$) correspond to the wave number of subsequent peaks of Fig. 4.4. It is interesting to note that the eigen function is not symmetric around the point of zero velocity for $k_z = 2, 3, 4$ (which correspond to wave numbers of the subsequent peaks in the growth rate).

In Fig. 4.5 the eigen function corresponding to no value of k_z is symmetric

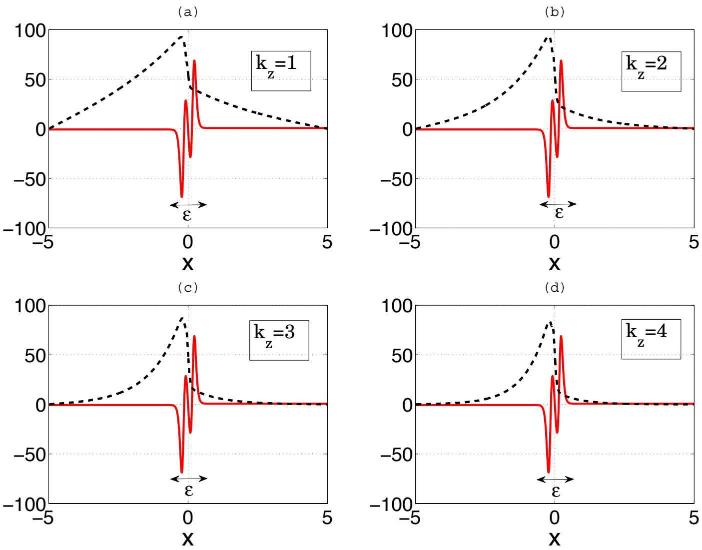

Figure 4.9: The four subplots show $v_0 - (\gamma_0 v_0)''$ (solid line) and the eigen function $\mid v_{x1} \mid^2$ (dashed line) as a function of x for the tangent hyperbolic equilibrium shear profile flow for different values of k_z. Here, $V_0 = 0.95$ and $\epsilon = 0.1$.

around $x = 0$. The appearance of additional zeroes in $v_{z0} - (\gamma_0 v_{z0})''$ ensures that the instability condition of Eq. (4.22) can be satisfied even by an asymmetric $\mid v_{x1} \mid^2$ which is not localized around $x = 0$ for these cases.

Furthermore, since the eigen function is asymmetrically placed with respect to the anti-symmetric tangent hyperbolic velocity shear profile, a Doppler shifted real frequency naturally appears in the eigen value. This can be compared with the appearance of a real Doppler shifted frequency in the eigen value even in the non-relativistic cases in a frame where the velocity profile is not anti-symmetric.

These observations, thus, point towards a novel extension of the KH mode of EMHD in relativistic regime arising solely due to the shear in the relativistic mass factor. It should be noted that for the case of the step velocity flow profile these features can not be observed. This is so because in that case the value of γ_0 also jumps exactly at the same location as that of the velocity discontinuity.

4.6 Summary

The sheared electron flow configuration is a ubiquitous feature in laboratory as well as astrophysical plasmas. The electron velocity in these situation is also often in the relativistic regime. For instance, the electron jets observed in astrophysical context have relativistic velocities. Also, with the advent of high intensity lasers, the laboratory experiments on laser plasma interaction routinely produces sheared electron flow at relativistic speeds. There have been suggestions that the velocity sheared flow instability for electron fluid might play a crucial role in the anomalous stopping mechanism of the energetic electrons within the compressed target core during the ignition phase of the Fast Ignition (FI) experiments [3, 5, 33]. The electrons in the experiment being strongly relativistic, the studies carried out here might have direct relevance to such experiments. The stability of sheared electron flow at relativistic velocities is therefore of interest both from fundamental as well as application point of view.

We have discussed in this chapter the role of relativistic effects on the electron velocity shear driven instability. The electron species being comparatively much lighter than the ions in the plasmas, the framework of the fluid Electron Magnetohydrodynamics (EMHD) model, which treats the ions as a neutralizing stationary background was adopted. The EMHD model was, however, generalized to incorporate the relativistic effects. The simplified incompressible limit of the relativistic EMHD model was then employed to study the KH instability in this regime. The assumption of incompressibility can be justified for dense plasmas where plasma frequency is very high, and where the time scales of the phenomena under consideration can be assumed to be slower than the plasma period. This implies, the density perturbations associated with the electron fluid can be ignored in the treatment.

Our studies demonstrate that the role of displacement current in this incompressible limit is considerably weak. Furthermore, it was also shown that the growth rate for the relativistic case differs only slightly from the one evaluated using the non-relativistic expression. Thus the typical order of magnitude estimate of the growth rate in the relativistic case, made from a non-relativistic treatment does not introduce any major error.

There are also a number of novel features that have been uncovered for the shear driven mode in the relativistic regime. We have shown that there exists two varieties of shear driven mode in relativistic regime. One which arises solely from the shear in the equilibrium velocity $v_0(x)$, the other which is due to the associated shear in the relativistic mass factor γ_0. The first variety of mode has features similar to the KH mode of the non relativistic case and primarily occurs in the weakly relativistic regime. It is a purely growing mode with its eigen function localized around the velocity null point (for a symmetric tangent hyperbolic velocity profile). The growth rate in this case plotted as a function of $k_z\epsilon$ (ϵ being the shear width of the velocity profile) displays a single maximum and vanishes both at $k_z = 0$ and for k_{zth}, where $k_{zth} < 1/\epsilon$. For this particular mode the maximum value of the growth rate Γ_{max}/V_0 and k_{zth} diminishes with increasing amplitude of V_0 indicating that it becomes increasingly more difficult to excite the mode in relativistic regime.

In contrast, the other variety of mode occurs at very high values of velocity (essentially close to the speed of light). In this case the growth rate curve does not show the universal single peak character as a function of $k_z\epsilon$. The mode is asymmetrically localized around the velocity null point and thereby acquires a real frequency (Doppler shifted frequency). The threshold wave number in this case is no longer restricted by $k_{zth} < 1/\epsilon$, in fact k_{zth} has been shown to exceed the inverse of the shear scale $1/\epsilon$. Thus much shorter scales get destabilized in the strongly relativistic regime. We have shown, this mode essentially arises due to the equilibrium shear associated with the relativistic mass factor γ_0. At intermediate velocity range, both kind of modes are present. The modes at lower/higher wave numbers are excited by the shear in velocity/relativistic mass factor in the intermediate case.

In this Chapter, we studied the various physical aspects of relativistic flow shear driven instability in EMHD. An analytical methodology to bridge strongly relativistic flow sheared instability would be desirable. In the next chapter, we employ perturbative analytic treatment to study the weakly relativistic flow shear driven instability.

Chapter 5

Perturbative analysis of sheared flow Kelvin-Helmholtz instability in a weakly relativistic magnetized electron fluid

The effect of relativistic flow on the Kelvin - Helmholtz like instability has been investigated in Chapter 4 using numerical technique. The growth rate, mode structure and the threshold wave number were obtained using well known numerical scheme of eigen value and eigen function determination. We adopt here a perturbative analytical treatment and confirm the numerical results obtained in Chapter 4 for the weakly relativistic case.

5.1 Introduction

The Kelvin Helmholtz (KH) instability has been investigated in the context of non-relativistic Electron-Magneto-Hydrodynamics (EMHD) Model in considerable detail [35]. In recent times, there are routine experiments which involve the interaction of intense laser pulses with compressed matter and/or plasma which can produce a relativistically sheared electron flow configuration. An example in this regard is the interaction of the ignitor laser pulse with the compressed target in the context of fast ignition experiments [6]. The inward propagation of these energetic electrons is countered by the background plasma reverse shielding current. It is well known that the combination of such a forward and reverse shielding current can undergo Weibel destabilization causing spatial separation of the forward and reverse shielding currents, which subsequently form current sheets. The tearing and coalescence of these sheets then form several current filaments. One such particular filament consists of the central core region carrying the inward electron current and the outer shell the reverse current [see Fig. 1.2]. The combination of the forward and reverse shielding current produces a sheared electron flow profile, which in general is susceptible to the KH destabilization process. However, the magnetized character of the electrons and the fact that their flow speed could be relativistic, produce certain distinct characteristic features to the properties of this well known fluid instability. These features have been identified by employing the Electron Magnetohydrodynamic (EMHD) fluid model and its relativistic generalization for the depiction of the electron fluid flow. The role of magnetized behaviour of electron flow on KH instability has been investigated in considerable detail in several publications [1, 2, 5, 19–21, 25, 26, 29–35, 39]. The additional effects arising in the weakly relativistic regime were investigated by us numerically [22] and have been presented in Chapter 4. In the weakly relativistic regime, the main features pointed out were the reduction in both the value of the growth rate as well as the threshold wave number of the instability. In this chapter, we show that these effects can be quantitatively understood by employing a perturbative analytic treatment [40, 41].

5.2 Governing Equations

The governing equations for electron time scale phenomena in relativistic regime comprises of the coupled set of Maxwell's and the relativistic electron fluid momentum equations. We assume that the ion species of the plasma forms a stationary neutralizing background of homogeneous density at the time scales of interest. Thus, the collisionless EMHD equations in dimensionless form when electron motion is relativistic is given by Eqs. (2.6) and (2.7). The electron fluid has been chosen to be either cold or at non-relativistic temperature. We consider a 2-D geometry with $\hat{y}$ as the symmetry direction and variations confined in the $x - z$ plane. The equilibrium flow velocity of electron is sheared along x and its flow is directed along $\hat{z}$, i.e. $\vec{v}_{e0} = v_0(x)\hat{z}$. This equilibrium flow produces an equilibrium magnetic field $\vec{B}_{0y}$ along $\hat{y}$ via Eq. (2.7). The electron flow velocity (both equilibrium and the perturbed) and consequently the associated current is assumed to lie in the 2-D, $x - z$ plane. Fourier analyzing the linearized equations in time and the z coordinate we retrieve Eq. (4.18).

5.3 Perturbative Treatment

The value of the threshold wave vector (k_z along the equilibrium flow direction) and the growth rate of the KH mode for non-relativistic sheared electron fluid are known from numerical eigen value calculation. The growth rate has a typical bell shaped form as a function of $k_z\epsilon$, where k_z is the wave number along the flow direction and ϵ is the shear width of the equilibrium flow [see Fig. 4.3]. The growth rate is zero at $k_z = 0$, maximizes and then again falls back to zero at a threshold value of wave number $k_z = k_{zth}$. It is observed that k_{zth} is typically of the order of $1/\epsilon$ and is exactly equal to $1/\epsilon$ for a tangent hyperbolic form of the sheared equilibrium flow velocity in the non relativistic case. In the weakly relativistic case, it was shown numerically by solving the eigen value equation that the threshold wave number as well as the growth rate diminishes. We, however, provide a perturbative analytic treatment to obtain an expression for the modification of the growth rate as well as the threshold wave number. We show that our perturbative analytical expression yields quantitative values which are in close agreement with the numerically obtained exact result.

We would seek the perturbative modification of the growth rate and the threshold wave number around the exact solution obtained by using the non-relativistic expression. The perturbative approach would be valid if the relativistic correction in the expression is weak. We show that this indeed is the case. Let $v_x^{(0)}$ be the exact solution when the non-relativistic expression is employed for the sheared system. We expand in terms of the small parameter of $\mathcal{O}(v_0^2/c^2)$ for the weakly relativistic case, around the zeroth order known non-relativistic result. The problem is then cast in various orders of expansion parameter $\eta = v_0^2$. Retaining terms only upto first order in the expansion parameter we have for the eigen function, wave vector and the eigen value

$$\begin{aligned} v_{x1} &= v_x^{(0)} + v^{(1)} \\ k_z &= k_z^{(0)} + k_z^{(1)} \\ \bar{\omega} &= \bar{\omega}^{(0)} + \omega^{(1)} \end{aligned} \tag{5.1}$$

respectively. Here, $\bar{\omega}^{(0)} = \omega^{(0)} - k_z v_0$. The superscript index inside the brackets represent the various orders of η, the function is dependent upon. Using the perturbative expansions of eigen function, wave vector and the eigen value, Eq. (4.18) can be rewritten as

$$\begin{aligned} &{\gamma_0}^3 \left(\bar{\omega}^{(0)} + \omega^{(1)}\right) \left\{ \frac{d^2(v_x^{(0)} + v^{(1)})}{dx^2} + 3\left(\log\gamma_0\right)' \frac{d(v_x^{(0)} + v^{(1)})}{dx} \right. \\ &\qquad \left. - \left(\frac{k_z^2}{{\gamma_0}^2} + \frac{1}{{\gamma_0}^3}\right)\left(v_x^{(0)} + v^{(1)}\right)\right\} \\ &+ k_z \left((\gamma_0 v_0)'' - v_0\right)\left(v_x^{(0)} + v^{(1)}\right) = 0 \end{aligned} \tag{5.2}$$

Expanding γ_0 and its higher powers, we get

$$\begin{aligned} &\left(\bar{\omega}^{(0)} + \omega^{(1)}\right) \left\{ \left(1 + \frac{3v_0^2}{2}\right)\left(v_x^{(0)} + v^{(1)}\right)'' + 3v_0 {v_0}' \left(1 + \frac{5v_0^2}{2}\right)\left(v_x^{(0)} + v^{(1)}\right)' \right. \\ &\qquad \left. - \left(k_z^2(1 + \frac{1}{2}v_0^2) + 1\right)\left(v_x^{(0)} + v^{(1)}\right)\right\} \\ &+ k_z \left((\gamma_0 v_0)'' - v_0\right)\left(v_x^{(0)} + v^{(1)}\right) = 0 \end{aligned}$$

The zeroth order of Eq. (5.2) is

$$\bar{\omega}^{(0)} \left(\frac{d^2 v_x^{(0)}}{dx^2} - \left(k_z^2 + 1\right) v_x^{(0)}\right) - k_z v_0 \left(1 - \frac{{v_0}''}{v_0}\right) v_x^{(0)} = 0 \tag{5.3}$$

First order expansion of Eq. (5.2) is given by the following equation

$$\omega^{(1)}\left(\frac{d^2 v_x^{(0)}}{dx^2}-\left(k_z^2+1\right)v_x^{(0)}\right)+k_z\left(3v_0{v_0'}^2+\frac{3}{2}{v_0}^2{v_x^{(0)}}''\right)v_x^{(0)}+$$
$$\left[\bar{\omega}^{(0)}\left(\frac{d^2 v_1}{dx^2}-\left(k_z^2+1\right)v^{(1)}\right)-k_z v_0\left(1-\frac{{v_0}''}{v_0}\right)v^{(1)}\right]+$$
$$\bar{\omega}^{(0)}\left(\frac{3}{2}{v_0}^2{v_x^{(0)}}''+3v_0{v_0}'{v_x^{(0)}}'-\frac{{k_z^{(0)}}^2 v_0^2}{2}v_x^{(0)}\right)=0 \tag{5.4}$$

We multiply Eq. (5.4) by $v_x^{(0)}$ and integrate over x from -∞ to $+\infty$. For the term in square bracket the x differentiations are transferred to v_{x0} from $v^{(1)}$ and using Eq. (5.3), it vanishes.

$$\omega^{(1)}=\frac{-\int\left(\bar{\omega}^{(0)}\left(3v_0(v_0 v_x^{(0)}/2''+{v_0}'{v_x^{(0)}}')-{k_z^{(0)}}^2 v_0^2 v_x^{(0)}/2\right)v_x^{(0)}\right)dx}{\int\left(\frac{d^2 v_x^{(0)}}{dx^2}-\left(k_z^2+1\right)v_x^{(0)}\right)dx}$$
$$-\frac{\int\left(3k_z v_0\left({v_0'}^2/2+v_0{v_x^{(0)}}''\right){v_x^{(0)}}^2\right)dx}{\int\left(\frac{d^2 v_x^{(0)}}{dx^2}-\left(k_z^2+1\right)v_x^{(0)}\right)dx} \tag{5.5}$$

By evaluating the integrals for the zeroth order wavefunction for specific shear profile we can obtain the value of $\omega^{(1)}$. The results have been shown for a typical shear flow equilibrium for weakly relativistic case for a tangent hyperbolic profile. The reason for choosing a tangent hyperbolic equilibrium velocity profile, in particular, is that an exact value of threshold wave vector can be calculated analytically for non-relativistic flows. Also, for the relativistic case, the exact results have been obtained numerically which shows that the growth rate reduces due to relativistic factor in the weakly relativistic regime.

In Fig. 5.1, we have compared the numerical and analytical values of the growth rate for $V_0 = 0.3$. The figure shows that they are in good agreement with the exact

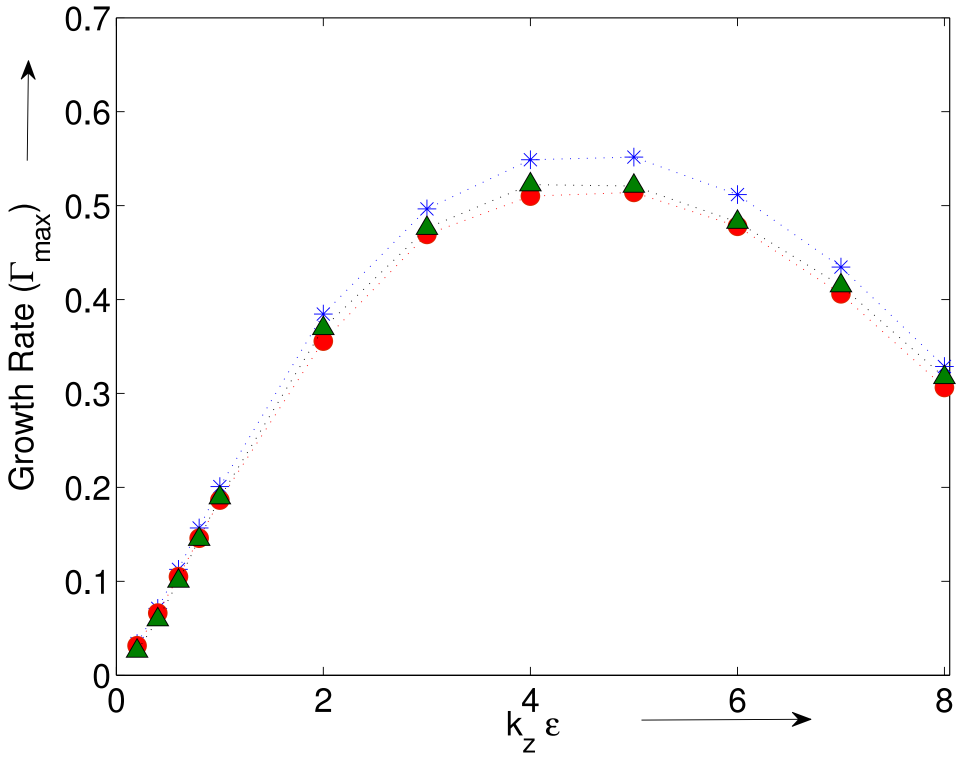

Figure 5.1: The comparison between the growth rate as a function of $k_z\epsilon$ for the weakly relativistic tangent hyperbolic sheared velocity profile. The plot for non-relativistic, perturbative and weakly relativistic has been shown by asterisk, filled circles and triangle respectively. Here $V_0 = 0.3$ has been taken.

result. It can be observed that even the first order perturbative corrections show impressive agreement with numerical results.

Using the same perturbative approach we will calculate the threshold wave vector. We now obtain the expression for the altered threshold wave number k_z for growth. To evaluate the threshold, we put $\omega = 0$ and look for the change in the value of k_z from its original non-relativistic value of $k_z^{(0)}$. For $\omega = 0$, Eq. (4.18) reduces to the following form

$$\frac{d^2 v_{x1}}{dx^2} + 3(\sqrt{1-v_0^2})\frac{d\left(1/\sqrt{1-v_0^2}\right)}{dx}\frac{dv_{x1}}{dx} -$$
$$\left(k_z^2(1-v_0^2) + \frac{(1-v_0^2)^{3/2}}{v_0}\left(\frac{v_0}{\sqrt{1-v_0^2}}\right)''\right) v_{x1} = 0 \tag{5.6}$$

Upon simplification, Eq. (5.6) can be written as:

$$\frac{d^2 v_{x1}}{dx^2} + 3v_0 {v_0}' \frac{dv_{x1}}{dx} - v_0^2 \frac{d^2 v_{x1}}{dx^2}$$
$$-\left(k_z^2 - 2v_0^2 k_z^2 + k_z^2 v_0^4 + \frac{{v_0}''}{v_0} - v_0 {v_0}'' + 3{v_0}'^2\right) v_{x1} = 0 \tag{5.7}$$

The zeroth order of Eq. (5.6) is

$$\frac{d^2 v_x^{(0)}}{dx^2} - \left(k_0^2 + \frac{{v_0}''}{v_0}\right) v_x^{(0)} = 0 \tag{5.8}$$

The first order expansion of Eq. (5.6) is given by the following equation

$$\frac{d^2 v_{x1}}{dx^2} - \left(k_0^2 + \frac{{v_0}''}{v_0}\right) v_1 + 3v_0 {v_0}' \frac{dv_x^{(0)}}{dx} - v_0^2 \frac{d^2 v_x^{(0)}}{dx^2}$$
$$-\left(2k_z^{(0)} k_z^{(1)} - 2{k_z^{(0)}}^2 v_0^2 - v_0 {v_0}'' + 3{v_0}'^2\right) v_x^{(0)} = 0 \tag{5.9}$$

We again apply the same technique of multiplying by $v_x^{(0)}$ and integrating from -∞ to $+\infty$ over x.

$$\int \left\{ \left(2k_z^{(0)} k_z^{(1)} - v_0 {v_0}'' - 2{k_z^{(0)}}^2 v_0^2 + 3{v_0}'^2\right) v_x^{(0)2} + \left(v_0^2 {v_x^{(0)}}'' - 3v_0 {v_0}' {v_x^{(0)}}'\right) v_x^{(0)} \right\} dx$$
$$= \int \left\{ \frac{d^2 v_{x1}}{dx^2} - \left({k_z^{(0)}}^2 + \frac{{v_0}''}{v_0}\right) v_1 \right\} v_x^{(0)} dx$$

For the first term on R.H.S. the x differentiations are transferred to $v_x^{(0)}$ from $v^{(1)}$.

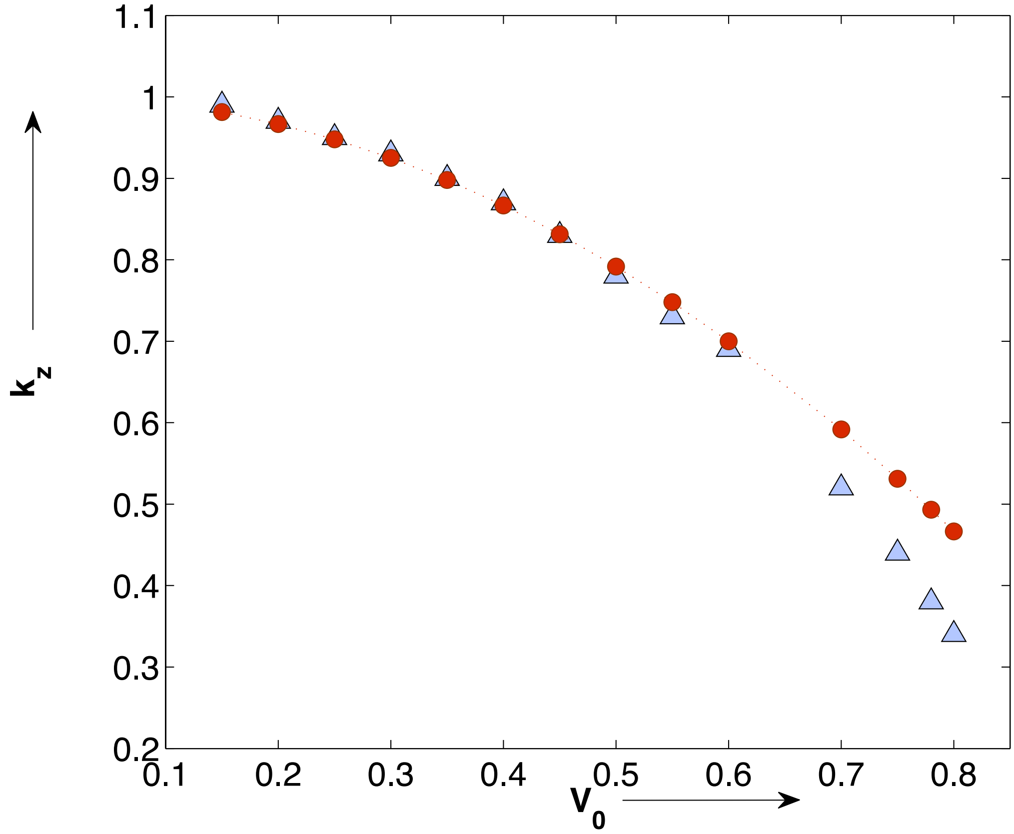

Figure 5.2: The comparison between the analytical and numerical wave vectors vs. V_0 for the weakly relativistic tangent hyperbolic sheared velocity profile. The line with circles shows the values of k_z obtained using perturbative analytic treatment while the triangles are the values obtained numerically.

Hence, using Eq. (5.8) the terms on R.H.S. vanish. Simplifying the remaining terms give us $k_z^{(1)}$ as follows

$$k_z^{(1)} = \frac{\int \left(\left(v_0 {v_0}'' + \int 2{k_z^{(0)}}^2 v_0^2 - 3{v_0'}^2 \right) v_x^{(0)2} + \left(3 v_0 {v_0}' {v_x^{(0)}}' - v_0^2 {v_x^{(0)}}'' \right) v_x^{(0)} \right) dx}{\int 2 k_z^{(0)} v_x^{(0)2} dx} \tag{5.10}$$

We have analytical equilibrium solution for the non-relativistic case for

$$v_0 = V_0 \tanh(x/\epsilon) \text{ as}$$

$$v_x^{(0)} = sech\left(\frac{x}{\epsilon}\right) \tag{5.11}$$

Substituting these in the Eq. (5.10), we get

$$k_z^{(1)} = \frac{{V_0}^2 \left(2{k_z^{(0)}}^2 \epsilon^2 - 7 \right)}{6 k_z^{(0)} \epsilon^2} \tag{5.12}$$

So, $k_z = k_z^{(0)} + k_z^{(1)}$ gives the exact solution to the perturbed system to the first order in the perturbation ϵ. In Fig. 5.2, we have compared the analytical values with the numerical ones. Here also, we can see that they are in good agreement. It can also be observed that the threshold value of the wave number decreases for the weakly relativistic case when compared with the non-relativistic results [22, 35].

5.4 Summary and Conclusion

The sheared electron flow configuration with electron speed in the relativistic regime can occur in wide ranging experiments concerning interaction of intense laser fields with overdense plasma. The sheared flow configuration of any fluid suffers destabilization through the well known fluid Kelvin Helmholtz (KH) instability. A detailed study of the KH instability in the context of electron fluids have been carried out in recent past [25, 35]. However, these studies could be conducted using numerical techniques for the eigen value evaluation. We have provided here a perturbative analytic expression for the first order correction in the growth rate as well as the threshold wave number in terms of the relativistic correction parameter of V_0^2/c^2. We show that these perturbative expressions provide close agreement to the exact numerical value. A physical interpretation of the reduction in the growth rate of the KH like mode in EMHD for weakly relativistic flows has also been provided.

Part II

Problem two

Chapter 6

Relativistic Electromagnetic solitons in cold plasmas

In this second part of the thesis (the present chapter 6 and chapter 7), we consider our studies for the coupled laser plasma system. The possible nonlinear coherent solutions for such system have been identified and an understanding of their formation in a particular parameter domain of the laser frequency and the group velocity has been provided. It has been shown that though the oscillating electric field of the laser light influences the electron species due to its smaller mass, when the structures form at small and/or zero group velocity the ion evolution has to be retained. It is shown that the retention of ion motion permits an even richer variety of solutions.

6.1 Introduction

The interaction of the electromagnetic field with plasma encapsulates a rich variety of nonlinear physics phenomena. A lot of which has been explored [3, 7–14] in recent times. The Ponderomotive pressure of the radiation field and the relativistic nonlinearities (typically associated with the dynamical response of the lighter electron species of the plasma at the available Peta - Watt range of laser power) are two major sources which alter the effective dielectric constant of the plasma. This leads to a nonlinear coupling between the transverse electromagnetic field and the longitudinal plasma wave. Several authors have sought exact solutions for this particular nonlinear coupled system, which has resulted in a rich variety of solutions in the form of propagating envelope solitary pulses. A further richer class of solutions results when the response of the heavier ion species is incorporated [42–55].

A detailed and complete characterization of the various kind of solutions in the parametric space of λ (associated with laser frequency) vs the group velocity β has, however, been lacking. We provide here, a detailed description of the possible solutions, both in the absence and the presence of ion response. We also comment on the main characteristic features of the possible solutions and physically interpret their formation in specific domain of the parameter space comprising the group speed and the frequency of the trapped electromagnetic wave.

6.1.1 One Dimensional Cold Plasma : Model Equations

The description of the propagation of intense circularly polarized laser pulse in a cold electron-ion plasma is provided by the coupled set of relativistic fluid equations and the wave equation for the vector potential of the electromagnetic radiation. We consider only one dimensional spatial variation along the propagation direction x. The evolution equations read as follows:

$$\frac{\partial n_e}{\partial t} + \frac{\partial (n_e u_e)}{\partial x} = 0 \tag{6.1}$$

$$\frac{\partial n_i}{\partial t} + \frac{\partial (n_i u_i)}{\partial x} = 0 \tag{6.2}$$

$$\left(\frac{\partial}{\partial t} + u_e \frac{\partial}{\partial x}\right)(\gamma_e u_e) = \frac{\partial \varphi}{\partial x} - \frac{1}{2\gamma_e}\frac{\partial {A_\perp}^2}{\partial x} \tag{6.3}$$

$$\left(\frac{\partial}{\partial t} + u_i \frac{\partial}{\partial x}\right)(\gamma_i u_i) = -\alpha\frac{\partial \varphi}{\partial x} - \frac{\alpha^2}{2\gamma_i}\frac{\partial {A_\perp}^2}{\partial x} \tag{6.4}$$

$$\frac{\partial^2 \varphi}{\partial x^2} = n_e - n_i \tag{6.5}$$

$$\frac{\partial^2 A_\perp}{\partial t^2} - \frac{\partial^2 A_\perp}{\partial x^2} = -\left(\frac{n_i \alpha}{\gamma_i} + \frac{n_e}{\gamma_e}\right) A_\perp \tag{6.6}$$

where $\alpha = m_e/m_i$. Here, Eqs. (6.1) and (6.2) are the continuity equations for electron and ion respectively, Eqs. (6.3) and (6.4) are the momentum equations for these species. Eq. (6.5) is the Poisson equation for the electrostatic potential φ and Eq. (6.6) is the wave equation for the vector potential $\vec{A}$, and other notations are standard. The equations (eqs. (6.1)–(6.6)) form the complete set of evolution equations for the propagation of an intense circularly polarized radiation in a cold plasma under the one dimensional approximation. The perpendicular components for the fluid velocities of electrons ($u_{e\perp}$) and ions ($u_{i\perp}$) have been eliminated by exact integration of the perpendicular momentum equations of the two species. The symbols γ_e and γ_i represent the relativistic factors for electrons and ions respectively, and are given by

$$\gamma_e = \sqrt{\frac{1 + A_\perp^2}{1 - u_e^2}}$$

and

$$\gamma_i = \sqrt{\frac{1 + A_\perp^2 \alpha^2}{1 - u_i^2}}$$

The set of equations (eqs. (6.1)–(6.6)) describe the governing model for the propagation of intense circularly polarized laser pulse in a cold electron - ion plasma in one-dimension.We have retained here the relativistic effects for both electron and ion species for the sake of completeness and also in view of the future possibility of laser amplitudes being high enough to drive even ions to relativistic velocities. The set of eqs. (6.1)–(6.6) has been employed for the study of the dynamical characteristics of the one dimensional exact nonlinear solutions. We choose to normalize electron and ion densities by a typical background value n_{00}, length by the corresponding skin depth c/ω_{pe0} (where $\omega_{pe0} = \sqrt{4\pi n_{00}e^2/m_e}$), time by the inverse of the plasma frequency ω_{pe0}^{-1} and the scalar and vector potentials by mc^2/e.

The coupled set of fluid-Maxwell equations [eqs. (6.1)–(6.6)] admits a variety of coherent nonlinear solutions. We use the coordinate transformation $\xi = x - \beta t$ (which represents the spatial coordinate in the frame moving with a group velocity β) and $\tau = t$. The choice of circularly polarized vector potential viz., $\vec{A} = [a(\xi)/2][\{\hat{y} + i\hat{z}\}exp(-i\lambda\tau) + c.c.]$ avoids the generation of harmonics. Using the coordinate transformation outlined above and seeking stationary solutions in the moving frame i.e. $\partial/\partial\tau = 0$, Eqs. (eqs. (6.1)–(6.4)) reduce to the form of ordinary differential equations. The equations upon integration give, $n_e(\beta - u_e) = \beta$, $n_i(\beta - u_i) = \beta$, $\gamma_e(1 - \beta u_e) - \varphi = 1$ and $\gamma_i(1 - \beta u_i) + \varphi\alpha = 1$. The integration constant is determined from the boundary condition of $u_e = u_i = 0, \varphi = 0$ and $n_e = n_i = 1, R = R' = 0$ at $\xi = \pm\infty$ corresponding to the bright solitonic structures [45, 46, 49, 56]. Eliminating n_e and n_i, the Poisson's equation [Eq. (6.5)] becomes

$$\varphi'' = \frac{\beta}{\beta - u_e} - \frac{\beta}{\beta - u_i}. \tag{6.7}$$

Here, prime($\prime$) denotes derivative with respect to ξ. Further, writing $a(\xi) = R\exp(i\theta)$, the wave equation [Eq. (6.6)] becomes

$$R'' + \frac{R}{1-\beta^2}\left[\left(\lambda^2 - \frac{M^2}{R^4}\right)\frac{1}{1-\beta^2} - \frac{\beta}{\beta - u_e}\frac{1-\beta u_e}{1+\varphi} - \alpha\frac{\beta}{\beta - u_i}\frac{1-\beta u_i}{1-\varphi\alpha}\right] = 0 \tag{6.8}$$

where $M = R^2[(1-\beta^2)\theta' - \lambda\beta]$ is a constant of integration and $R^2 = A_x^2 + A_y^2$. Eqs. (6.7) and (6.8) form a coupled set of second-order differential equations for the fields φ and R. The parallel fluid velocities for electron and ion species can be expressed in terms of R and φ as shown below

$$u_e = \frac{\beta(1+R^2) - (1+\varphi)[(1+\varphi)^2 - (1-\beta^2)(1+R^2)]^{1/2}}{(1+\varphi)^2 + \beta^2(1+R^2)} \tag{6.9}$$

and

$$u_i = \frac{\beta(1+R^2\alpha^2) - (1-\varphi\alpha)[(1-\varphi\alpha)^2 - (1-\beta^2)(1+R^2\alpha^2)]^{1/2}}{(1-\varphi\alpha)^2 + \beta^2(1+R^2\alpha^2)} \tag{6.10}$$

In the next two sections, we present the exact nonlinear solutions provided by the set of Eqs. (6.7) and (6.8) with u_e and u_i given by Eqs. (6.9) and (6.10) respectively, for various values of the parameters λ and β. These solutions have been obtained earlier by several authors [10–13, 42–45, 48] in separate contexts. Here, we provide a comprehensive detailed picture of the possible solutions in the parameter domain of λ - β space.

6.2 The Nonlinear Solutions with electron response alone

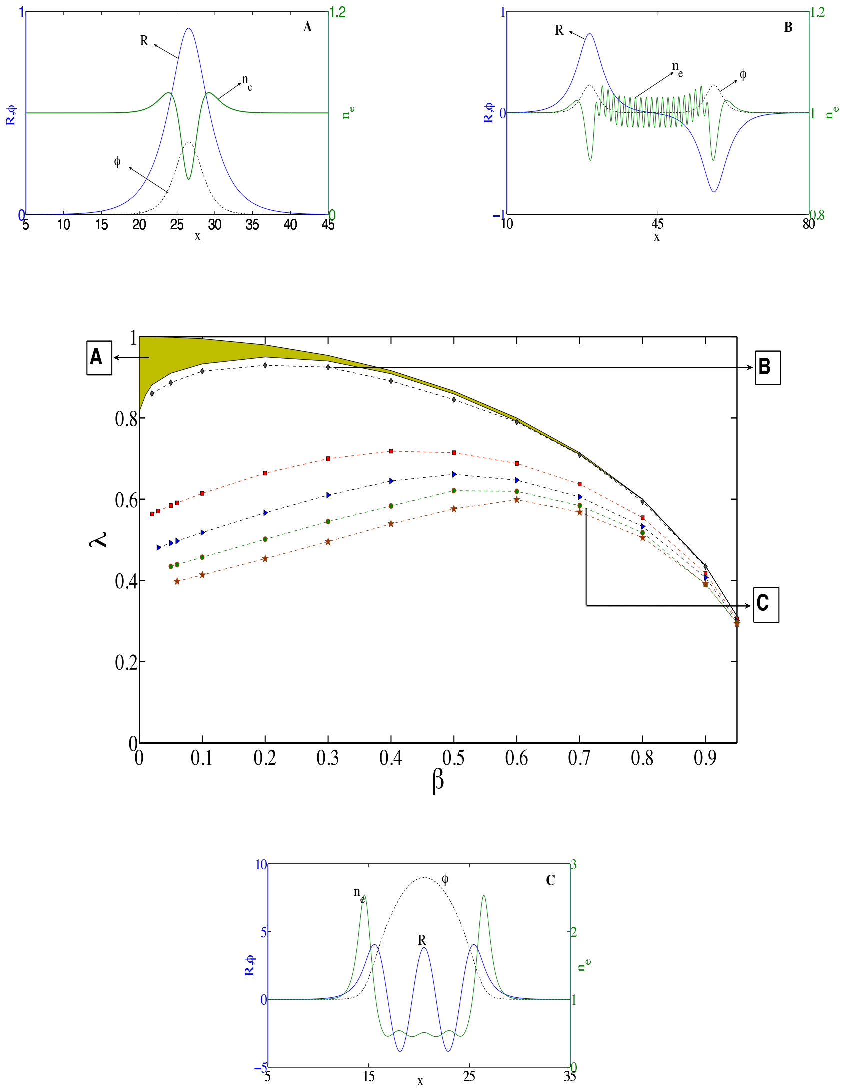

Figure 6.1: The $\lambda - \beta$ spectrum in subplot 'S' indicating the existence region for possible soliton solutions in static ion case viz. the single peak solutions, paired solutions, and multi peak solutions tagged with 'A', 'B', and 'C', respectively. The profile of vector potential(R), scalar potential(φ), and electron density(n_e) for the solutions of each variety are shown in subplots with the same tags.

In Fig. 6.1, we show the possible varieties of solutions for $\alpha = 0$ (infinitely massive ions) and the region in the λ vs β plane where they occur. The figure

(Fig. 6.1) shows that in this case, there are essentially three varieties of solutions. These solutions have been termed as (i) the single peak solutions, (ii) the paired solutions, and (iii) the multiple peak solutions. We now briefly discuss all possible varieties of solutions one by one.

1. **Single peak solutions:**

   These are structures shown in subplot (A) of Fig. 6.1. These solutions have a **single peak** in both vector R and scalar φ potentials. The normalized amplitude of the scalar potential φ for these structures is typically smaller than that of vector potential,R. The central subplot (S) of Fig. 6.1 shows the region of existence of these particular variety of solutions in the λ vs. β plane by an arrow pointing at the box enclosing the alphabet **A**. It shows that they exist for a continuum range of values of λ and β contained by the region enclosed by the two topmost lines of the subplot (S). As can be seen that these solutions are possible even when the group velocity β goes to zero. An analytical form of the solutions for the simple case of $\beta = 0$ was obtained by Esirkepov *et al.* [42]. At a fixed value of β, the amplitude of these solutions increases upon decreasing the value of λ. It has been shown in our earlier work [49] that these solutions are very robust and stable. The smaller amplitude solutions amidst this variety of structures (i.e. solutions for high value of λ) have the dynamical characteristics of exact soliton solutions of the Nonlinear Schrödinger (NLS) equation. It was shown that they preserve their identity after colliding with other similar structures. Their group velocity was shown to get altered as they propagate through an inhomogeneous plasma. At higher density, the group speed was found to reduce, as a result of which the structure reflects when it encounters a plasma density beyond a certain critical value. This behaviour presents no surprise as in the small amplitude limit one can analytically show that the coupled set of Eqs. (6.7) and (6.8) reduces to the form of NLS equation. The higher amplitude solutions obtained for somewhat lower values of λ, however, display dynamical features distinct from the NLS solitons. Though these solutions show stable propagation at their respective group speed, they do not behave like solitons upon collision. While solitons with same amplitude propagating in opposite directions reflect off each other, when those with dis-similar amplitude collide, the structures simply loose their identity.

2. **Paired structures:**

   The second variety of solutions depicted in subplot (B) has been termed as **Paired structures** [55]. Basically, they represent a spatial coupling of two single peak solutions with opposite polarity of the field R via an intermediate sandwiched region comprising of plasma oscillations. These solutions also exist for a continuum range of the parameter values λ and β shown by an arrow pointing at **B** in subplot S of the $\lambda-\beta$ plane. The possible values of the λ hovers below (in subplot(S)) the region for which single peak structures of kind **A** exist. We have conducted preliminary study of their dynamical evolution and observe that they disintegrate after about 100 plasma periods.

3. **Multi-peak solutions :**

   This is a third possible variety of structures having **multiple - peaks** of the vector potential R as shown in subplot (C). These solutions have several peaks of the vector potential R which reside in a cavity from where electron density has been almost evacuated. The electron density evacuation is due to the ponderomotive pressure of the light wave and results in a build up of huge space charge field. This produces a high amplitude single peak φ which envelopes the structure. There are no standing multi-peak solutions possible, *i.e.* β is always finite for these solutions. Another aspect associated with these solutions is that they correspond to a discrete spectrum of λ values. A structure with a particular number of extremas in R can have only one possible value of λ for any given β, as depicted by the various curves in subplot (S) of Fig. 6.1. This is essentially due to the nonlinear discrete eigenvalue condition arising from the fact that the structure has to accommodate a particular number of extremas in R within a certain width. In subplot (S), the lines with dots, triangles, crosses and stars represent the values of λ and β for which solutions with 2, 3, 4 and 5 extremas in R are possible, respectively. It has been shown by some of us in an earlier publication [49] that these Multi - peak solutions, when evolved in time, survive only for several $10's$ of plasma periods. They are observed to be unstable and emit radiation from their trailing edge as they propagate. The instability has been identified as the Stimulated forward Raman scattering instability.

6.3 Physical interpretation of soliton formation with electron response only

The soliton structures that we have discussed in the previous section have a localized structure in space for all the associated fields, which go asymptotically to zero at both the boundaries $x = \pm\infty$. The spatial form of the R and φ fields are governed by the second order ODE Eqs. (6.7) and (6.8). Clearly, for φ and R to have a localized form, φ'' and R'' should be negative at the place of maxima and at the edges it should change sign. This suggests that for the case when only electrons respond, φ'' can be negative to produce a maxima in the φ profile only if electrons are evacuated from center. These evacuated electrons accumulate at the edge such that $n_e > 1$; making φ'' change sign and rendering φ profile asymptote smoothly at infinity.

Simultaneously it is important that similar conditions on R'', for the R field to be localized, should also be satisfied. This entails that the coefficient of R viz.,

$$\mathcal{A} = \frac{\lambda^2}{(1-\beta^2)} - \frac{n_e}{\gamma_e}$$

in Eq.(6.8) (for $M = \alpha = 0$) is positive at the center of the solution and it is negative at the edge. Note that at the center of the structure, n_e reduces as the electrons get evacuated; the minimum value that n_e can attain for a structure moving with speed β, occurs when u_e is negative and equal to -1 such that $n_e = \beta/(\beta+1)$. Thus, higher evacuation of electron density implies an increase in the value of $\mid u_e \mid$. Furthermore, evacuation of electron density happens due to high radiation pressure. Thus, a higher evacuation also implies a higher value of R. Both

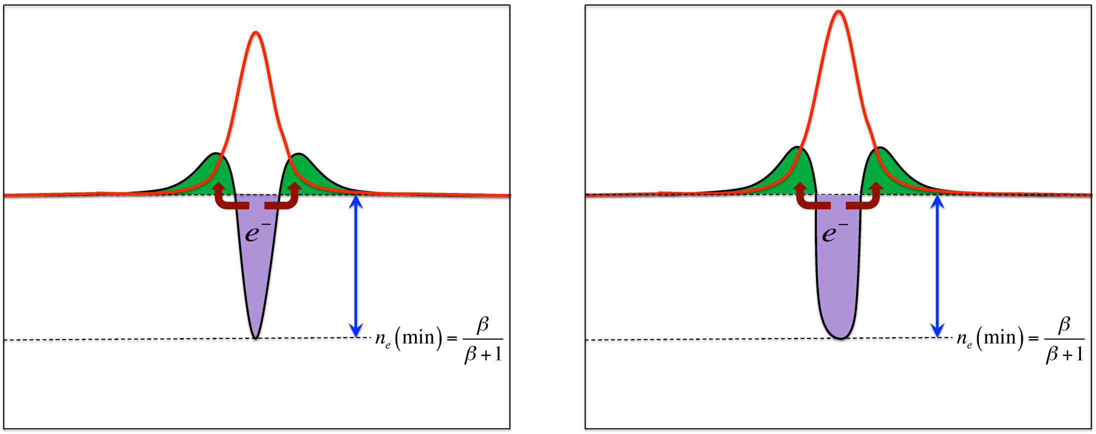

Figure 6.2: Schematic of the formation of single peak solution.

a high $\mid u_e \mid$ and a high R in turn increase γ_e. Eventually, at the centre (n_e/γ_e would typically be small compared to its value at the edges and with increasing amplitude of solitons it would decrease further.

At the edge, $\mathcal{A}$ is supposed to be negative. This is possible since the evacuated n_e accumulates (changing the sign of φ'') at the edge. Also, $n_e > 1$ implies that u_e is positive and less than β. The value of R also drops down away from the center. Thus, γ_e can reduce, making n_e/γ_e larger in the edge region to satisfy the condition of $\mathcal{A}$ being negative. The analysis clearly shows that the dependencies are consistent and the possibility of soliton solution exists. We now ask the question as to what restricts the parameter values of λ and β, and why the different kinds of structures form in distinct domain of the parameter space. Let us first analyze the uppermost curve in the λ vs. β space, below which only, solutions can exist. We conjecture that uppermost curve represents infinitesimally small amplitude solitons. Thus, on the curve $R \approx 0$, $n_e \approx \gamma_e \approx n_e/\gamma_e \approx 1$ almost everywhere with very little variation from centre to edge. Thus, $\lambda^2/(1-\beta^2)$ should be equal to 1 to satisfy both the edge and the centre conditions of having $\mathcal{A}$ as negative and positive respectively. The upper boundary is thus described by the relation $\lambda^2 = 1-\beta^2$. This agrees with the form of the uppermost curve shown in Fig. 6.1.

We now show that by choosing any high finite amplitude of R, one can get solutions only below the $\lambda^2/(1-\beta^2) = 1$ curve. At the boundaries, $n_e/\gamma_e = 1$ for all solutions. In order to have a localized confined structure for R for all solutions, at the edge where n_e/γ_e would exceed briefly the value of unity, it is necessary that $\lambda^2/(1-\beta^2) < 1$. Thus, solutions above the curve $\lambda^2 = 1-\beta^2$ are not permitted. As noted earlier, higher amplitude solitons have higher R at centre. As a result, both n_e and γ_e behave in a fashion so as to have a lower $(n_e/\gamma_e) < 1$ at the center with the increasing amplitude of solitons. The requirement for $\mathcal{A}$ to be positive at the center can now be satisfied for $\lambda^2/(1-\beta^2) < 1$. The reason for $\lambda^2/(1-\beta^2)$ to decrease and not stay put at the value of unity can also be understood by realizing that as n_e/γ_e at the centre reduces, and if $\lambda^2/(1-\beta^2)$ is held fixed, then $\mathcal{A} = k_c^2$ (the wave number at the centre for R structure) would increase as well. Solutions with single peak in R would keep making the structures narrow. The amount of electrons evacuated from the narrow region is less. These electrons evacuated from the centre have to accumulate at the edge to shield R at the edge. Larger amplitude of R and weakening of the electron number available for shielding would rule out the existence of the formation of soliton. Thus, as R increases, the value of $\lambda^2/(1-\beta^2)$ has to decrease so that k_c^2 does not become large enough to disturb the balance. It is, thus, clear that the solutions with increasing amplitude of R form only when $\lambda^2/(1-\beta^2)$ reduces. This also explains the observations that the higher amplitude solutions get narrower. The plots of Fig. 6.1 also show that the single peak solutions are not permitted beyond the lower second curve. A possible reason may be that defining the lower boundary for specific range of β values. The minimum value that the electron density can take for a moving soliton structure is when $u_e = -1$ and is $n_M = \beta/(\beta+1)$. However, this can happen iff (see Eq. (6.9) for the expression for u_e) $\varphi >> 1$ and $\varphi >> R$. For single peak solutions, φ is always less than R, so this can never be met. The lowest value of density n_{e_min} in the solutions is higher than n_M. Hence, minimum value of density beyond which n_e cannot be evacuated further from the centre is n_{e_min}. The moment, the central density reaches the value of $n_c = n_{min}$, no more electrons can be scooped from the center. At higher R, even lesser electrons would be available as the structure keeps narrowing down. It would then become impossible at the edge to build up sufficient density to shield the radiation R from leaking to form an isolated structure. This can be understood from the schematic of Fig. 6.2. The subplot (a) of Fig. 6.2 shows single peak solitons. As we go for lower values of λ (i.e. increase R), it needs higher number of electrons to be scooped out from the center(shown here by violet color) to the edges (shown here by green color) to confine the radiations. Since no more electrons could be scooped out due to the minimum density criteria, it results in flattening of the density profile [see subplot (b) of fig. 6.2].

Just below the single peak solutions the paired solutions are observed. For a single peak solution, the electron scooped out from the central region have to pile up so as to satisfy the criteria of non-transmittance of R at the two edges. Two such solitons would have twice the electrons available from central region. Separately, they have to satisfy the criteria at four edges. When they pair up as in

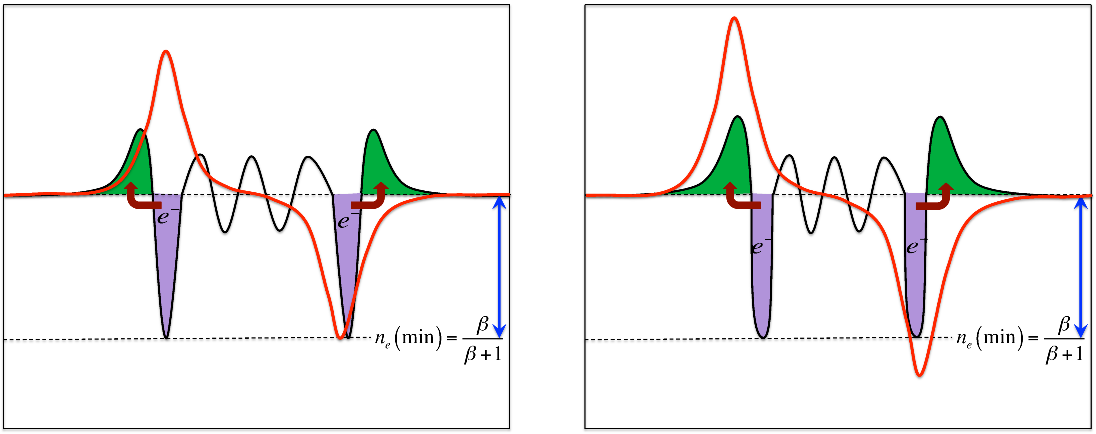

Figure 6.3: Schematic of the formation of paired structures.

paired structures, they satisfy the non - transmittance criteria at two edges only. In the central region of the paired structure R is allowed to get transmitted from one to the other structure. The formation also clearly suggests that two opposite polarity solutions in R would form for this case. Thus, at values of λ below the permissible curve of single peak solutions, these structures are observed. At still further lower values of λ, even the electrons scooped out by two solutions are insufficient to satisfy the non - transmittance of R at the two edges [see Fig. 6.3]. Then only, multiple peak solutions of R form, with higher and higher number of peaks as for discrete values of λ. The λ in this case has discrete specific value for a given β and a given number of peaks in the solution. The appearance of discrete eigen spectrum has already been discussed earlier by some authors [11, 49, 56]. We would here simply like to state that the oscillatory R in the center provides a wider domain from where electron density can be evacuated. These solutions, therefore, have a φ which is typically higher than R. The larger number of electrons available can then easily screen the radiation at the two edges.

6.3.1 Nonlinear Solutions for both electron and ion response

We choose a finite value of α to take account of ion participation in the formation of the nonlinear solutions of the coupled laser plasma system. We have chosen an unrealistic high value of the electron to ion mass ratio, namely $\alpha = 0.01$ here, for the purpose of convenience. For the true α value of 0.0005 also the solutions have been obtained, however, the changes in the value of λ to get various kinds of solutions are very small to be depicted clearly in a single figure.

The various possible solutions have been shown in Fig. 6.4. It is clear that a much richer variety is possible in this particular case. There are in fact six possible varieties which have been shown in the subplots (A) to (F) of Fig. 6.4. The central subplot (S) again identifies the possible values of the parameter λ and β for which each of these solutions can be obtained.

1. **Single peak solutions:**

   The first kind of solution is shown in the subplot (A). It is similar to the **single peak** solutions of Fig. 6.1. However, the permissible range of these solutions in the λ and β parameter space gets restricted when ions are involved. For instance, it can be observed that now there are no solutions possible below a critical value of $\beta = \beta_c$ bordering the left side of the upper two curves in the subplot **S** of Fig. 6.4.

2. **Flat top solutions:**

   In the neighbourhood of the forbidden low β values where the single peak solutions discussed in the previous paragraph cease to exist, a new variety of solution emerges. This has been denoted by blue colored thick line in the color online version of subplot (S) of Fig. 6.4. The arrow pointing from the alphabet **B** also depicts this region. The solutions have been shown in the subplot (B) of Fig. 6.4. These solutions are termed as the **flat top solutions** [57] as they have a central spatial region of flat profiles for all the fields, the vector potential R, scalar potential φ, the electron and ion densities n_e, n_i and their velocities u_e, u_i. It can be shown that the structure is almost quasineutral, n_e and n_i being very similar. The amplitude of R is considerably much higher than that of φ. It is worth noting that the field profiles for the flat-top solutions are broader than the neighbouring single peak solutions. The narrow spectrum of these flat-top solutions, in the eigen space, essentially provides a transition boundary between the localized single peak solutions and indefinitely extended wavefront solutions (shocks or dark solitons) [48]. In fact, it is found that there occurs a smooth transition from a single peak solution with a given group velocity to a flat-top solution with the same group velocity as the value of λ is decreased. The detailed characteristic features of these solutions along with their dynamical evolution studies have been presented in detail in one of our recent work [23]. These solutions were shown to get destabilized after several plasma periods through an interesting Brillouin backscattering process. The plasma being cold, the scattering occurs through a quasi mode for which the electron quiver velocity in the laser field plays the role of the effective temperature. We will discuss the details of the flat-top solutions in the next chapter.

3. **High amplitude single peak solutions:**

The incorporation of ion response causes another modification in the eigen spectrum of λ vs. β. The lower line enclosing the continuum single peak solutions instead of hitting the $\beta = 0$ axis, curves backwards and traces higher β values again, this time albeit for a different and lower value of λ. This essentially produce another branch of solutions which have been depicted in subplot (C) of Fig. 6.4. It can be seen from the plot that solutions for this second branch have much higher amplitudes than the usual single peak solutions observed in the topmost continuum domain of the λ vs. β. The electron density evacuation in this case is stronger compared to the **single peak** solutions of region **A**. Thus, these solutions have a larger space charge field in the central region. These solutions have an upper threshold in β beyond which no solutions are found. The last point of this curve has been shown by a thick red diamond symbol about which we will discuss later.

4. **Paired solution:**

   The fourth variety of possible solutions are the **paired solutions** depicted by subplot (D), which are also found when only electron species is involved, as we have already shown while discussing Fig. 6.1. These solutions also have a continuum spectrum hovering below region **A** and have been depicted by arrow pointing towards the character **D**.

5. **Multi-peak solutions:**

   The fifth variety are the **multi-peak** solutions (subplot (E)) with discrete spectrum shown by solid curve with full circle, open triangles, crosses and stars corresponding to 2, 3, 4 and 5 extremas in R respectively in the central subplot (S) of Fig. 6.4. As depicted in Fig. 6.1, here too, the solutions cease to exist below a certain group velocity β. However, in contrast to the previous case of **multi-peak** solutions shown in Fig. 6.1, the curve does not stop at certain β value but curves back to produce a second branch of solutions at lower λ values. This is very similar to the behaviour described above for the single peak structures. Thus, two distinct values of λ are permitted for solutions with a particular number of extremas in R when ions participate in the formation of the solutions. The solution corresponding to lower branch of λ has an upper threshold value of β beyond which there are no solutions. The last point of all these curves are special and have a singular form of the shape of cusp in their potential profile. We call them as **cusp solitons** and discuss their behaviour below.

6. **Cusp solitons**

   The typical single and multiple peak solutions have a structure in which the electron density is evacuated from the central region (where the light intensity peaks) and accumulate at the two edges of the structure whereas the ion density in all of these solutions peak at the central region.

   The upper threshold on β occurs when for these high amplitude solutions, the ion density reaches a wave breaking limit. At the wave breaking point, the solutions acquire an interesting shape of cusp. These cusp solutions occurring right at the ion wave breaking point were obtained by Bulanov *et al.* [43].

   The cusp solutions exist at the ion wave breaking point and have been shown in the subplot (F) of Fig. 6.4. At that point, the ion longitudinal velocity (which is maximum at the center of the soliton) hits the group velocity of the structure. Thus, the ion density becomes singular at the center of these solutions. Though the scalar potential φ remains continuous, its derivative shows a discontinuity. The eigen values λ and β for the cusp structures have been shown in the central subplot (S) of Fig. 6.4 by thick red diamonds and correspond to a point beyond which the second higher amplitude branch ceases to exist.

We see, therefore that in the presence of ion dynamics, additional three new kinds of solutions (viz., flat top, cusp and the second high amplitude branch of solutions) are possible which have no counterparts for the case of infinitely massive ions depicted in Fig. 6.1. The **high amplitude second branch for both single and multiple peak solutions** are essentially the second branch of solutions which appear due to ion species in addition to electrons also getting involved in the dynamics.

Out of these three new varieties, we have investigated the dynamical evolution characteristics of flat-top solutions. The result of this study will be reported in the next Chapter (Chapter 7).

6.4 Physical interpretation of soliton formation with both electron and ion response

The new features observed in the presence of response from heavier ion species are the appearance of (i) a lower limit of the group velocity below which the solitons do not exist, (ii) a second branch of high amplitude solutions for both single as well as multiple peak structures in R, and (iii) new additional variety of flat top solution and the cusp structures.

The Poisson equation, in the presence of ion response is governed by both

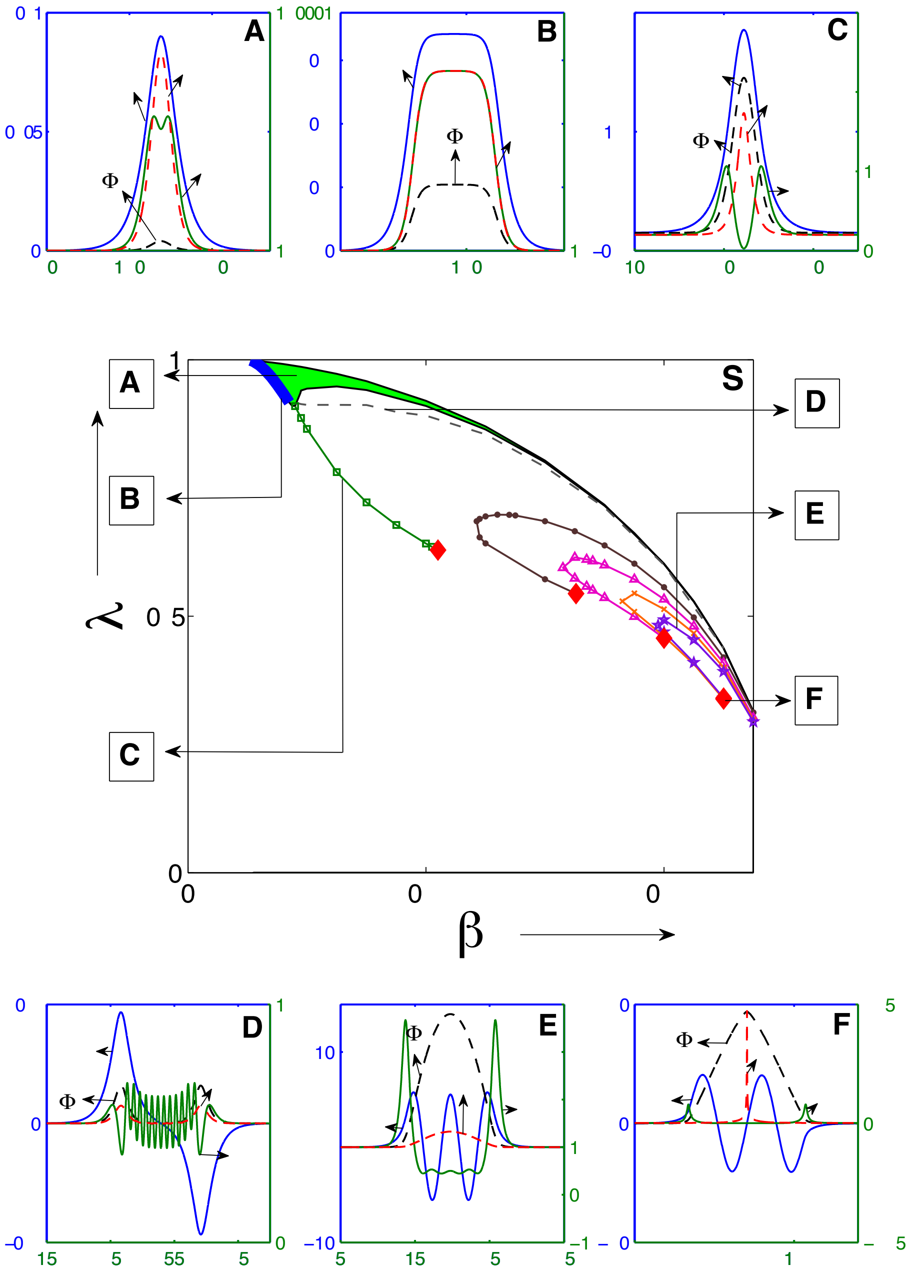

Figure 6.4: The $\lambda - \beta$ spectrum in subplot 'S' indicating the existence region for possible soliton solutions in movable ion case viz. the single peak solutions, flat-top solutions, single peak solutions with higher amplitudes, paired solutions, multi peak and cusp solutions tagged with 'A', 'B', 'C', 'D', 'E' and 'F' respectively. The profile of vector potential (R), scalar potential (φ), electron density (n_e) and ion density (n_i) for the solutions of each variety are shown in subplots with the same tags.

electron and ion densities. Thus, unlike the electron only case where the φ structure was determined by having $n_e < 1$ at centre and $n_e > 1$ at the edge, in the present case, this comparison is with respect to the ion density n_i at the center and the edge.

Thus, while the electron only case had solitonic structures only when the electrons were evacuated from centre, in this case, there can also be piling of electron density at the centre. The only condition should be that n_i is higher than n_e. This is indeed borne out from Fig. 6.4 subplot **A** and had also been analytically demonstrated in an earlier publication [45].

When the soliton speed is typically less than α, the ion dynamics will wipe out any possible electrostatic potential structure in the plasma. Thus, the possibility of electromagnetic radiation trapping in the localized region by the electrostatic potential is essentially ruled out at low group velocities. This is the physics behind the existence of a threshold on β below which the solitons do not form in this case.

A small amplitude expansion upto $\mathcal{O}(R^3)$ has clearly shown that the soliton amplitude approaches zero, when $\beta^2 = \alpha$. Just at the edge, where $\beta^2 = \alpha$, if one retains higher order expansion, the resulting equations yield the flat-top solutions. This has been enunciated in detail in one of our recent publications [23] and will be presented in next Chapter. This explains the formation of flat-top structures for the low β regime of single peak structures.

The multiple peak solutions have higher amplitude. At higher amplitudes, the ions can respond even if the group speed is comparatively higher. Thus, for multiple peak solutions (structures with increasing amplitude for higher number of peaks in R), the threshold of the group velocity β below which the solutions

Table 6.1: Scalar potential φ of cusp solitons for various β values.

β	λ	φ	$\beta^2/2\alpha$
0.420	0.6289599000	8.899	8.8200
0.652	0.5440000000	24.040	21.2552
0.800	0.4570000953	39.010	32.0000
0.900	0.3402846592	54.740	40.5000

cannot be found, increases. This is evident from Fig. 6.4.

The appearance of the second branch can be understood by realizing that for an electron - ion system having disparate masses, two different modes of response automatically exist. One, in which the electron and ion have an in-phase response. The other, when their response is out of phase. Typically, the in-phase response will occur at slower and/or weaker amplitudes of the scalar potential. The out of phase will occur at faster and/or higher amplitudes. Thus, at the same group velocity, when the ion and electron species respond in phase, a weak space charge field gets generated. This is the case, for instance, when at the centre both ion and electron accumulate. The solitons then, are of small amplitude and hence occur at higher values of λ (as per the explanation provided for the electron only case). When the two species respond out of phase, a greater space charge separation gets created. Thus, these structures form at lower values of λ. However, as one increases β, the amplitude of the solution keeps growing, the space charge potential keeps building up at the centre due to ion accumulation there. A situation then arises when $u_i \rightarrow \beta$, thereby meeting the condition for ion wave breaking. This happens for the second branch of each and every kind (differing in regard to the existence of number of peaks) of soliton structure. Beyond this β value, a smooth

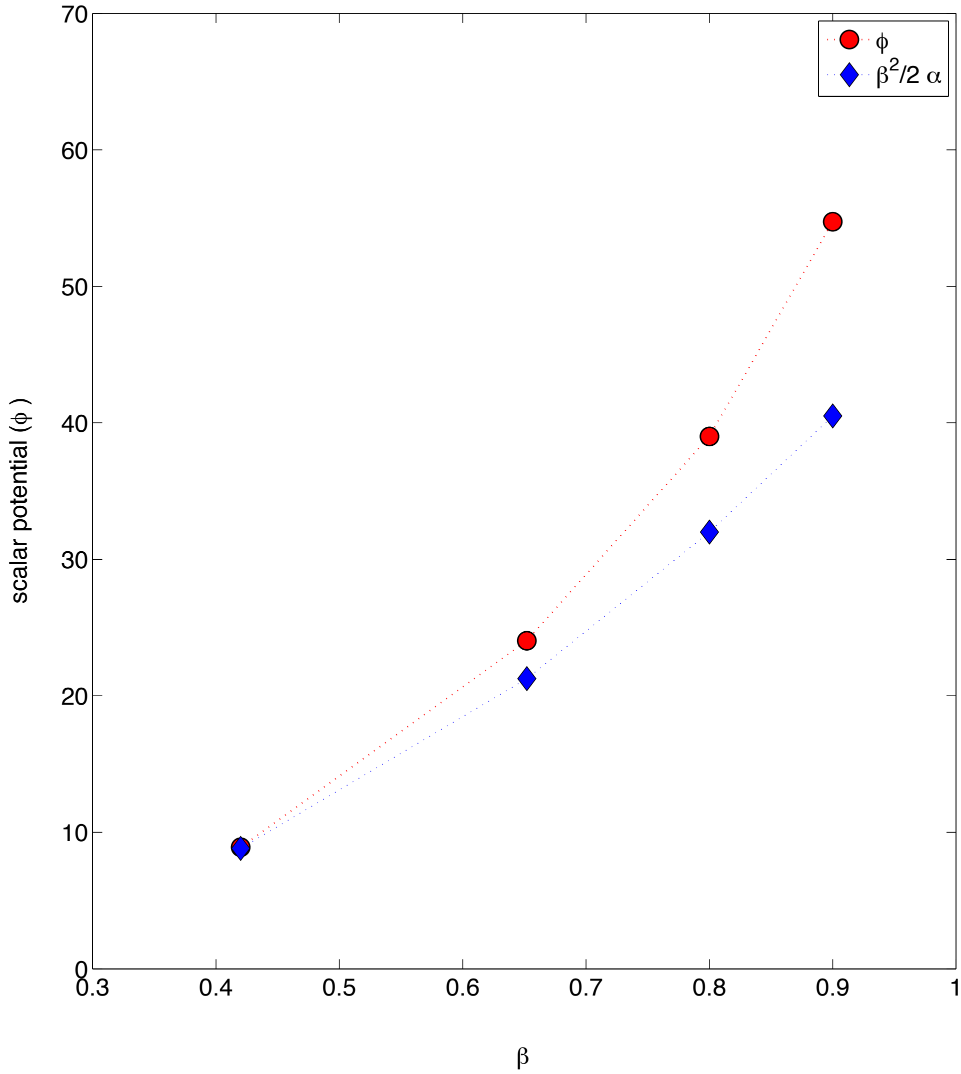

Figure 6.5: Plot showing cusps with higher amplitude of solitons form at higher β values. The filled red circle shows the scalar potential of the cusp solitons observed in simulations. Comparison with $\beta^2/(2\alpha)$ is shown alongside with blue diamond.

soliton solution ceases to exist.

At the ion wave breaking point, shown by red squares in Fig. 6.4, the potential takes the form of a cusp structure. The ion density tends to infinity as $u_i \to \beta$. This condition is met when $(1-\alpha\varphi)^2 = (1-\beta^2)(1+\alpha^2 R^2)$. Retaining the dominant orders, under the assumption of small α and small β limits, we have an approximate estimate of the wave breaking amplitude of the solutions as $\varphi = \beta^2/2\alpha$. Clearly, it is evident from Fig. 6.5 that the cusps with higher amplitude of solitons form at higher β values.

6.5 Summary

We have found a plethora of soliton solutions for a laser plasma interacting system. A detailed characterization of the eigen spectrum (in the frequency vs. the group velocity space) has also been provided. We show that when ion response (typically important for slow moving solutions and also for high power lasers) is taken into account, a much richer variety of solutions are possible. The ion dynamics forbids the formation of stationary nonlinear solutions. Bright soliton solutions are possible only above β_c. Furthermore, an additional feature of the solutions in this case is the emergence of a second branch of solutions at a lower λ value, which typically have larger amplitudes.

Some new physical phenomena resulting in new kinds of solutions which have no counterpart in the immobile ion case are also possible. One such feature is the possibility of ion wave breaking of the high amplitude second branch of solutions. The longitudinal velocity of ions maximize at the center of the structure. When this velocity becomes equal to the group velocity of the structure, the ion density profile becomes singular. There are no solutions possible beyond this value of β. However, solutions which are poised at the wave breaking point acquire interesting form. The singular ion density produces a cusp in the scalar potential.

Another new variety of solution that form in the presence of ion dynamical response are the flat- top solutions. These solutions have a very weak space charge field as $n_e \sim n_i$ and they form at the boundary separating the forbidden low group velocity regime for bright solitons and the continuum single peak solutions. The dynamical evolution and the susceptibility of these solutions to a backward scattering Brillouin process will be shown in the next chapter.

Chapter 7

Stability of relativistic electromagnetic flat-top solutions

In Chapter 6, detailed characterization of the 1-D laser pulse solitons along with the eigen spectrum of their formation in the parameter space in the absence and presence of ion dynamics has been presented. The inclusion of ion response in the study of relativistically intense electromagnetic laser pulse propagation in plasma yields certain new solitonic structures. A flat-top slow moving structure (for which the various fields have flat profile over a wide spatial range) is one such solution. In the present Chapter, the evolution of this particular flat-top soliton solution is studied in detail with the help of coupled fluid Maxwell set of equations. The study shows that the flat-top solution is unstable. The instability is characterized as the backward Brillouin instability for which the electron quiver velocity plays the role of the effective temperature.

7.1 Introduction

The interaction mechanism of the intense electromagnetic pulses with plasma is rich in a variety of nonlinear physics phenomena. Some of which has been explored [3, 7–14, 58] and a lot still needs to be examined. Several authors have sought exact nonlinear solutions in the form of propagating envelope solitary pulses for the coupled system of light field and the electron fluid. Some of these nonlinear solutions move very slowly and/or are even stationary. For these slowly moving solutions (and also in the eventuality of a major breakthrough leading to a next generation of high power lasers), the heavier ion species would also respond. Work along this direction has been initiated in some recent studies [42–55, 59].

It has been shown that the inclusion of ion response rules out the existence of static single peak solutions that have been obtained when electron species alone is considered [43]. The single peak solutions, for a continuum band in the parameter space of λ (associated with laser frequency defined in earlier studies [11]) vs group propagation speed β, do not touch the $\beta = 0$ axis, when ion response is incorporated. The single peak solutions now start from a small finite value of the curve defined by a critical value of $\beta = \beta_c$ (which is dependent on electron to ion mass ratio as well as the parameter λ). It has been shown in some papers [46, 48] that the gap from $\beta = 0$ to β_c supports dark solitonic structures. This transition from the dark to the bright soliton, however, does not occur drastically. Within a single peak and the dark soliton solutions, there exist new variety of spatially extended solutions having flat spatial profile at the centre. These solutions appear to be a deformation of the single peak solutions, as though their maxima have been spatially extended. The ion and electron density profiles are also observed to be identical for these solution, and hence the entire structure is essentially quasineutral.

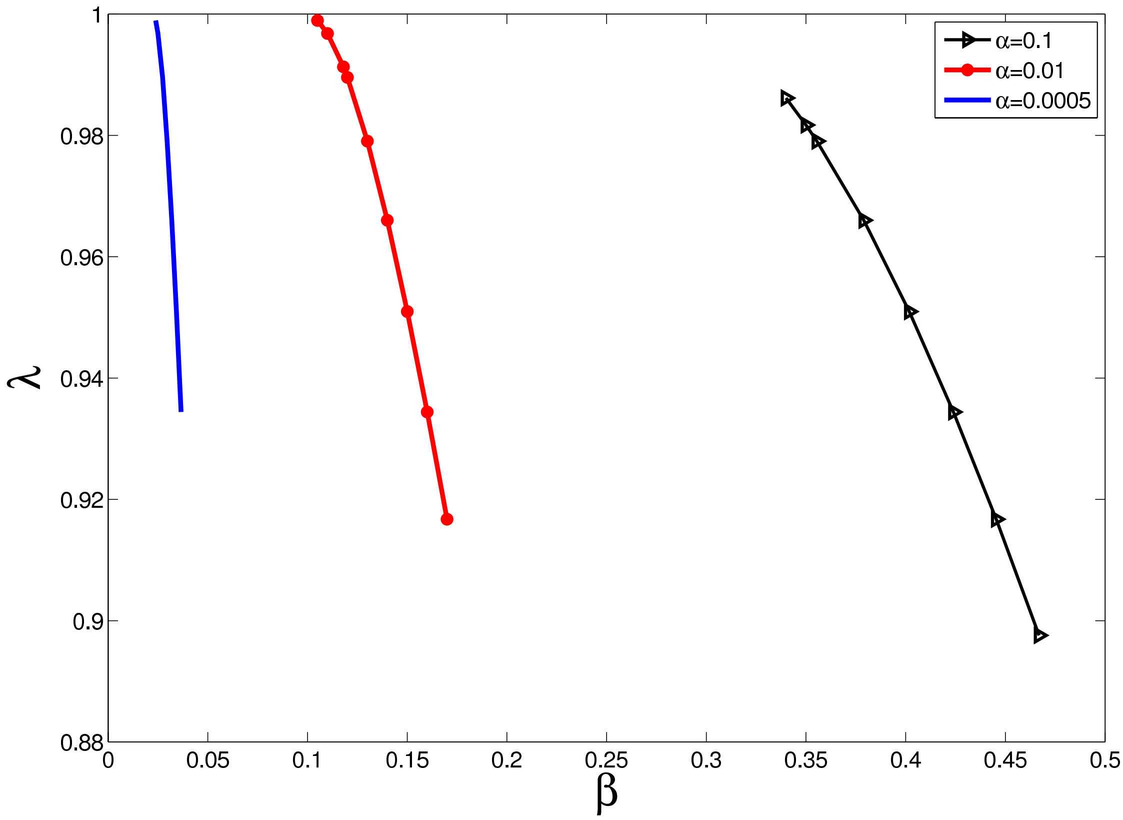

Figure 7.1: The plot of critical group velocity $\beta = \beta_c$ above which the single peak solutions are permissible for various values of α parameter.

We present in this chapter the numerical fluid simulation studies for these flat-top solutions. It is shown that they survive for a long time but later develop an instability. The instability eventually leads to the complete disintegration of the structure. The instability is shown to be linked to a Brillouin scattering process. In a cold plasma, there are no modes associated with ions. In this case, however, the scattering generates a quasi-ion mode where the role of temperature is provided by the quiver velocity of electrons in the electromagnetic field.

7.2 The flat-top nonlinear solution

The governing equations for an interacting laser plasma system discussed in Chapter 6 clearly represents a rich nonlinear set of equation. The numerical solutions of the coupled set of Eqs. (6.7) and (6.8) using the expression for u_e and u_i from Eqs. (6.9) and (6.10) leads to several varieties of exact one dimensional localized solutions. For a fixed value of the group speed β, only certain specific values of λ are permitted for obtaining solutions. These solutions have been obtained earlier by several authors [10–13, 42–45, 48].

In the presence of ion response, no stationary solution can be found. In fact, the continuum band (in λ vs β space) of single peak solutions [43] now has a forbidden gap from $\beta = 0$ to a critical value β_c. The curve $\beta = \beta_c$ as a function of λ for three different values of α is shown in Fig. 7.1 (in the λ vs β space) where α is the mass ratio,m_e/m_i.

It can be observed from the figure (Fig. 7.1) that for any given value of λ, forbidden gap shrinks as we decrease α. The plot for three different values of α, viz., 0.1, 0.01 and 0.0005 (the realistic value for electron-proton plasma) denoted by black line with triangles, red line with filled circles and solid blue line respectively have been shown in the figure.

For a fixed α, the single peak solutions exist only for $\beta > \beta_c$ for any given λ. At $\beta = \beta_c$, just as the single peak solution ceases to exist, a new variety of solutions emerge. These solutions are termed as the **flat-top solutions** [57] as they have a central spatial region of flat spatial profile for all fields as shown in Fig. 7.2 by the solid lines in various subplots corresponding to the profile of the vector potential R, scalar potential φ, the electron and ion densities n_e, n_i and their velocities u_e, u_i. It can be seen that the structure is quasineutral as n_e and

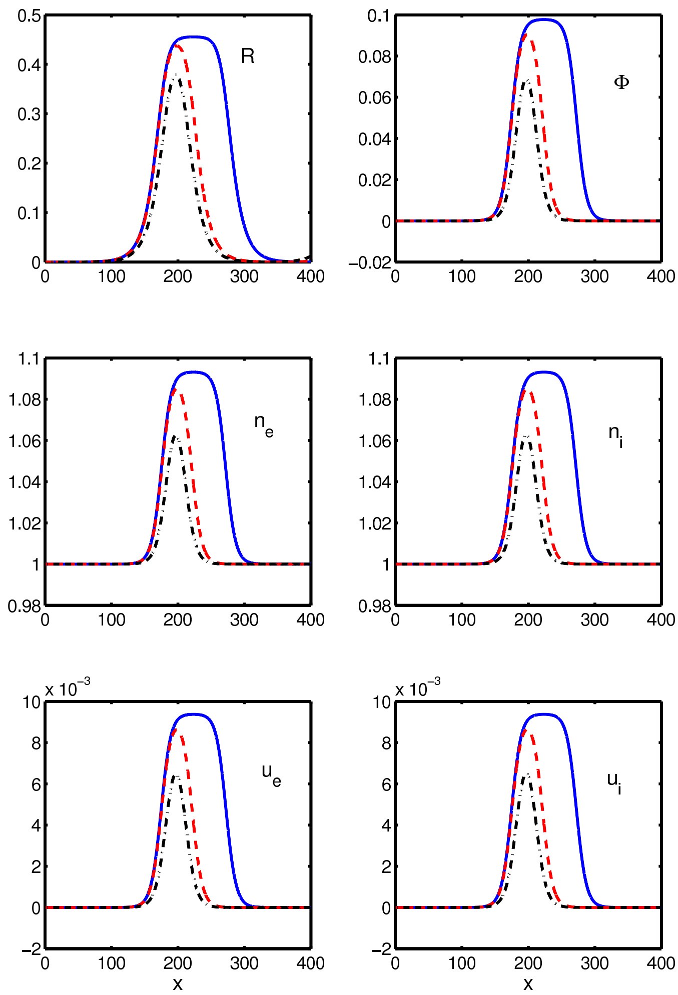

Figure 7.2: The profile of flat-top solution in various field are shown by solid lines in different subplot of the figure. The value of $\beta = 0.11$ and $\lambda = 0.99680694$ for this solution. For the same mass ratio $\alpha = 0.01$ and group velocity $\beta = 0.11$, as the value of λ is increased to 0.99682 and 0.997 the single peak solutions shown by dashed and dashed dot lines are obtained.

n_i are same. The amplitude of R is considerably much higher than that of φ. The flat-top structure in this plot corresponds to $\beta_c = 0.11$, $\lambda = 0.99680694$ and $\alpha = 0.01$. The width and the amplitude of these flat-top solitons get decided by the values of the spectral parameters β and λ. A flat-top solution with a lower

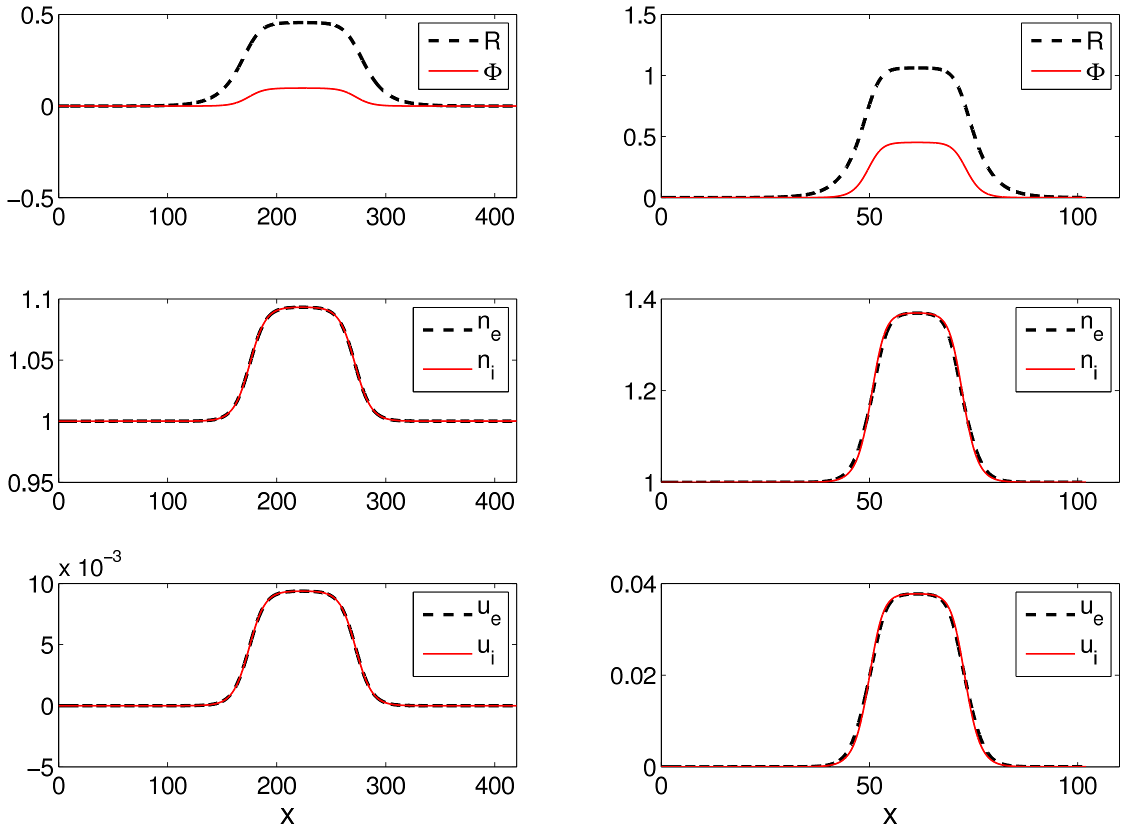

Figure 7.3: A comparison of two flat-top solutions with $\beta = 0.11$, $\lambda = 0.99680694$ and $\beta = 0.14$, $\lambda = 0.9660155$ has been shown in the left and right subplots of the figure respectively.

value of β (higher λ) has smaller amplitude and larger width than a solution with higher value of β (smaller λ). We compare two such solutions in Fig. 7.3.

The left column of subplots corresponds to $\beta = 0.11$ and $\lambda = 0.99680694$ whereas the parameter values for the right column of subplots are $\beta = 0.14$ and $\lambda = 0.9660155$. These solutions correspond to $\alpha = 0.01$ which is unrealistically high. In Fig. 7.4, we show how the flat-top solutions get modified as α is reduced to its realistic value.

The plot corresponds to a fixed value of $\lambda = 0.9167206$, the group velocity β is off course different when α is changed.

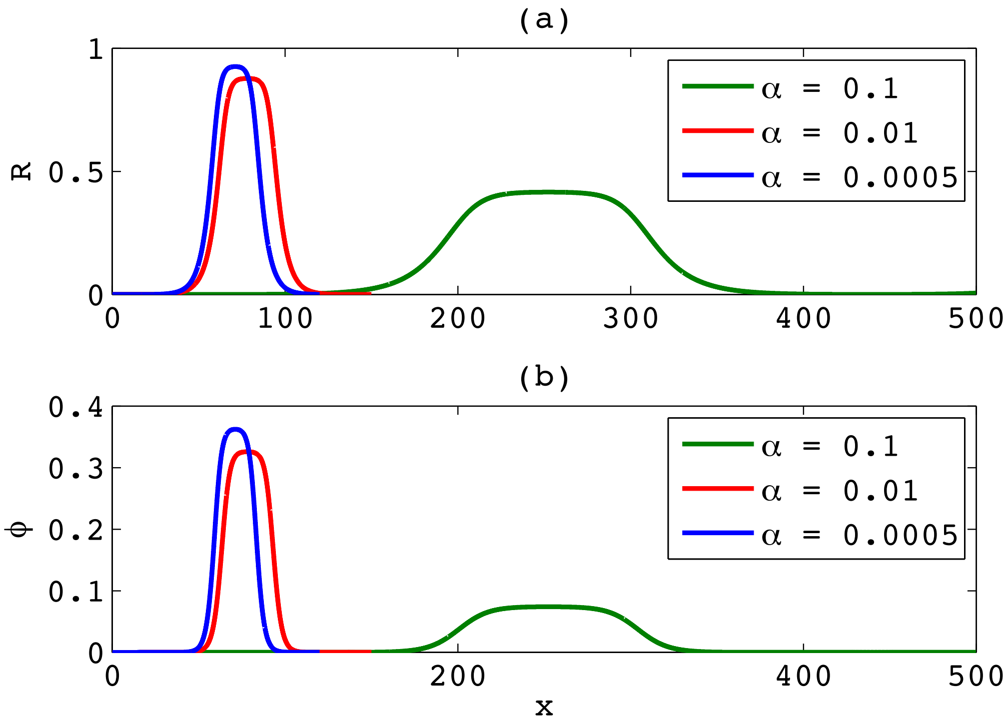

Figure 7.4: A comparison of flat-top solutions for different values of α parameter at fixed group velocity $\beta = 0.17$. Subplots (a) and (b) show the structure of scalar and vector potential respectively.

These flat-top solutions, in eigen space, provide a transition boundary between the localized single peak solutions and indefinitely extended wave-front solutions (shocks or dark solitons) [48, 60]. In fact, it is found that there occurs a smooth transition from a single peak solution with given group velocity to a flat-top solution with the same group velocity as the value of λ is decreased. This is clearly evident from the other plots shown in Fig. 7.2. The profiles shown by dashed and the dash-dot lines correspond to those solutions for which $\beta = 0.11$ (the same value as the flat-top structure), however, the value of λ is 0.99682 and 0.997 respectively.

The formation of the flat-top solutions at the transition boundary between single peak bright solitons and the dark structures at $\beta = \beta_c$ can be illustrated by a small mathematical analysis. We also provide an explanation for a particular relationship that λ and β have to satisfy for the formation of such flat-top structures. Such an analytical study is, however, carried out in the small amplitude limit. The observations show that the small amplitude solutions (both flat-top and single peak solitons) are essentially quasineutral, i.e. $n_e \approx n_i = n$. This also implies $u_e \approx u_i = u$ from the continuity equation of the two species.

Using the quasi-neutrality condition and eliminating φ from $\gamma_e(1-\beta u_e)-\varphi = 1$ and $\gamma_i(1 - \beta u_i) + \varphi\alpha = 1$ we get

$$(\gamma_i + \alpha\gamma_e)(1 - \frac{\beta^2(n-1)}{n})) - (1+\alpha) = 0 \qquad (7.1)$$

At low amplitude, the density response being weak one chooses, $n = 1 + \epsilon$, where ϵ is a small parameter. We then obtain an expression for ϵ from Eq. (7.1) as

$$\epsilon = [(1+\alpha) - (\gamma_i + \alpha\gamma_e)]/[(1-\beta^2)(\gamma_i + \alpha\gamma_e) - (1+\alpha)]$$

In the weakly relativistic limit, we then expand $\gamma_e \approx 1 + R^2/2 + ...$ and $\gamma_i \approx 1$ for the small amplitude flat-top soliton solutions. This yields

$$\epsilon = \frac{\alpha R^2}{2\beta^2(1+\alpha)} + \frac{\alpha^2 R^4(1-\beta^2)}{4\beta^4(1+\alpha)^2} + ... \tag{7.2}$$

$$\frac{n}{\gamma_e} = 1 - \frac{R^2}{2} + \frac{\alpha R^2}{2\beta^2(1+\alpha)} + \frac{\alpha^2 R^4}{4\beta^4(1+\alpha)^2}(1-\beta^2) - \frac{\alpha R^4}{4\beta^2(1+\alpha)} + ... \tag{7.3}$$

$$\frac{n}{\gamma_i} = 1 + \frac{\alpha R^2}{2\beta^2(1+\alpha)} + \frac{\alpha^2 R^4}{4\beta^4(1+\alpha)^2}(1-\beta^2) + ... \tag{7.4}$$

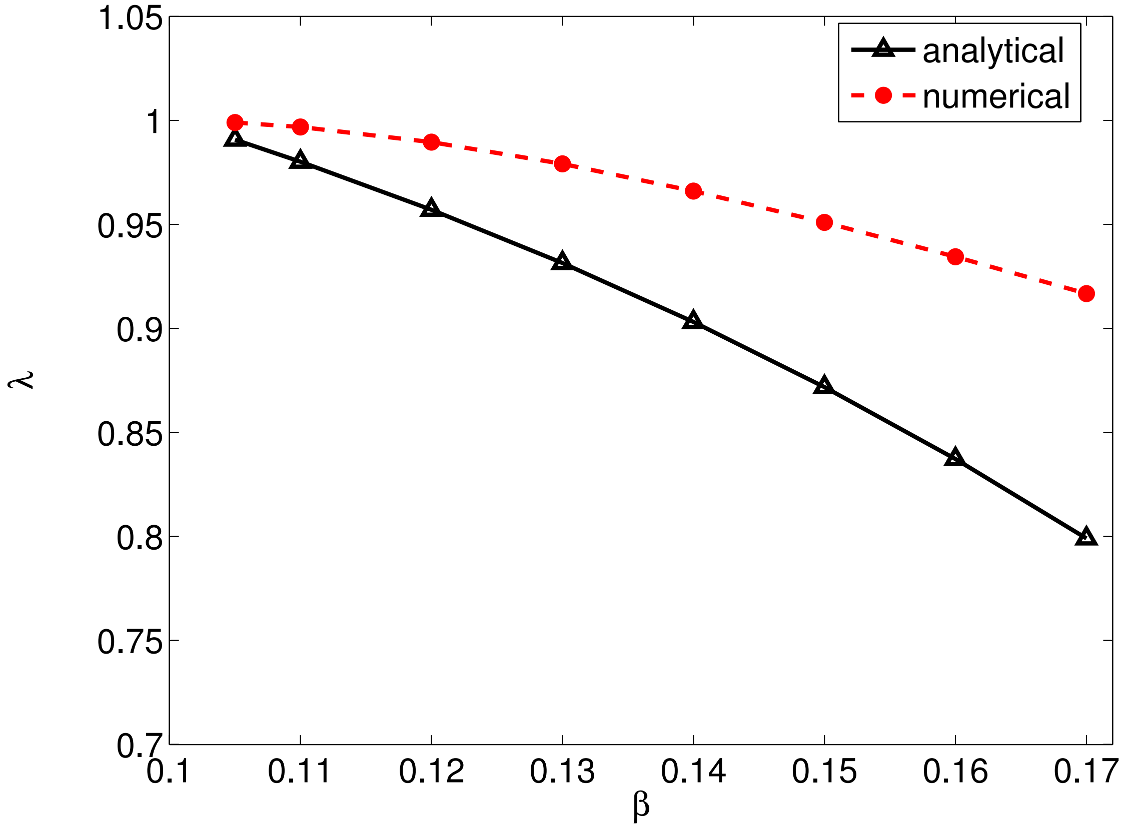

Figure 7.5: A comparison of λ vs β curve for the analytical and numerical values at $\alpha = 0.01$.

We take the conventional case of $M = 0$, and use the above expansion for n/γ_e and n/γ_i in Eq. (6.2). In an earlier work by Poornakala *et al.* [46] the low amplitude dark and bright solitonic structures were obtained by seeking such an expansion for a finite temperature plasma. In that work, only terms upto order R^3 were retained to get an expression of the form $R'' + AR + BR^3 = 0$. Considering the limit of a cold plasma, their study shows that the transition from dark to bright form of the solution occurred when $\beta = \beta_c = \sqrt{\alpha}$. At $\beta = \beta_c$, it can be shown that the coefficient B goes to zero. Thus, as $\beta^2 - \alpha$ changes sign, the sign of coefficient B changed giving rise to bright and dark solitonic structures. However, we show here that if we retain higher order terms in the expansion, flat-top solutions form at this boundary. Thus, retaining the next higher term in the expansion we obtain the following equation

$$\begin{aligned} R'' + \frac{R}{1-\beta^2}\left[\frac{\lambda^2}{1-\beta^2} - (1+\alpha)\right] + \frac{R^3}{2(1-\beta^2)}\left[\frac{\beta^2-\alpha}{\beta^2}\right] \\ + \frac{R^5}{4(1-\beta^2)}\left[\frac{\beta^2\alpha(1+\alpha)-\alpha^2}{\beta^4(1+\alpha)}\right] = 0 \end{aligned}$$

which has the form of $R'' + AR + BR^3 + CR^5 = 0$, where the coefficients are

$$A = \frac{\lambda^2 - (1+\alpha)(1-\beta^2)}{(1-\beta^2)^2}$$

$$B = \frac{\beta^2 - \alpha}{2\beta^2(1-\beta^2)}$$

and

$$C = \frac{\beta^2\alpha(1+\alpha)-\alpha^2}{4\beta^4(1-\beta^2)(1+\alpha)}$$

It should be noted that by ignoring terms of higher power in α, we regain the expression obtained by Poornakala *et al.* [46]. We integrate once to achieve

$$\frac{R'^2}{2} + A\frac{R^2}{2} + B\frac{R^4}{4} + C\frac{R^6}{6} = K \tag{7.5}$$

The constant K can be chosen to be zero for localized bright solutions including the flat-top structures which vanish at $\pm\infty$. Hence, using $K = 0$ and making the substitution $f = R^2$ we get

$$\frac{f'^2}{f^2} + \frac{8C}{6} f^2 + 2Bf + 4A = 0 \tag{7.6}$$

This is an elliptic differential equation. The positive solution of this equation is

$$f(\xi) = \frac{2 f_1 f_2}{(f_1 + f_2) - (f_1 - f_2) \cosh\left(2\kappa\sqrt{f_1 |f_2|}\xi\right)} \tag{7.7}$$

where $\kappa = \sqrt{C/3}$ and f_1, f_2 are the solutions of the quadratic equation:

$$\frac{8C}{6} f^2 + 2Bf + 4A = 0 \tag{7.8}$$

When $f_1 \to f_2$, we get flat-top solutions as has been shown by Akhmediev *et al.* [61]. For any other arbitrary value of f_1 and f_2 one obtains single-peak soliton solutions. When $f_1 \to f_2$, we have $B^2 = 16AC/3$ which in turn gives us:

$$\lambda^2 = (1 + \alpha)\left(1 - \beta^2\right)\left[1 - \frac{3}{16\alpha} \frac{\left(\beta^2 - \alpha\right)^2}{\beta^2 (1 + \alpha) - \alpha}\right] \tag{7.9}$$

This is the eigen value condition for small amplitude flat-top structures. This eigen value condition (λ vs β curve) in comparison with the numerical values for the flat-top structures has been shown in Fig. 7.5. It can be seen from the plot that the eigen values obtained analytically are consistent with the numerical values in the small β limit. This is in accordance with the approximations of weakly relativistic solitons. Deviation at large β values is due to the approximations made in deriving the analytical values. The flat-top solutions form in the neighbourhood of the

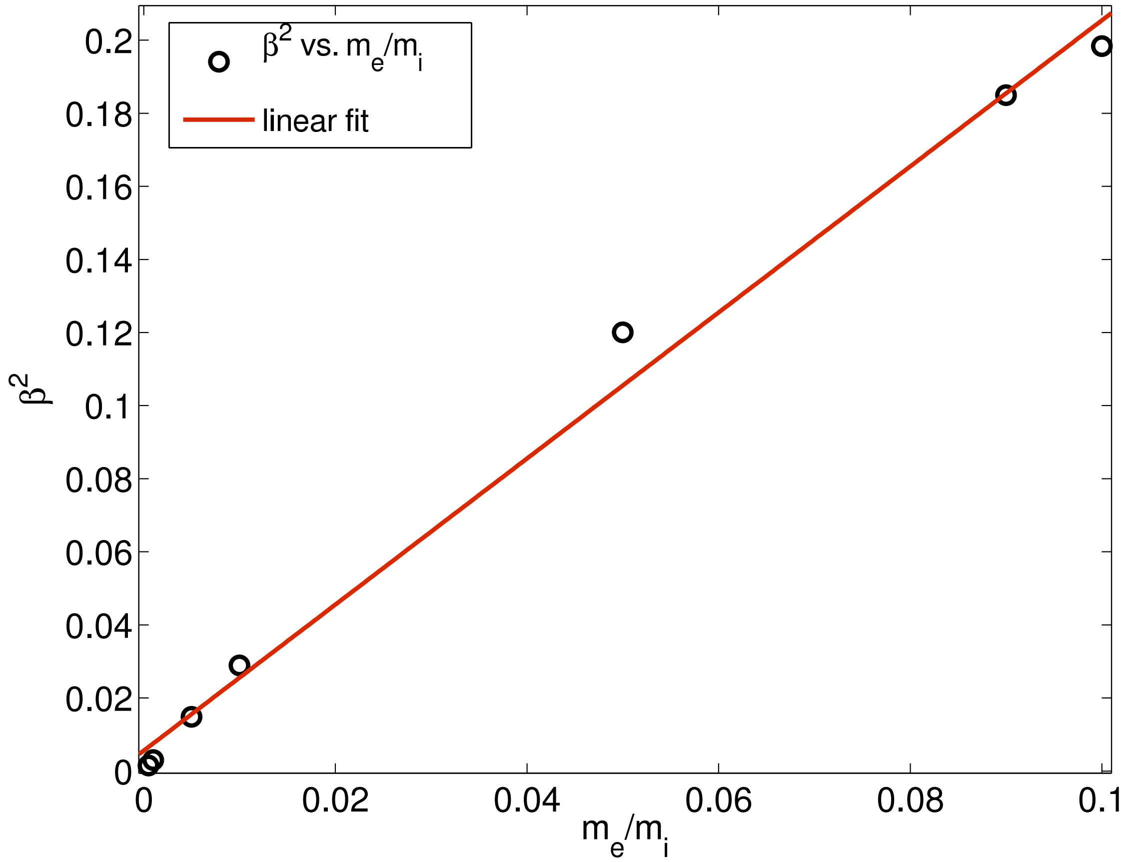

Figure 7.6: A plot of β^2 vs α for the flat-top solutions showing a linear relation between β^2 and α.

condition $\beta^2 \to \alpha$. This has been shown in Fig. 7.6, where the plot of β^2 vs α for various flat-top solutions have been shown as hollow circles.

The points fall on a straight line as expected. If we look at the coefficients A, B and C carefully, we find that these coefficients have the same order for any value of α for $\beta^2 \to \alpha$, where the flat-top structures form. Thus, at $\beta \approx \sqrt{\alpha}$, the boundary which separates dark and bright solitons in reference [46] there exists an infinitesimal domain of $\beta_2 = \alpha + \delta$ where the flat-top solitons form.

We next address the question of the stability of these flat-top solutions. Analytically this can be addressed by using the Vakhitov-Kolokolov criteria [62, 63]. In this case, the soliton solution will be unstable if

$$\frac{dP_0}{dA} > 0 \tag{7.10}$$

where $P_0 = \int_{-\infty}^{\infty} R^2 d\xi$. The expression for $P_0(\lambda)$ for the analytical flat-top soliton solution from Eq. (7.7) can be evaluated and is given by

$$P_0\left(\lambda\right) = \frac{2k_1}{\kappa} \tag{7.11}$$

where k_1 is a positive constant. Here, we have taken positive values of f_1 and f_2 and $f_1 < f_2$. Thus

$$\frac{dP_0}{dA} = \frac{2k_1}{\kappa^2}\left(\frac{1}{2\sqrt{(3C)}}\right)\frac{dC}{dA} > 0 \tag{7.12}$$

Hence, according to the condition (7.10), the flat-top soliton solutions turn out to be unstable. We have also evaluated P_0 for the exact numerical soliton solutions and checked its variation with respect to the parameter A. This has been shown in Fig. 7.7. The curve of P_0 vs A clearly demonstrates that $dP_0/dA > 0$, showing that the solutions can be unstable.

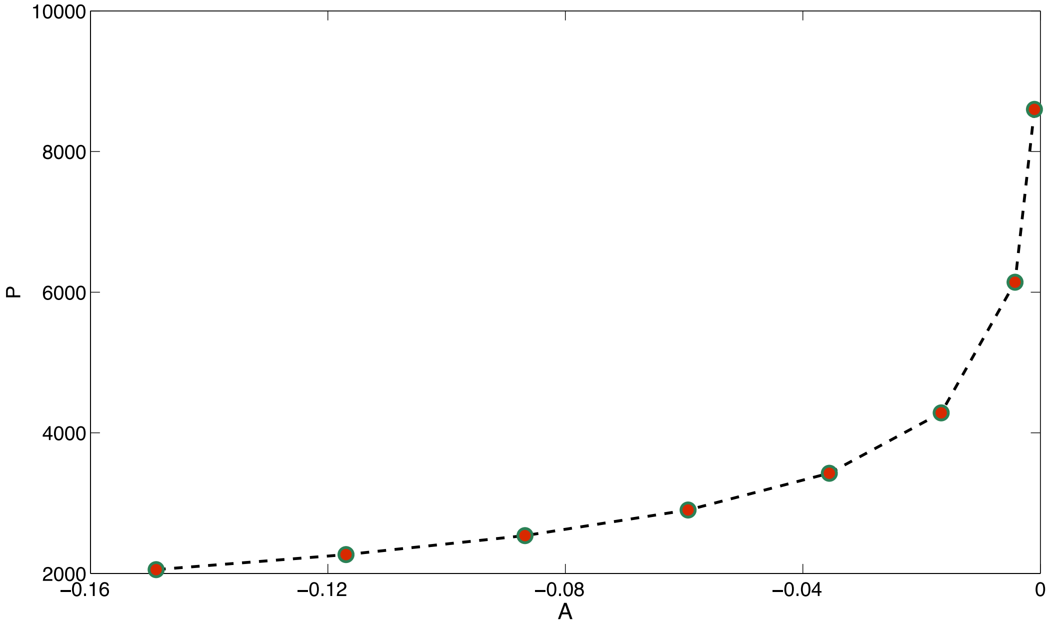

Figure 7.7: A plot of P_0 vs A for the flat-top solutions showing a positive slope.

In the next section, we describe the dynamical trait of this particular variety of solution in detail. Our numerical simulation studies demonstrate that the flat-top solutions persist for several plasma periods. However, later they exhibit a development of an instability as a result of back scattering process.

7.3 Dynamical evolution of the flat-top solutions

For the numerical simulation studies, electron and ion continuity and parallel momentum equations have been solved using the flux corrected scheme of Boris *et al.* [64]. The second order time differentiation for the vector potential has been tackled by separating it into two first order equations. We choose the field profile of the flat-top solution as our initial condition for investigation.

The various stages of the evolution of the fields R and φ for a particular flat-top

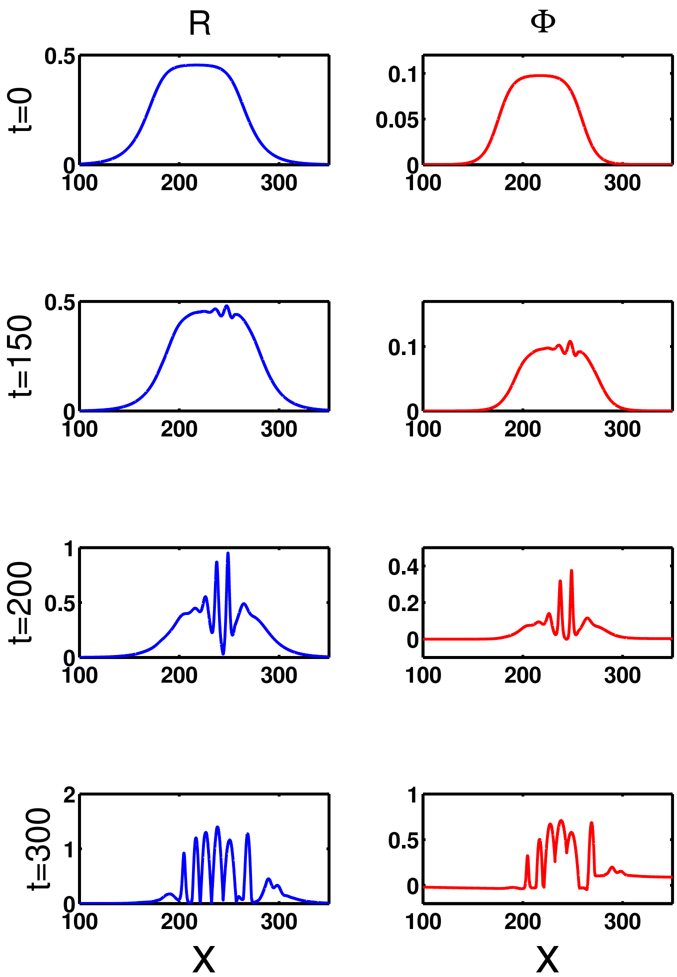

Figure 7.8: The evolution of the fields R and φ for a flat-top solution with $\beta = 0.11, \lambda = 0.996807$ has been shown at various times. The appearance of the unstable perturbations at the front edge of the structure and then propagating backwards can be observed. The entire structure disintegrates subsequently as a result of this instability.

solution with $\beta = 0.11, \lambda = 0.996807$ has been shown in the subplots of Fig. 7.8. One observes that the solution propagates without perceptible distortion for > 100 plasma periods. At a later time it can be observed that the front end of the solution gets distorted. The disturbance seems to travel backwards, grows and engulfs the entire solution at later time. In Fig. 7.9, the amplitude of the perturbed fields R and φ at $t = 100$ electron plasma periods has been shown.

The thin dashed dotted line shows the electron density profile of the original

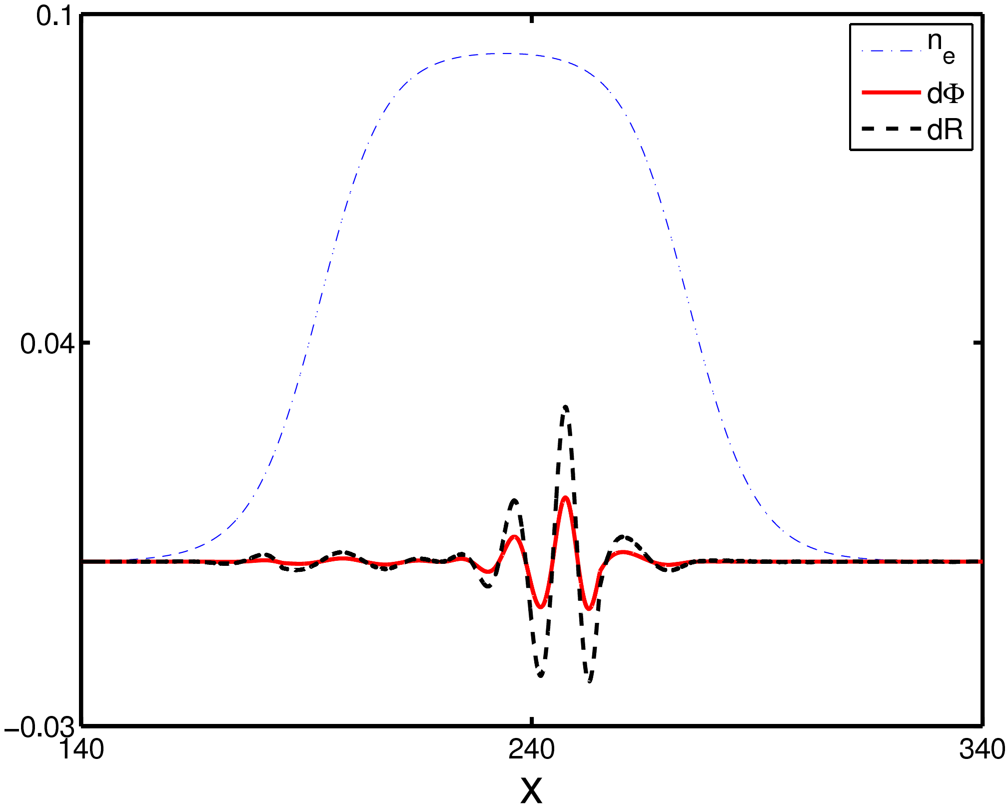

Figure 7.9: A comparison of the perturbed scalar φ and vector R potential in space which shows that their length scales are typically identical. The thin dashed dot line shows the original flat-top structure. It can be seen that the perturbations typically maximize at the front edge of the flat-top structure.

flat-top solutions. This has been shown to place the location of the perturbation with respect to the original structure at this time. It is interesting to note that the perturbed scalar φ and vector R potentials have typically identical scales.

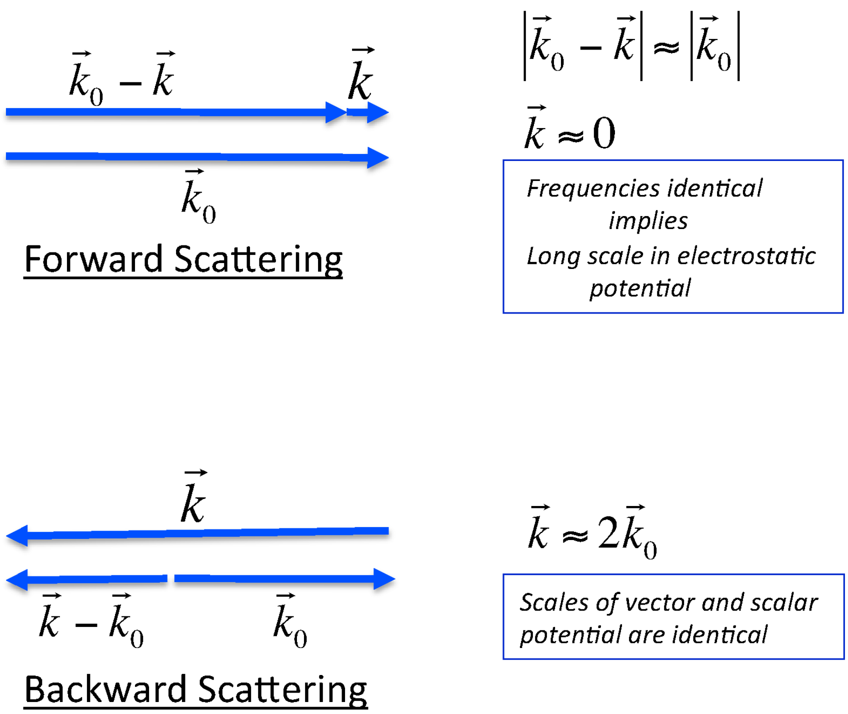

Figure 7.10: Schematic showing the mechanism of forward and backward scattering in 1-D

Let us now comment on the possible instability mechanism which is responsible for the break up of the flat-top solutions. If we treat the light wave associated with the structure as the pump wave, then under the constraint of 1-D dynamics it can either suffer a forward and /or backward scattering [see Fig. 7.10] . Such a scattering process can generate either a plasma wave and/or a wave associated

Table 7.1: Growth rate for quasi-mode of Brillouin scattering

β	λ	ω_0	k_0	v_{os}	Γ_{kruer}	Γ_{kaw}	Γ_{Liu}	$\Gamma_{numerical}$
0.105	0.99894732	1.0101	0.1061	0.2933	0.0656	0.1202	0.0931	0.04844
0.11	0.99680700	1.0090	0.1110	0.4137	0.0825	0.1512	0.1061	0.06552
0.12	0.98956944	1.0040	0.1205	0.5638	0.1012	0.1855	0.1208	0.10643
0.13	0.97907410	0.9959	0.1295	0.6594	0.1120	0.2053	0.1304	0.14585
0.14	0.96601600	0.9853	0.1379	0.7274	0.1190	0.2182	0.1375	0.18114
0.15	0.95096800	0.9729	0.1459	0.7814	0.1241	0.2275	0.1434	0.22129
0.16	0.93440570	0.9590	0.1534	0.8186	0.1277	0.2340	0.1482	0.19200
0.17	0.91672060	0.9440	0.1605	0.8465	0.1300	0.2383	0.1523	0.30170

with ion dynamics. In the case of forward scattering (the scattered radiation being of almost similar frequency), the scalar potential reflecting the scattered plasma and/or ion wave will have a wave length which would be much longer than the wavelength of the scattered radiation field. In our case, we see from Fig. 7.9 that this is not the case. The two scales are almost identical. This suggests that it is a backward scattering process. We now address the question whether the instability scatters a plasma wave and/or a wave associated with ions. The plot in Fig. 7.11 shows that the ion and electron perturbed densities are in phase.

This suggests that the scattering is from a slow wave associated with ion response. There is, however, no conventional ion wave that can be supported in a cold plasma medium. We feel that the quiver velocity of the electrons play the role of effective temperature for the ion wave produced in the medium which scatters the pump radiation. This suggests that the instability associated with the flat-top solitons is essentially a Brillouin backscattering process.

To put this assertion on a firmer footing, we evaluate the numerical growth rate for various flat-top solutions identified by various distinct values of the group velocity. This has been shown in Fig. 7.12 by triangular data points. We have also

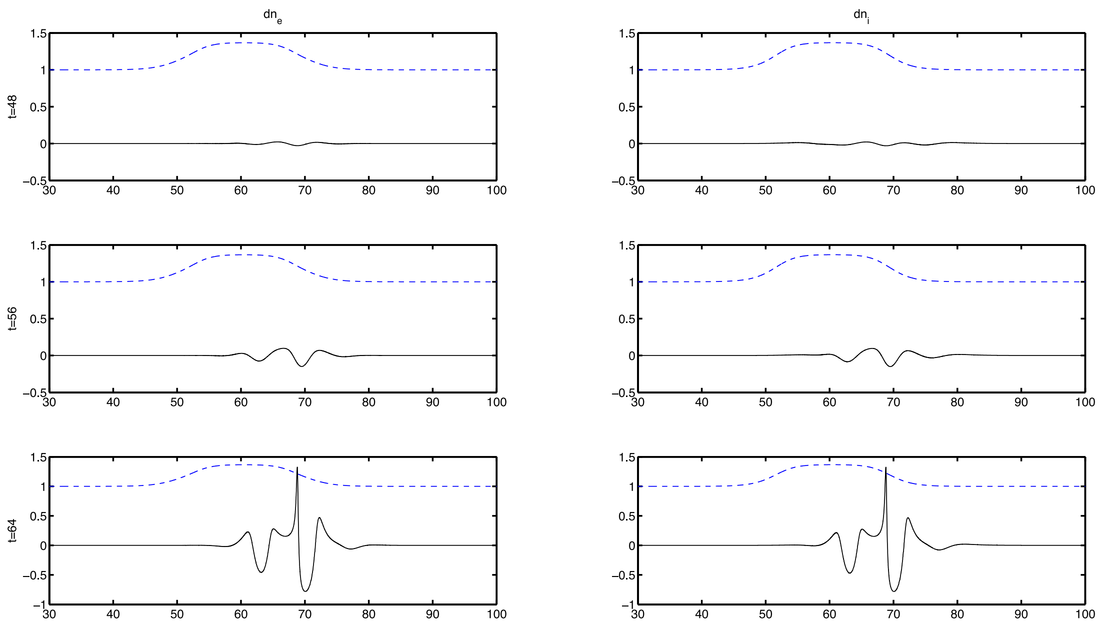

Figure 7.11: The perturbed ion and electron densities during the linear phase of the instability has been shown. The figure clearly shows that the density perturbations are in phase.

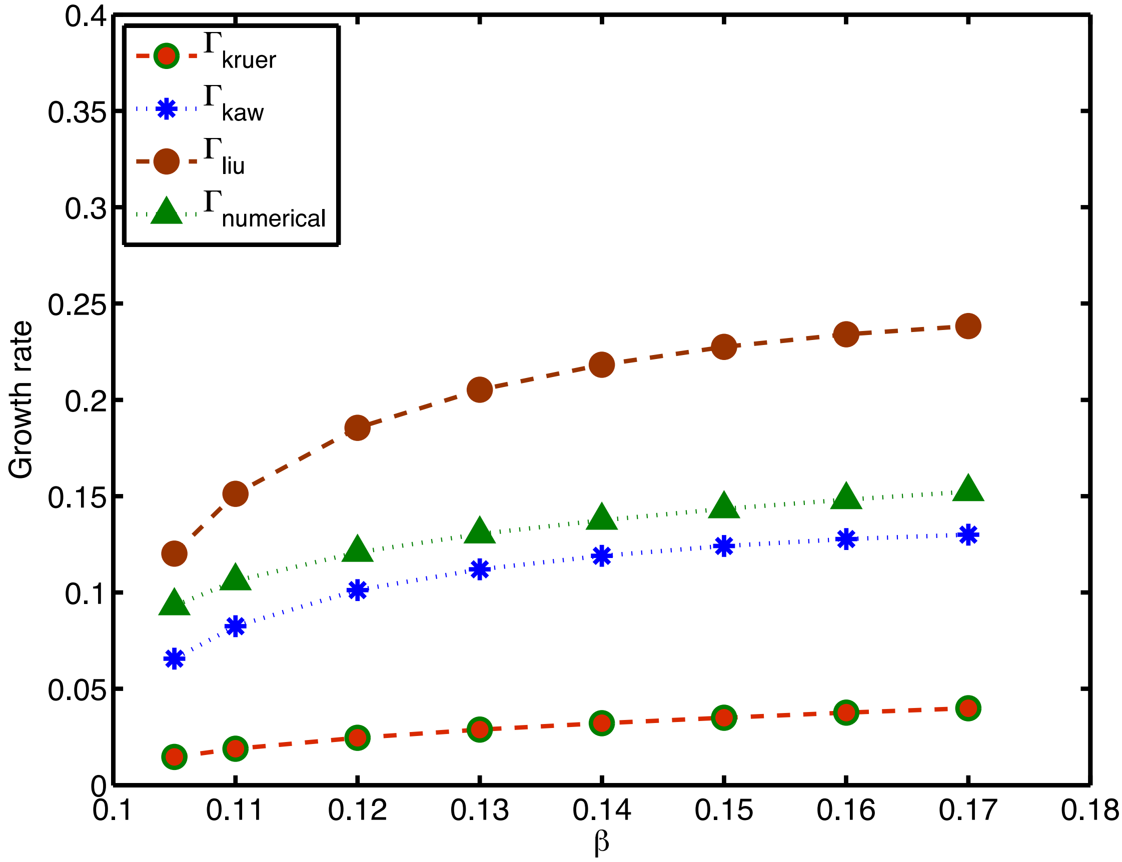

Figure 7.12: A comparison of the numerically obtained growth rate with the analytical expressions [15–17].

alongside shown the analytical growth rate of the Brillouin backscattering process obtained from the expression of Liu *et al.* [15]. In the strong field limit, the growth rate for quasi-mode of Brillouin scattering is given by:

$\mathbf{\Gamma_{Kruer}} = (\sqrt{\mathbf{3}}/\mathbf{2})(\mathbf{k_0^2 v_{os}^2}\omega_{\mathbf{pi}}^{\mathbf{2}}/2\omega_0)^{1/3}$

$\mathbf{\Gamma_{Kaw}} = \mathbf{2^{1/3}}(\mathbf{v_{os}^2}\omega_{\mathbf{pi}}^{\mathbf{2}}\omega_{\mathbf{0}})^{1/3}$

$\mathbf{\Gamma_{Liu}} = (\sqrt{\mathbf{3}}/\mathbf{2^{1/3}})(\mathbf{k_0 v_{os}}\omega_{\mathbf{pi}}^{\mathbf{2}})^{1/3}$

The analytical and numerical growth rates show a decent match. We notice that the approximate analytical growth rate expression obtained by different authors [15–17] for this instability, differ from each other typically by similar order, due to the nature of the approximation. In the light of which the agreement between numerical and analytical estimates are fairly reasonable.

7.4 Summary

The nonlinear exact solutions of the coupled laser plasma system obtained by ignoring ion response predict the existence of stationary as well as slowly moving structures. For these structures, it would be incorrect to a-priori neglect the ion dynamical response. The incorporation of ion response rules out the existence of static solutions. Solutions are permissible only beyond a certain critical value of group speed. For group speeds below this value there are no permissible bright solitons. At the critical group velocity, a new kind of structures are permitted by the equations. These structures have a flat and broad spatial profile for all concerning fields. A detailed characterization of these flat-top solutions has been provided in this chapter.

We have investigated in this chapter the dynamical evolution of these flat-top solutions. It is observed that these solutions survive for several plasma periods but ultimately develop an instability which breaks the structure. This particular destabilization process has been identified as the backward Brillouin scattering process.

It should be noted that the coupled laser plasma system permits a wide variety of solutions. These structures can have practical relevance provided questions related to their accessibility, stability and the time scale of growth for unstable case are understood and explored thoroughly. Our dynamical evolution study has been motivated towards addressing these issues. In an earlier work [56], it has been shown that the high amplitude multiple peak solutions are unstable to forward Raman scattering process. In the present work, we have shown that the flat-top variety of solutions observed with ion dynamical response develop a backward Brillouin scattering instability.

Chapter 8

Summary of the thesis and Scope for Further Research

The development of high power lasers and fast diagnostics have opened up the possibility of exploring an entirely new regime of plasma behaviour. This is associated with the fast electron time scale response of the medium. The goal of this thesis is to theoretically look into some of these phenomena in plasmas. In this respect, we have chosen two specific phenomena for our study, namely (i) the KH like instabilities when the electron flow has a shear configuration and (ii) the coupled laser plasma system. Issues pertaining to these two phenomena have been addressed in the thesis which we summarize below. The future scope has also been outlined.

8.1 Summary of the thesis

The two phenomena chosen for study in the thesis are interesting from fundamental point of view and they also have relevance in a variety of frontier applications such as fast ignition concept of inertial confinement fusion studies, plasma switches, fast magnetic reconnection etc.

8.1.1 Governing Models

We have chosen to depict the fast electron time scale phenomena by employing a relativistic fluid model for the electron species. The ions are typically chosen to provide merely a stationary background as the relevant times are too fast for their response. The Maxwell's equations provide a coupling of the electron fluid evolution to the field evolution. A detailed description of such a governing model has been provided in the second chapter of the thesis. The various simplifications in different limits have also been discussed in detail. These model set of equations have been employed in the subsequent chapters to explore certain physical phenomena.

8.1.2 Physics of flow shear driven instabilities in EMHD

A sheared flow of electron fluid produces instabilities which is akin to the Kelvin - Helmholtz instability of the neutral fluid. However, since the electron fluid is a charged fluid, the magnetized character of the fluid produces some interesting differences with the pure KH mode of the neutral fluid. Furthermore, the flow of the charge fluid also defines the current in the plasma medium. The current shear flow driven instabilities can also arise in this context. Therefore, the instability has a combined characteristics. In Chapter 3, these issues associated with the shear driven instability have been discussed in detail. A physical understanding of the instability has been provided. The free energy source of the flow has been identified. Simplified physical reasoning has been given for understanding the characteristic traits of the instability in terms of the threshold wavenumber, the typical order of magnitude of the growth rate etc.

8.1.3 Electron velocity shear driven instability in relativistic regime

The electron velocity shear driven instability has been often invoked in the context of fast ignition laser fusion scheme. However, the electrons involved in the shear flow in this case may have relativistic energies. An interesting aspect to notice is that the sheared electron flow would have an additional manifestation in the relativistic case as the relativistic mass of the fluid would also have a sheared configuration. We have explored the role of this effect on the growth rate. In a weakly relativistic case, the growth rate of the KH mode shows reduction. The unstable wavenumber domain also shrinks. This can be understood by realizing that the increase in the inertia makes the fluid more rigid to be susceptible to the KH instabilities.

However, at higher flow speed, an interesting effect emerges. The growth rate again increases and the unstable wave number domain also expands. Our detailed study has shown that the instability exhibits these novel features due to the sheared relativistic mass of the medium. Chapter 4 contains a detailed discussion of this effect. This clearly suggests that in the context of fast ignition where the flows can be strongly relativistic, this instability can still have a role primarily arising through the shear in the relativistic mass factor.

We have also carried out a perturbative analytical treatment in the weakly relativistic domain. The numerically observed growth rate and the threshold wavenumber change are seen to compare well with the analytical results obtained from perturbative calculations. This has been discussed in Chapter 5.

8.1.4 Relativistic electromagnetic soliton structures in a cold plasmas

The electron response is typically triggered in plasma by a laser. Keeping this in view we have investigated the coupled system of laser plasma. In particular, we have studied the possible coherent solutions that can be permitted by such a coupled system in a simplified 1-D scenario in the second part of the thesis, comprising Chapter 6 and 7.

A detailed characterization of the possible one dimensional exact solutions of circularly polarized electromagnetic pulse in a cold, collisionless plasma has been provided. It should be noted that though the laser field has typically a fast evolution time scale associated with its frequency, in the plasma medium it can get trapped and form structures moving at very slow group velocity. For such slow moving structures ion response also becomes crucial. It was shown that the ion involvement in the dynamics results in several new varieties of solutions. A comprehensive description and physical understanding of the possible solutions in the parametric domain of laser frequency vs. the group speed of the structure has been provided in Chapter 6.

8.1.5 Evolution of flat top soliton

A special variety of soliton which forms in the context of the presence of ion response, has a flat top at the centre for all the concerning fields. A detailed evolution study of this structure was carried out using 1-D simulations of the coupled set of fluid Maxwell system with a flux corrected code. The flat top structure was found to be unstable at ion time scales. The instability was identified as the backward Brillouin scattering instability. In a cold plasma, this occurs as the electron quiver velocity in the laser field plays the role of effective temperature. This study has been presented in Chapter 7.

8.2 Future Directions for Research

We have studied two specific problems in the context of plasma behaviour occurring at the fast electron time scales. We identify below the aspects which are open for further investigation in these two set of phenomena.

8.2.1 Electron velocity shear driven instability

- We have carried out the linear stability analysis of relativistic shear driven flow which is valid as long as the perturbation amplitude is small and there is no coupling between various modes. In the realistic situation the instability amplitude would soon grow to a large value when nonlinear mode coupling effects would become important and crucial in defining the final state. It is, therefore, important that the nonlinear simulation in the context of relativistic shear driven instability be done. The nonlinear simulation studies would also be important from the context of spectral cascade features.

- In addition to relativistic flows, the electron fluid can have temperature in the relativistic domain in experiments and astrophysical scenario where the shear flow instability has a role to play. It would, therefore, be of interest to carry out studies of the shear driven modes for the case with finite temperature effects.

8.2.2 Laser plasma coupled system

- In this thesis, we have presented a detailed characterization of the Relativistic Electromagnetic solitons in cold plasmas in the absence and presence of ion dynamics. Incorporation of ion response results in three new varieties of solitary structures i.e. high amplitude single peak solitons, flat-top solitons and cusp solitons. We have carried out the the dynamical evolution of flat-top solitons. It would be interesting to study the evolution of other variety of solitonic structures. In addition, the interaction, the propagation through inhomogeneous plasma etc., are other features which need to be extensively simulated.

- The stability of the soliton structures in 1-D have been studied for some of the main variety of solutions. It has been shown by earlier workers [49] that the single peak structures are typically very robust in 1-D and the multiple peak variety of solutions suffer the forward Raman scattering instability. We have shown that the flat top structures develop a backward Brillouin scattering instability. In this context, the 2-D studies should therefore be carried out to see whether the stable single peak solutions are susceptible to side scattering instabilities.

- At the wave breaking of the ion fluid, the cusp solitons are formed. In certain other plasma systems, such cusp variety of solitons are observed to be very stable [65]. These structures have been observed to dither around the wave breaking point. It has also been found that an initial large amplitude perturbation spontaneously evolves towards the formation of such cusp structures. Keeping these developments in view, the similar exercise for the cusp solutions of the coupled laser plasma system should be carried out.

- We have focussed in this thesis on the cold plasma case. The effect of temperature on the formation, evolution etc., of the structures need to be carried out.

- We had limited ourselves in our study to a circularly polarized laser light. The case of linear polarization typically leads to harmonic generation. The possibility of stable confined solutions in this case needs to be looked at.

Bibliography

[1] Neeraj Jain, Amita Das, Predhiman Kaw, and Sudip Sengupta. Nonlinear electron magnetohydrodynamic simulations of sausage-like instability of current channels. *Physics of Plasmas*, 10(1):29–36, 2003.

[2] Neeraj Jain, Amita Das, and Predhiman Kaw. Kink instability in electron magnetohydrodynamics. *Physics of Plasmas*, 11(9):4390–4398, 2004.

[3] Max Tabak, James Hammer, Michael E. Glinsky, William L. Kruer, Scott C. Wilks, John Woodworth, E. Michael Campbell, Michael D. Perry, and Rodney J. Mason. Ignition and high gain with ultrapowerful lasers@f|. *Physics of Plasmas*, 1(5):1626–1634, 1994.

[4] Neeraj Jain and A. Surjalal Sharma. Electron scale structures in collisionless magnetic reconnection. *Physics of Plasmas*, 16(5):050704, 2009.

[5] Sharad Kumar Yadav, Amita Das, Predhiman Kaw, and Sudip Sengupta. Anomalous energy dissipation of electron current pulses propagating through an inhomogeneous collisionless plasma medium. *Physics of Plasmas*, 16(4):040701, 2009.

[6] K. A. Tanaka, R. Kodama, K. Mima, Y. Kitagawa, H. Fujita, N. Miyanaga, K. Nagai, T. Norimatsu, T. Sato, Y. Sentoku, K. Shigemori, A. Sunahara,

T. Shozaki, M. Tanpo, S. Tohyama, T. Yabuuchi, J. Zheng, T. Yamanaka, P. A. Norreys, R. Evanse, M. Zepf, K. Krushelnic, A. Dangor, R. Stephens, S. Hatchett, M. Tabak, and R. Turner. Basic and integrated studies for fast ignition. *Physics of Plasmas*, 10(5):1925–1930, 2003.

[7] A. I. Akhiezer and R. V. Polovin. Theory of wave motion of an electron plasma. *Soviet Physics - JETP*, 3(5):696–705, 1956.

[8] T. Katsouleas and W. B. Mori. Wave-breaking amplitude of relativistic oscillations in a thermal plasma. *Phys. Rev. Lett.*, 61(1):90–93, Jul 1988.

[9] N. L. Tsintsadze and D. D. Tskhakaya. On the theory of electrosound waves in a plasma. *Soviet Physics - JETP*, 45(2):252–255, 1977.

[10] V. A. Kozlov, A. G. Litvak, and E. V. Suvorov. Envelope solitons of relativistic strong electromagnetic waves. *Soviet Physics - JETP*, 49(1):75–80, 1979.

[11] P. K. Kaw, A. Sen, and T. Katsouleas. Nonlinear 1d laser pulse solitons in a plasma. *Phys. Rev. Lett.*, 68(21):3172–3175, May 1992.

[12] H. H. Kuehl and C. Y. Zhang. One-dimensional, weakly nonlinear electromagnetic solitary waves in a plasma. *Phys. Rev. E*, 48(2):1316–1323, Aug 1993.

[13] R. N. Sudan, Y. S. Dimant, and O. B. Shiryaev. One-dimensional intense laser pulse solitons in a plasma. *Physics of Plasmas*, 4(5):1489–1491, 1997.

[14] W. B. Mori, C. Joshi, J. M. Dawson, D. W. Forslund, and J. M. Kindel. Evolution of self-focusing of intense electromagnetic waves in plasma. *Phys. Rev. Lett.*, 60:1298–1301, Mar 1988.

[15] C. S. Liu, Marshall N. Rosenbluth, and Roscoe B. White. Raman and brillouin scattering of electromagnetic waves in inhomogeneous plasmas. *Physics of Fluids*, 17(6):1211–1219, 1974.

[16] C. S. Liu and P. K. Kaw. *Advances in plasma physics. Vol. 6.* 1976.

[17] William L. Kruer. *Frontiers in Physics: The Physics of Laser Plasma Interactions.* Wesley Publishing company.

[18] Energy doubling of 42 gev electrons in a metre-scale plasma wakefield accelerator. *Nature*, 445(7129):741, 2007.

[19] A. S. Kingsep, K. V. Chukbar, and V. V. Yankov. *Reviews on Plasma Physics*, 16(243), 1990.

[20] Amita Das. Nonlinear aspects of two-dimensional electron magnetohydrodynamics. *Plasma Physics and Controlled Fusion*, 41(3A):A531, 1999.

[21] Sharad Kumar Yadav, Amita Das, and Predhiman Kaw. Propagation of electron magnetohydrodynamic structures in a two-dimensional inhomogeneous plasma. *Physics of Plasmas*, 15(6):062308, 2008.

[22] Amita Das, Neeraj Jain, Predhiman Kaw, and Sudip Sengupta. Sausage instabilities in the electron current layer and its role in the concept of fast ignition. *Nuclear Fusion*, 44(1):98, 2004.

[23] Sita Sundar, Amita Das, Vikrant Saxena, Predhiman Kaw, and Abhijit Sen. Relativistic electromagnetic flat top solitons and their stability. *Physics of Plasmas*, 18(11):112112, 2011.

[24] P. G. Drazin and W. H. Reid. Hydrodynamic stability.

[25] Amita Das and Predhiman Kaw. Nonlocal sausage-like instability of current channels in electron magnetohydrodynamics. *Physics of Plasmas*, 8(10):4518–4523, 2001.

[26] Amita Das and P. H. Diamond. Theory of two-dimensional mean field electron magnetohydrodynamics. *Physics of Plasmas*, 7(1):170–177, 2000.

[27] S. V. Bulanov, F. Pegoraro, and A. S. Sakharov. Magnetic reconnection in electron magnetohydrodynamics. *Physics of Fluids B: Plasma Physics*, 4(8):2499–2508, 1992.

[28] D. Biskamp, E. Schwarz, A. Zeiler, A. Celani, and J. F. Drake. Electron magnetohydrodynamic turbulence. *Physics of Plasmas*, 6(3):751–758, 1999.

[29] N. Attico, F. Califano, and F. Pegoraro. Fast collisionless reconnection in the whistler frequency range. *Physics of Plasmas*, 7(6):2381–2387, 2000.

[30] F. Califano, N. Attico, F. Pegoraro, G. Bertin, and S. V. Bulanov. Fast formation of magnetic islands in a plasma in the presence of counterstreaming electrons. *Phys. Rev. Lett.*, 86(23):5293–5296, Jun 2001.

[31] John C. Dorelli and Joachim Birn. Electron magnetohydrodynamic simulations of magnetic island coalescence. *Physics of Plasmas*, 8(9):4010–4019, 2001.

[32] L. Chacón, Andrei N. Simakov, and A. Zocco. Steady-state properties of driven magnetic reconnection in 2d electron magnetohydrodynamics. *Phys. Rev. Lett.*, 99(23):235001, Dec 2007.

[33] Neeraj Jain, Amita Das, Predhiman Kaw, and Sudip Sengupta. Role of current shear driven turbulence in anomalous stopping of energetic electrons. *Physics Letters A*, 363(1-2):125 – 129, 2007.

[34] F. Califano, R. Prandi, F. Pegoraro, and S. V. Bulanov. Two-dimensional electron-magnetohydrodynamic instabilities. *Physics of Plasmas*, 6(6):2332–2339, 1999.

[35] Gurudatt Gaur, Sita Sundar, Sharad K. Yadav, Amita Das, Predhiman Kaw, and Sarveshwar Sharma. Role of natural length and time scales on shear driven two-dimensional electron magnetohydrodynamic instability. *Physics of Plasmas*, 16(7):072310, 2009.

[36] G. Bodo, A. Mignone, and R. Rosner. Kelvin-helmholtz instability for relativistic fluids. *Phys. Rev. E*, 70:036304, Sep 2004.

[37] T Yabuuchi, A Das, G R Kumar, H Habara, P K Kaw, R Kodama, K Mima, P A Norreys, S Sengupta, and K A Tanaka. Evidence of anomalous resistivity for hot electron propagation through a dense fusion core in fast ignition experiments. *New Journal of Physics*, 11(9):093031, 2009.

[38] S. Hain and P. Mulser. Fast ignition without hole boring. *Phys. Rev. Lett.*, 86:1015–1018, Feb 2001.

[39] Sita Sundar and Amita Das. Free energy source for flow shear driven instabilities in electron-magnetohydrodynamics. *Physics of Plasmas*, 17, 2010.

[40] B. M. Veeresha, S. K. Tiwari, A. Sen, P. K. Kaw, and A. Das. Nonlinear wave

propagation in strongly coupled dusty plasmas. *Phys. Rev. E*, 81:036407, Mar 2010.

[41] Sanat Kumar Tiwari, Amita Das, Predhiman Kaw, and Abhijit Sen. Kelvin–helmholtz instability in a weakly coupled dust fluid. *Physics of Plasmas*, 19(2):023703, 2012.

[42] T. Zh. Esirkepov, F. F. Kamenets, S. V. Bulanov, and N. M. Naumova. Low-frequency relativistic electromagnetic solitons in collisionless plasmas. *JETP Letters*, 68(1):36–41, 1998.

[43] D. Farina and S. V. Bulanov. Relativistic electromagnetic solitons in the electron-ion plasma. *Phys. Rev. Lett.*, 86(23):5289–5292, Jun 2001.

[44] D. Farina and S. V. Bulanov. Dark solitons in electron-positron plasmas. *Phys. Rev. E*, 64(6):066401, Nov 2001.

[45] S. Poornakala, A. Das, A. Sen, and P. K. Kaw. Laser envelope solitons in cold overdense plasmas. *Physics of Plasmas*, 9(5):1820–1823, 2002.

[46] S. Poornakala, A. Das, P. K. Kaw, A. Sen, Z. M. Sheng, Y. Sentoku, K. Mima, and K. Nishikawa. Weakly relativistic one-dimensional laser pulse envelope solitons in a warm plasma. *Physics of Plasmas*, 9(9):3802–3810, 2002.

[47] Maurizio Lontano, Matteo Passoni, and Sergei V. Bulanov. Relativistic electromagnetic solitons in a warm quasineutral electron–ion plasma. *Physics of Plasmas*, 10(3):639–649, 2003.

[48] Daniela Farina and Sergei V Bulanov. Dynamics of relativistic solitons. *Plasma Physics and Controlled Fusion*, 47(5A):A73–A80, May 2005.

[49] Vikrant Saxena, Amita Das, Abhijit Sen, and Predhiman Kaw. Fluid simulation studies of the dynamical behavior of one-dimensional relativistic electromagnetic solitons. *Physics of Plasmas*, 13(3):032309, 2006.

[50] Hsing-Hen Chen and Chuan-Sheng Liu. Solitons in nonuniform media. *Phys. Rev. Lett.*, 37(11):693–697, Sep 1976.

[51] Maurizio Lontano, Sergei Bulanov, and James Koga. One-dimensional electromagnetic solitons in a hot electron-positron plasma. *Physics of Plasmas*, 8(12):5113–5120, 2001.

[52] G. Lehmann, E. W. Laedke, and K. H. Spatschek. Stability and evolution of one-dimensional relativistic solitons on the ion time scale. *Physics of Plasmas*, 13(9):092302, 2006.

[53] M. Borghesi, S. Bulanov, D. Campbell, R. Clarke, T. Esirkepov, M. Galimberti, L. Gizzi, a. MacKinnon, N. Naumova, F. Pegoraro, H. Ruhl, a. Schiavi, and O. Willi. Macroscopic Evidence of Soliton Formation in Multiterawatt Laser-Plasma Interaction. *Physical Review Letters*, 88(13):1–4, March 2002.

[54] W. Lu, C. Huang, M. Zhou, W. B. Mori, and T. Katsouleas. Nonlinear theory for relativistic plasma wakefields in the blowout regime. *Phys. Rev. Lett.*, 96(16):165002, Apr 2006.

[55] Hitoshi HOJO, Tsuguhiro WATANABE, and Kazuhiro AKIMOTO. Stationary solitary electomagnetic waves generated in relativistic laser-plasma interaction. *Journal of Plasma and Fusion Research*, 78(6):495–496, 2002.

[56] Vikrant Saxena, Amita Das, Sudip Sengupta, Predhiman Kaw, and Abhijit Sen. Stability of nonlinear one-dimensional laser pulse solitons in a plasma. *Physics of Plasmas*, 14(7):072307, 2007.

[57] S. Poornakala. Interaction of intense electromagnetic pulse with plasma: A thesis.

[58] Claire Ellen Max, Jonathan Arons, and A. Bruce Langdon. Self-modulation and self-focusing of electromagnetic waves in plasmas. *Phys. Rev. Lett.*, 33(4):209–212, Jul 1974.

[59] P. Kaw, G. Schmidt, and T. Wilcox. Filamentation and trapping of electromagnetic radiation in plasmas. *Physics of Fluids*, 16(9):1522–1525, 1973.

[60] D. Farina and S. Bulanov. Slow electromagnetic solitons in electron-ion plasmas. *Plasma Physics Reports*, 27:641–651, 2001. 10.1134/1.1390536.

[61] N. N. Akhmediev, V. V. Afanasjev, and J. M. Soto-Crespo. Singularities and special soliton solutions of the cubic-quintic complex ginzburg-landau equation. *Phys. Rev. E*, 53:1190–1201, Jan 1996.

[62] N. G. Vakhitov and A. A. Kolokolov. Stationary solutions of the wave equation in a medium with nonlinearity saturation. *Radiophysics and Quantum Electronics*, 16:783–789, 1973. 10.1007/BF01031343.

[63] Lj. Hadžievski, M. S. Jovanović, M. M. Škorić, and K. Mima. Stability of one-dimensional electromagnetic solitons in relativistic laser plasmas. *Physics of Plasmas*, 9(6):2569–2574, 2002.

[64] J. P. Boris and D. L. Book. Solution of the continuity equations by the method of flux-corrected transport. *Methods in Computational Phys.*, 16.

[65] Sanat Kumar Tiwari, Amita Das, Predhiman Kaw, and Abhijit Sen. Observation of sharply peaked solitons in dusty plasma simulations. *New Journal of Physics*, 14(6):063008, 2012.